UNIVERSIDADE DE BRASÍLIA - UnB
INSTITUTO DE GEOCIÊNCIAS - IG
CURSO DE PÓS-GRADUAÇÃO EM GEOLOGIA

INTRUSÕES MÁFICAS-ULTRAMÁFICAS DO DOMÍNIO RIO GRANDE DO NORTE, PROVÍNCIA BORBOREMA: AMBIENTE TECTÔNICO E POTENCIAL PARA DEPÓSITOS MAGMÁTICOS

DISSERTAÇÃO DE MESTRADO Nº 354

Alanielson da Câmara Dantas Ferreira

Brasília-DF, novembro de 2015

UNIVERSIDADE DE BRASÍLIA - UnB
INSTITUTO DE GEOCIÊNCIAS - IG
CURSO DE PÓS-GRADUAÇÃO EM GEOLOGIA

Intrusões máficas-ultramáficas do Domínio Rio Grande do Norte, Província Borborema: ambiente tectônico e potencial para depósitos magmáticos

Alanielson da Câmara Dantas Ferreira

Orientador:

Prof. Dr. Cesar F. Ferreira Filho

Coorientador:

Prof. Dr. Valmir da Silva Souza

Banca Examinadora:

_____

Prof. Dr. Cesar F. Ferreira Filho - (UnB)

_____

Dr. Francisco Valdir Silveira - (CPRM)

_____

Prof. Dr. Claudinei Gouveia de Oliveira - (UnB)

Brasília-DF, Novembro de 2015

AGRADECIMENTOS

- Aos professores e funcionários dos laboratórios do Instituto de Geociências da Universidade de Brasília pelos ensinamentos e comprometimento sem os quais não seria possível a construção desta dissertação. Em especial, ao Prof. Cesar pela condução e exemplo professor e pesquisador.
- Aos companheiros de pós-graduação com os quais convivi esses últimos dois anos, em especial ao Hudson, Luiz, Igor, Lauro, Ana Rita, Mariana, Hammel, Marco, Bernardo, Rafael, Diego, Raquel, Daniel, Mateus, Catarina, Leonardo e Sergio.
- Por fim, e principalmente a Amarilys, pelo carinho e por ter me possibilitado as condições de concluir esta etapa.

“Que a vida não gosta de esperar,

A vida é pra valer,

A vida é pra levar”

Chico Buarque / Toquinho

SUMÁRIO

ÍNDICE DE FIGURAS

ÍNDICE DE TABELAS

RESUMO

Intrusões máfica-ultramáficas afloram de forma descontinua ao longo de um trend NNE-SSW de 32 km no Terreno Rio Piranhas, porção central do Domínio Rio Grande do Norte (Província Borborema). Estas intrusões permitem a abertura de uma nova janela para exploração de depósitos de Ni-Cu (PGE) na Província Borborema. As intrusões máfico-ultramáficas afloram em geral como pequenos corpos lenticulares (<500 metros de comprimento) constituídos por proporções variadas de wehrlito (Ol + Cpx + Chr cúmulus), clinopiroxenito (Cpx cúmulus) e troctolito (Ol + Pl cúmulus) hospedados principalmente em ortognaisses e migmatitos. A mineralogia e a textura primária das intrusões são caracterizadas por cristais bem desenvolvidos de granulação média a grossa, sem orientação preferencial, localizados nos núcleos das intrusões. Estas características magmáticas são obliteradas nas margens das intrusões, pela substituição gradativa em direção as bordas dos minerais primários por anfibólios, os quais marcam o contato com as rochas encaixantes e exibem uma foliação metamórfica bem definida. As encaixantes são constituídas principalmente por ortognaisses e migmatitos, subordinadamente anfibolitos e supracrustais. A paragênese metamórfica presente nos ortognaisse é composta por quartzo-microclina-plagioclásio-hornblenda indicativa de metamorfismo no fácies anfibolito. A composição da olivina cúmulus nas diferentes intrusões, e rochas, variam de $Fo_{80,6}$ a $Fo_{67.6}$. A composição mais primitiva de olivina é obtida em wehrlitos, indicando magma parental com composições moderadamente primitivas ($Fo_{80,6}$ e ~ 2000 ppm de Ni). A composição do plagioclásio cúmulus em equilíbrio com a olivina cúmulus nos troctolitos apresenta elevados teores de An ($An_{89,0}$ a $An_{79,9}$) correlacionáveis com as composições de magma descritos em arcos magmáticos gerados em ambientes de subducção. A geoquímica de rocha total das máficas-ultramáficas é controlada principalmente por diferentes proporções de olivina, clinopiroxênio e plagioclásio. Na mesma intrusão composições químicas das amostras com minerais e texturas ígneas primárias preservadas são semelhantes às amostras com mineralogia totalmente transformada, indicando que a recristalização metamórfica não promoveu uma mudança significativa na composição dos elementos maiores. Os teores de Cr_2O_3 mostram uma significativa diferença entre as rochas máfica-ultramáficas. A combinação Mg # e Cr_2O_3 sugerem que as intrusões situadas na porção sul foram cristalizadas a partir de magmas saturados em cromita relativamente primitivos (Mg # entre 73,3 e 80,5), enquanto intrusões da parte norte

foram geradas por magmas insaturados em cromita e mais fracionados (Mg # entre 57,0 e 68,7). Perfis dos elementos traços normalizados pelo condrito mostram que as rochas são fracionadas, evidenciado pelo enriquecimento relativo em íons de grande raio (*large ion lithophile elements* – LILE) e depleção relativa de elementos de alto campo de força (*high field strength elements* – HFSE). Várias amostras exibem pronunciadas anomalias negativas de Nb e Ta, estas anomalias são mais evidentes quando Nb e Ta são comparados com elementos adjacentes mais resistentes a alteração (por exemplo, Th e La). Perfis dos elementos traços são semelhantes para as mesmas litologias das diferentes intrusões. Idades U-Pb em zircão indicam que as intrusões máfica-ultramáficas foram cristalizadas em 2195 ± 5 Ma. Idades U-Pb em zircão das encaixantes ortognáissicas indicam cristalização a partir de magmas félsicos entre 2220-2230 Ma. Portanto ocorre uma estreita janela de tempo (cerca de 30 Ma) entre os eventos de plutonismo félsico e máfico. Idades U-Pb em zircão de rochas encaixantes incluem idades mais antigas (cerca de 2,50 - 2,71 Ga), indicando retrabalhamento crustal de rochas siderianas-arqueanas durante magmatismo máfico e félsico riaciano. Magmatismo máfico-ultramáfico e félsico (cálcio-alcalino) de 2,15 - 2,25 Ga é correlacionado a arcos magmáticos relatado em estudos anteriores no Terreno Rio Piranhas do Domínio Rio Grande do Norte. O magmatismo máfico-ultramáfico é interpretado como originado em arco magmático, possivelmente resultante da fusão parcial da cunha do manto acima da zona de subducção durante as fases finais da orogênese.

ABSTRACT

A recently identified 32 km long NNE-SSW trending array of mafic-ultramafic intrusions occur in the paleoproterozoic Rio Piranhas terrain of the Rio Grande do Norte domain (Borborema Province). The cluster of mafic-ultramafic intrusions described in this study provides a new window for exploration for Ni-Cu-(PGE) deposits in the Borborema Province. The mafic-ultramafic intrusions outcrop as small lensoid bodies (< 500 meters long) hosted mainly by orthogneiss and migmatites. Mafic-ultramafic rocks of four intrusions investigated in detail consist of variable proportions of wehrlite (Ol + Cpx ± Chr cumulate), clinopyroxenite (Cpx cumulate) and troctolite (Ol + Pl cumulate). The primary igneous textures and mineralogy are partially replaced by amphibolite facies metamorphic assemblages and tectonic fabric. These intrusions usually consist of medium- to coarse-grained domains where primary magmatic textures and minerals are preserved, and medium-to fine-grained massive to foliated domains where metamorphic fabric and minerals prevail. Primary magmatic features predominate in the core whereas a metamorphic minerals and texture characterize the contact with host rocks. The later consist of orthogneiss and migmatite associated with minor amphibolite and supracrustal. Metamorphic parageneses of banded orthogneiss, consisting of microcline-quartz-plagioclase-hornblende, indicate amphibolite facies of metamorphism. The compositions of cumulate olivine in different intrusions and rocks types range from $Fo_{80,6}$ to $Fo_{67.6}$. The composition of the most primitive olivine in wehrlite indicates parental magmas with moderately primitive compositions ($Fo_{80,6}$ and ~ 2,000 ppm Ni). The compositional range of cumulus plagioclase coexisting with cumulus olivine in troctolites is characterized by very high An content ($An_{89,0}$ to $An_{79,9}$), similar to magma compositions described in subduction-related magmatic arcs. The bulk compositions of mafic-ultramafic rocks are mainly controlled by different amounts of olivine, clinopyroxene and plagioclase. Chemical compositions of samples where primary igneous minerals and textures are preserved are similar to highly transformed samples from the same intrusion, thus supporting that the metamorphic recrystallization did not promoted a significant change in major element composition. Cr_2O_3 contents for mafic-ultramafic rocks from different intrusions are highly different. Combined Mg# and Cr_2O_3 contents suggest that the intrusions located in the south crystallized from relatively primitive (Mg# between 73.3 and 80.5) chromite saturated magmas, while intrusions located in the north crystallized from more fractionated chromite unsaturated magmas (Mg# between 57.0 and 68.7). Chondrite-normalized

trace element profiles of mafic-ultramafic rocks are fractionated, as indicated by relative enrichment in large ion lithophile elements (LILE) and relative depletion high field strength elements (HFSE). Several samples have pronounced negative Nb and Ta anomalies, a feature that becomes more evident when Nb and Ta are compared with adjacent alteration-resistant elements (e.g., Th and La). Trace-element profiles are similar for similar rock types from different intrusions. U-Pb zircon ages indicate that mafic-ultramafic intrusions crystallized at ca. 2195±5 Ma. U-Pb zircon ages of host orthogneiss indicate that they crystallized from felsic magmas at ca. 2220-2230 Ma, thus providing a narrow window of time (ca. 30 Ma) for the reported events of felsic and mafic plutonism. U-Pb zircon ages of host rocks also include older ages (ca. 2.50-2.68 Ga) indicating that older crustal components are reworked during mafic and felsic magmatism. The mafic-ultramafic and felsic (calc-alkaline) magmatism is correlated with the ca. 2.15-2.25 Ga magmatic arc reported in previous studies of the Rio Piranhas terrain of the Rio Grande do Norte domain. The mafic-ultramafic magmatism is interpreted as originated in a magmatic arc, possibly resulting from partial melting of a mantle wedge above the subduction zone in final stages of the orogeny.

1. INTRODUÇÃO

1.1 Apresentação e Objetivos

Intrusões máfica-ultramáficas foram descobertas na porção central do Estado do Rio Grande do Norte (Domínio Rio Grande do Norte) entre os anos de 2008 e 2012 durante campanhas sistemáticas de mapeamento geológico desenvolvido pela empresa "L & L Empreendimentos Minerais Ltda". Essas intrusões afloram ao longo de um trend NNE-SSW de mais de 30 km, localizado a leste da cidade de Lajes-RN, são hospedadas em ortognaisse e migmatitos associados ao Terreno Rio Piranhas (Almeida et al., 1981; Delgado et al., 2003). Intrusões e encaixantes foram afetadas pelos episódios deformacionais e magmáticos do Ciclo orogênico Brasiliano (640-540 Ma). Portanto, a configuração geológica da área de estudo apresenta as complexidades que caracterizam o embasamento paleoproterozoico de alto grau do Domínio Rio Grande do Norte (Jardim de Sá, 1994; Fetter et al., 2000; Brito Neves et al., 2000; Van Schmus et al., 2003; Souza et al, 2007; Dantas et al., 2008; Holanda et al., 2011; Sá et al., 2014).

Depósitos de classe mundial de Ni-Cu-PGE são tipicamente associados à tectônica extensional na crosta (Naldrett, 2004; Barnes and Lightfoot, 2005), porém depósitos significativos também são associados a terrenos orogênicos de diferentes idades (Song e Li., 2009; Su et al., 2011; Mota-e-Silva et al., 2011; Ferreira Filho et al., 2013). A descoberta do depósito de Ni-Cu-PGE em Limoeiro (Mota-e-Silva et al., 2013; 2015), primeiro depósito de sulfeto de níquel da Província Borborema, abriu novos alvos prospectivos na província. Depósitos de níquel sulfetado relacionados a intrusões máfica-ultramáficas de diferentes tamanho e composição são originados em diferentes ambientes petrotectônicos. Estes depósitos consistem geralmente em condutos de magmas que ocorrem ao longo de zonas de fraqueza da crosta (Naldrett, 2004; Lightfoot e Evans-Lamswood, 2014). A identificação do tipo de estrutura magmática em terrenos geologicamente complexos é um desafio. Porém, o entendimento da instalação, evolução e fonte dessas rochas é de suma importância para a compreensão geotectônica de uma área ou região, bem como de seu potencial metalogenético.

Neste trabalho apresentaremos dados de afloramentos, petrografia, mineralogia, química mineral, bem como a caracterização litogeoquímica e geocronológica de intrusões máfica-ultramáficas, além de correlacioná-las a um contexto geodinâmico.

A proposta desta dissertação, portanto, é contribuir para a produção de novos dados geológicos, geoquímicos e geocronológicos, e de forma geral, no acréscimo do conhecimento dos processos de evolução crustal desta porção da Província Borborema. Além da possibilidade de abrir caminhos para um novo potencial metalogenético a ser avaliado.

1.2 Localização

A área de estudo dessa dissertação localiza-se na porção central do Estado do Rio Grande do Norte, entre as cidades potiguares de Lajes e Angicos (Fig.1). O acesso principalmente dá-se pela BR-304 (rodovia Natal-Mossoró). Ocorre uma abundância de estradas vicinais que permitiram fácil acesso as unidades investigadas.

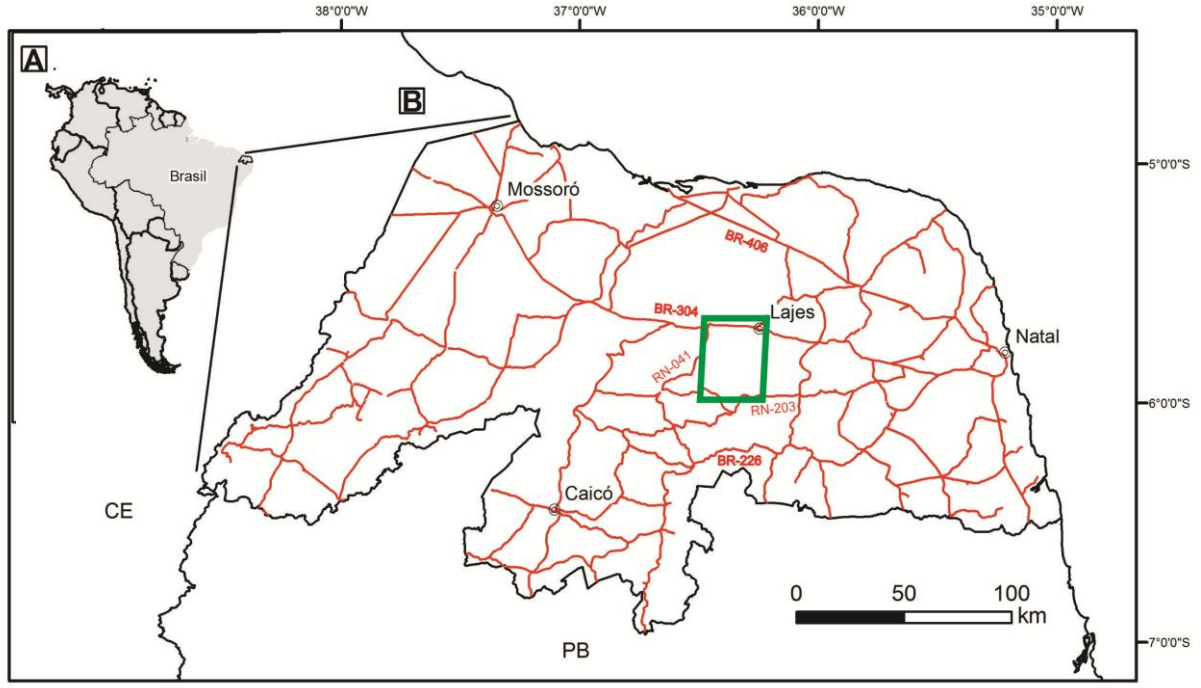

Figura 1: Mapa de localização e acesso da área estudada. A) Contorno da América do Sul. B) Contorno do Estado do Rio Grande do Norte.

1.3 Importância do Estudo

A relevância desta pesquisa destaca-se sobre os seguintes aspectos principais:

- Primeiros dados petrográficos, mineralógicos, litogeoquímicos e geocronológicos sistemáticos de intrusões máfica-ultramáficas riacianas (~2,19 Ga) da porção central do Domínio Rio Grande do Norte.
- As intrusões apresentam mineralogia (Ol + Cpx + Chr cúmulus) e características ígneas primárias muito bem preservadas, configurando-se como um excelente objeto de estudo para o entendimento dos processos

magmáticos formadores dos complexos máfico-ultramáficos: fracionamento magmático e magma parental.

- Magmas primitivos (i.e. alto Mg#) intrusivos em crosta siálica têm favorecido o processo de segregação de líquidos imiscíveis de sulfetos magmáticos, tornando-se alvos potenciais para conter depósitos de Ni-Cu sulfetado, a exemplo do depósito de Limoeiro localizado na Zona Transversal da Província Borborema (Mota-e-Silva et al., 2013; 2015).
- A presente pesquisa promove um avanço do conhecimento geológico e geocronológico do Terreno Rio Piranhas. O estudo também pode contribui para uma melhor compreensão do período riaciano bem como fornece subsídios à discussão do modelo evolutivo do embasamento do Grupo Seridó.

1.4 Escopo da Dissertação

Esta dissertação apresenta-se estruturada na forma de artigo a ser submetido para publicação em periódico científico especializado sobre o tema. O artigo é intitulado "Paleoproterozoic Mafic-Ultramafic Intrusions in the Rio Grande do Norte Domain of the Borborema Province, Northeast Brazil: tectonic setting and potential for magmatic deposits of a 2.2 Ga magmatism", elaborado entre os anos de 2014 e 2015.

O objetivo principal do artigo é apresentar a caracterização petrográfica, petrológica, litogeoquímica e geocronológica das intrusões máfica-ultramáficas da porção central do Domínio Rio Grande do Norte. Abordando discussões sobre o magma parental e a evolução das rochas máfica-ultramáficas, bem como seu significado na geologia regional.

O artigo ("Capítulo 2") é precedido por um Capítulo de Apresentação, no qual estão contidas informações gerais da dissertação: Apresentação e Objetivos, Localização, Importância do Estudo e este Sub-capítulo, "Escopo da Dissertação".

O Capítulo de Conclusões apresenta de forma sintetizada os resultados da pesquisa previamente discutidos no artigo.

Ao final do volume, o Capítulo de Anexo, no qual inclui os resultados de química mineral não apresentados no corpo do artigo.

1.5 Referências

Almeida, F. F. M., Hasui, Y., Brito Neves, B. B., Fuck, R. A., 1981. Brazilian structural provinces: an introduction. Earth Sci. Rev., v.17, pp. 1-29.

Barnes, S. J., Lightfoot P.C., 2005. Formation of magmatic nickel sulfide ore deposits and processes affecting their copper and platinum group element contents. In: Hedenquist JW, Thompson JFH, GoldfarbRJ, Richards JP (eds) Economic Geology, One Hundredth Anniversary Volume, pp. 179-214.

Brito Neves, B. B., Dos Santos, E. J., Van Schmus, W. R., 2000. Tectonic history of the Borborema Province, Northeastern Brazil. In: Cordani, U., Milani, E. J., Thomaz Filho, A., Campos, D. A., (Eds.). Tectonic evolution of South America. 31st International Geological Congress, Rio de Janeiro, Brazil, pp. 151–182.

Dantas, E.L., Negrão, M.M., Buhn, B., 2008. 2,3 Ga continental crust generation in the Rio Grande do norte terrane, NE-Brazil (VI SSAGI, San Carlos Bariloche, 2008). Book of Abstracts. In: VI South American Symposium on Isotope Geology. pp. 40. also in CD-rom.

Delgado, I.M., Souza, J.D., Silva, L.C., Silveira Filho, N.C., Santos, R.A., Pedreira, A.J., Guimarães, J,T, Angelim, L.A.A., Vasconcelos, A.M., Gomes, I.P., Lacerda Filho, J.V., Valente, C.R., Perrotta, M.P., Heineck, C.A., 2003. Geotectônica do Escudo Atlântico. In: Bizzi, L.A., Schobbenhaus, C., Vidotti, R.M., Gonçalves, J.H., eds., 2003. Geologia, tectônica e recursos minerais do Brasil. Brasília, CPRM, pp. 259-291.

Ferreira Filho, C. F., Cunha, J.C., Cunha, E.M. and Canela, J.H.C., 2013. Depósito de níquel, cobre sulfetado de Santa Rita, Itagibá, Bahia, Brasil. Série Arquivos Abertos, v. 39, Companhia Baiana de Pesquisa Mineral (CBPM), Salvador-Bahia, 59 pp.

Fetter, A. H., Van Schmus, W. R., Santos, T. J. S., Neto, J. A. N., Henriarthaud, M., 2000. U-Pb and Sm-Nd geochronological constraints on the crustal evolution and basement architecture of Ceará State, NW Borborema Province, NE Brazil: Implications for the existence of the Paleoproterozoic supercontinent Atlantica., v. 30, pp. 102-106.

Hollanda, M. H. B. M., Archanjo, C. J., Souza, L. C., Dunyi, L., Armstrong, L., 2011. Long-lived Paleoproterozoic granitic magmatism in the Seridó-Jaguaribe domain, Borborema Province-NE Brazil. Journal of South American Earth Sciences, v. 32, pp. 287-300.

Jardim de Sá, E.F., 1994. A Faixa Seridó (Província Borborema, Ne Brasil) e o seu Significado Geodinâmico na Cadeia Brasiliana/Pan-Africana. Unpublished Ph.D. Thesis, Universidade De Brasília, 803pp.

Lightfoot, P.C., Evans-Lamswood, D., 2014. Structural controls on the primary distribution of mafic–ultramafic intrusions containing Ni–Cu–Co–(PGE) sulfide mineralization in the roots of large igneous provinces. Ore Geology Reviews, v. 64, pp. 354–386.

Mota-e-Silva, J., Ferreira Filho, C.F., Bühn, B., Dantas, E.L., 2011, Geology, petrology and geochemistry of the “Americano do Brasil” layered intrusion, central Brazil, and its Ni-Cu sulfide deposits: Mineralium Deposita, v. 46, pp. 57–90.

Mota-e-Silva, J., Ferreira Filho, C.F., Giustina, M.E.S., 2013. The Limoeiro deposit: Ni-Cu-PGE sulfide mineralization hosted within an Ultramafic tubular magma conduit in the Borborema Province, Northeastern Brazil. Econ Geol, v. 108, pp. 1753–1771.

Mota-e-Silva, J., Prichard, H.M., Ferreira Filho, C.F., Fisher, P.C., McDonald, I., 2015. Platinum-group minerals in the Limoeiro Ni–Cu–(PGE) sulfide deposit, Brazil: the effect of magmatic and upper amphibolite to granulite metamorphic processes on PGM formation. Miner Deposita, DOI 10.1007/s00126-015-0585-0.

Naldrett, A.J., 2004. Magmatic Sulfide Deposits – Geology, Geochemistry and Exploration. Germany, Springer Berlin, 724pp.

Sá, J. M., Souza, L. C., Legrand, J. M., Galindo, A. C., Maia, H. N., Fillippi, R. R., 2014. U-Pb and Sm-Nd data of the Rhyacian and Statherian Orthogneisses from Rio Piranhas-Seridó and Jaguaribeano Terranes, Borborema Province, Northeast of Brazil. Geol. USP, Sér. cient, v.14, pp. 97-110.

Song, X.Y., Li, X.R., 2009, Geochemistry of the Kalatongke Ni-Cu-(PGE) sulfide deposit, NW China: Implications for the formation of magmatic sulfide mineralization in a postcollisional environment. Mineralium Deposita, v. 44, pp. 303−327.

Souza, Z. S., Martin, H., Peucat, J. J., Jardim De Sá, E. F., Macedo, M. H. F., 2007. Calc-Alkaline Magmatism At The Archean-Proterozoic Transition: The Caicó Complex Basement (Ne Brasil). Jounal of Petrology, v. 48, pp. 2149-2185.

Su, B.X., Qin, K.Z., Sakyi, P.A, Li, X.H., Yang, Y.H., Sun, H., Tang, D.M., Liu, P.P., Xiao, Q.H., Malaviarachchi, S.P.K., 2011. U–Pb ages and Hf–O isotopes of zircons from Late Paleozoic mafic–ultramafic units in southern Central Asian Orogenic Belt: tectonic implications and evidence for an Early-Permian mantle plume. Gondwana Res., v. 20, pp. 516–531.

Van Schmus, W. R., Brito Neves, B.B., Williams, I. S., Hackspacher, P. C., Fetter, A. H., Dantas, E. L., Babinski, M., 2003. The Seridó Group of NE Brazil, a late Neoproterozoic pre-to syn-collisional basin in West Gondwana: insights form SHRIMP U-Pb detrital zircon ages and Sm-Nd crustal residence (TDM) ages. Precambrian Research, v. 127, pp. 287-327.

2. PALEOPROTEROZOIC MAFIC-ULTRAMAFIC INTRUSIONS IN THE RIO GRANDE DO NORTE DOMAIN OF THE BORBOREMA PROVINCE, NORTHEAST BRAZIL: TECTONIC SETTING AND POTENTIAL FOR MAGMATIC DEPOSITS OF A 2.2 GA MAGMATISM

Alanielson da C. D. FERREIRA[1], Cesar F. FERREIRA FILHO[1] , Elton L. DANTAS[1], Valmir da Silva SOUZA[1]

[1]Instituto de Geociências, Universidade de Brasília, 70910-900 Brasília-DF, Brasil.

Corresponding author: Alanielson da C. D. Ferreira (ferreira.acd@gmail.com)/ Cesar Fonseca Ferreira Filho (cesarf@unb.br)

Abstract

A recently identified 32 km long NNE-SSW trending array of mafic-ultramafic intrusions in the paleoproterozoic Rio Piranhas terrain, Rio Grande do Norte domain (Borborema Province). The cluster of mafic-ultramafic intrusions described in this study provides a new window for exploration for Ni-Cu-(PGE) deposits in the Borborema Province. The mafic-ultramafic intrusions outcrop as small lensoid bodies (< 500 meters long) hosted mainly by orthogneiss and migmatites. Mafic-ultramafic rocks of four intrusions investigated in detail consist of variable proportions of wehrlite (Ol + Cpx ± Chr cumulate), clinopyroxenite (Cpx cumulate) and troctolite (Ol + Pl cumulate). The primary igneous textures and mineralogy are partially replaced by amphibolite facies metamorphic assemblages and tectonic fabric. These intrusions usually display medium- to coarse-grained domains where primary magmatic textures and minerals are preserved, and medium-to fine-grained massive to foliated texture where metamorphic fabric and minerals prevail. Primary magmatic features predominate in the core whereas a metamorphic minerals and texture characterize the contact with host rocks. The later consist of orthogneiss and migmatite associated with minor amphibolite and supracrustal. Metamorphic parageneses of banded orthogneiss, consisting of microcline-quartz-plagioclase-hornblende, indicate amphibolite facies of metamorphism. The compositions of cumulate olivine in different intrusions and rocks types range from $Fo_{80.6}$ to $Fo_{67.6}$. The composition of the most primitive olivine in wehrlite indicates parental magmas with moderately primitive compositions ($Fo_{80.6}$ and ~ 2,000 ppm Ni). The

compositional range of cumulus plagioclase coexisting with cumulus olivine in troctolites is characterized by very high An content ($An_{89.0}$ to $An_{79.9}$), similar to magma compositions described in subduction-related magmatic arcs. The bulk compositions of mafic-ultramafic rocks are mainly controlled by olivine, clinopyroxene and plagioclase in different amounts. Chemical compositions of samples where primary igneous minerals and textures are preserved are similar to highly transformed samples from the same intrusion, supporting that the metamorphic recrystallization did not promoted a significant change in major element composition. Cr_2O_3 contents for mafic-ultramafic rocks from different intrusions are highly different. Combined Mg# and Cr_2O_3 contents suggest that the intrusions located in the south crystallized from relatively primitive (Mg# between 73.3 and 80.5) chromite saturated magmas, while intrusions located in the north crystallized from more fractionated chromite unsaturated magmas (Mg# between 57.0 and 68.7). Chondrite-normalized trace element profiles of mafic-ultramafic rocks are fractionated, as indicated by relative enrichment in large ion lithophile elements (LILE) and relative depletion high field strength elements (HFSE). Several samples have pronounced negative Nb and Ta anomalies, a feature that becomes more evident when Nb and Ta are compared with adjacent alteration-resistant elements (e.g., Th and La). Trace-element profiles are similar for similar rock types from different intrusions. U-Pb zircon ages indicate that mafic-ultramafic intrusions crystallized at ca. 2195±5 Ma. U-Pb zircon ages of host orthogneiss indicate that they crystallized from felsic magmas at ca. 2220-2230 Ma, thus providing a narrow window of time (ca. 30 Ma) for the reported events of felsic and mafic plutonism. U-Pb zircon ages of host rocks also include older ages (ca. 2.50-2.71 Ga) indicating that older crustal components are reworked during mafic and felsic magmatism. The mafic-ultramafic and felsic (calc-alkaline) magmatism is correlated with the ca. 2.15-2.25 Ga magmatic arc reported in previous studies of the Rio Piranhas terrain. The mafic-ultramafic magmatism is interpreted as originated in a magmatic arc, possibly resulting from partial melting of a mantle wedge above the subduction zone in final stages of the orogeny.

Keywords: mafic-ultramafic intrusion, U-Pb geochronology, mineral chemistry, lithogeochemistry, Borborema Province

2.1 Introduction

World-class Ni-Cu-PGE deposits are typically associated with extensional tectonics in the crust (Naldrett, 2004; Barnes and Lightfoot, 2005), but significant deposits are now considered to be closely associated with orogenic terrains of different ages (*e.g*. Song and Li, 2009; Su et al., 2011; Mota-e-Silva et al., 2011; Ferreira Filho et al., 2013). The discovered of the Limoeiro Ni-Cu-PGE deposit (Mota-e-Silva et al., 2013; 2015), the first nickel sulfide deposit of the Borborema Province, unleashed the interest for exploration for nickel sulfides in this region. Intrusion related nickel sulfide deposits are associated with mafic-ultramafic bodies of different size and composition originated in different petro-tectonic settings. Mineralized intrusions usually consist of open system magma channels or conduits and occur as irregular small bodies along major fault zones in the crust (Lightfoot and Evans-Lamswood, 2014). The identification of this type of magmatic structures in poorly exposed or geologically complex terrains is a challenge.

A cluster of mafic-ultramafic intrusions was discovered in 2008 during geological mapping developed for mineral exploration for iron ore deposits by "L & L Empreendimentos Minerais", a Brazilian junior company, in the central portion of the Rio Grande do Norte State. These intrusions, located nearby the town of Lajes cite, are hosted by paleoproterozoic gneiss and migmatites and occur along a 32 km long NNE trend. Host rocks and layered intrusions were affected by the deformational, metamorphic and magmatic episodes linked to the Neoproterozoic Brasiliano orogenic cycle. Therefore, the geological setting where these mafic-ultramafic intrusions occur has the complexities that characterize the basement high-grade terrains of the Borborema Province (Jardim de Sá, 1994; Brito Neves et al., 2000; Van Schmus et al., 2003; Souza et al., 2007; Hollanda et al., 2011).

In this study we present the first geological, petrographic and geochemical results for mafic-ultramafic intrusions located in the central portion of the Rio Grande do Norte domain. Together with geochronological results for the intrusions and host rocks, these studies provide constraints for the petro-tectonic setting of this mafic-ultramafic magmatism, and open a new window for exploration for Ni-Cu-PGE deposits in the Borborema Province.

2.2 Regional Geology

The Borborema Province (Almeida et al., 1981) in northeastern South America is a typical branch of the Neoproterozoic Brasiliano orogenic system (Fig. 2A). The Borborema Province (BP) consists of magmatic and sedimentary Precambrian rocks of different ages (Fig. 2B). The crustal evolution of the BP includes Paleoproterozoic orogenic and taphrogenic cycles (Siderian, Rhyacian, Orosirian and Statherian) (Brito Neves, 2011) and the Brasiliano/Pan-African orogeny (0.7 to 0.5 Ga) (Jardim de Sá, 1994; Santos, 1996; Van Schmus et al., 2008). Another orogenic cycle, denominated Cariris Velhos (1.0 to 0.9 Ga), is identified just in the southern portion of the Patos lineament (Brito Neves et al.1995; 2000; Santos et al., 2010). Crustal scale shear zones (Fig. 2B) with associated magmatism, developed during the Brasiliano orogeny, separate different domains of the BP (Brito Neves, 1975; Jardim de Sá, 1994; Brito Neves et al., 2000; Van Schmus et al., 2011).

Mafic-ultramafic complexes occur in different geological settings of the BP. They include, among others, the ~ 3.08 Ga Riacho da Telha Complex in the São José Campestre massif (Jesus, 2011), the PGE and chromite mineralized 2036 Ma Tróia Complex in the Ceará domain (Da Costa et al., 2014), the ~ 950 Ma Floresta Complex in the Zona Tranversal domain (Lages, 2014), the ~ 830 Ma Brejo Seco Complex in the Riacho do Pontal domain (Salgado et al., 2014), the Ni-Cu-PGE mineralized Limoeiro chonolith in the Rio Capibaribe terrane (Mota-e-Silva et al., 2013) (Fig. 2B). These complexes have highly different compositions, magmatic intrusions and crystallization ages, indicating that they originated from different magmatic event and have distinct potential to host magmatic deposits.

The Rio Grande do Norte Domain (RGND) consists of different crustal segments juxtaposed during the Brasiliano orogeny (Fig. 2 and 3). The RGND, limited by the Patos Lineament (PaL) to the south and Senador Pompeu Lineament (SPL) to the west. The RGND includes crustal segments of Archean age (São José do Campestre massif, Dantas et al., 2004), extensive domains of paleoproterozoic gneiss and migmatites (Caby, 1989; Bertrand & Jardim de Sá, 1990; Caby et al., 1991; Jardim de Sá, 1994; Fetter et al., 2000; Souza et al., 2007), meso- to neo-proterozoic supracrustal sequences (e.g. Seridó and Orós belt, Van Schmus et al., 1995, 2003; Sá et al., 1995; Arthaud et al., 2008; Hollanda et al., 2015), and extensive sin- to pos-tectonic plutons (640-540Ma, Jardim de Sá, 1994; Hollanda et al., 1999; Nascimento et al., 2008; 2014). Mafic-ultramafic intrusion in the RGND is

restricted to the Riacho da Telha complex is (Jesus, 2011). This 3.03 Ga intrusion, consisting of interlayered serpentinite, websterite and gabbro, is hosted by ca 3.5 Ga ortho and paragneiss of the São José do Campestre Massif (Jesus, 2011).

The paleoproterozoic Rio Piranhas terrane of the RGND (Fig. 2 and 3) forms the basement rocks of the neoproterozoic supracrustal belt (Seridó Fold Belt). They include variable calc-alkaline quartz-feldspathic rocks, including banded gneiss, granitic to dioritic gneiss and migmatite, associated with metamafic and supracrustal rocks (Jardim de Sá, 1994; Van Schmus et al., 1995; Fetter et al., 2000; Souza et al., 1993, 2007; Sá et al., 2014). Different ages were obtained for this paleoproterozoic magmatism in the RGND (Dantas et al., 2008; Hollanda et al., 2011).

Systematic U-Pb zircon geochronological studies indicate magmatic ages of ca. 2.16-2.13 Ga for orthogneiss and metagabro of the São Vicente-Florânia region (Hackspacher et al.,1990; Dantas, 1992; Van Schmus et al., 1995), ca. 2.24-2.25 Ga for calc-alkaline granitic to dioritic orthogneiss of the Caicó region (Legrand et al., 1991, 1997; Medeiros et al., 2012), and different ages for orthogneiss from distinct plutonic bodies (i.e. 2.25 Ga for São José do Seridó pluton; 2.21 Ga for Santana do Matos pluton; 2.17 Ga Antônio Martins pluton) of the Rio Piranhas terrane (Hollanda et al., 2011).

The older tectonic fabric in these orthogneisses is a highgrade banding (D1~Sn-1) associated with isoclinal to intrafolial folds and strong transposition, followed by an event of tangential kinematics (D2~Sn). The last tectono-metamorphic event (D3~Sn+1) is marked by transcurrent to oblique shear zones and emplacement of the late Neoproterozoic granitoids. The associated metamorphism ranges from upper amphibolite to granulite facies (near plutonic intrusions and crustal-scale shear zones) to greenschist facies.

Mafic-ultramafic intrusions were not described in previous studies of the paleoproterozoic terrane of the RGND and, therefore, our results will provide additional constraints for the tectonic setting.

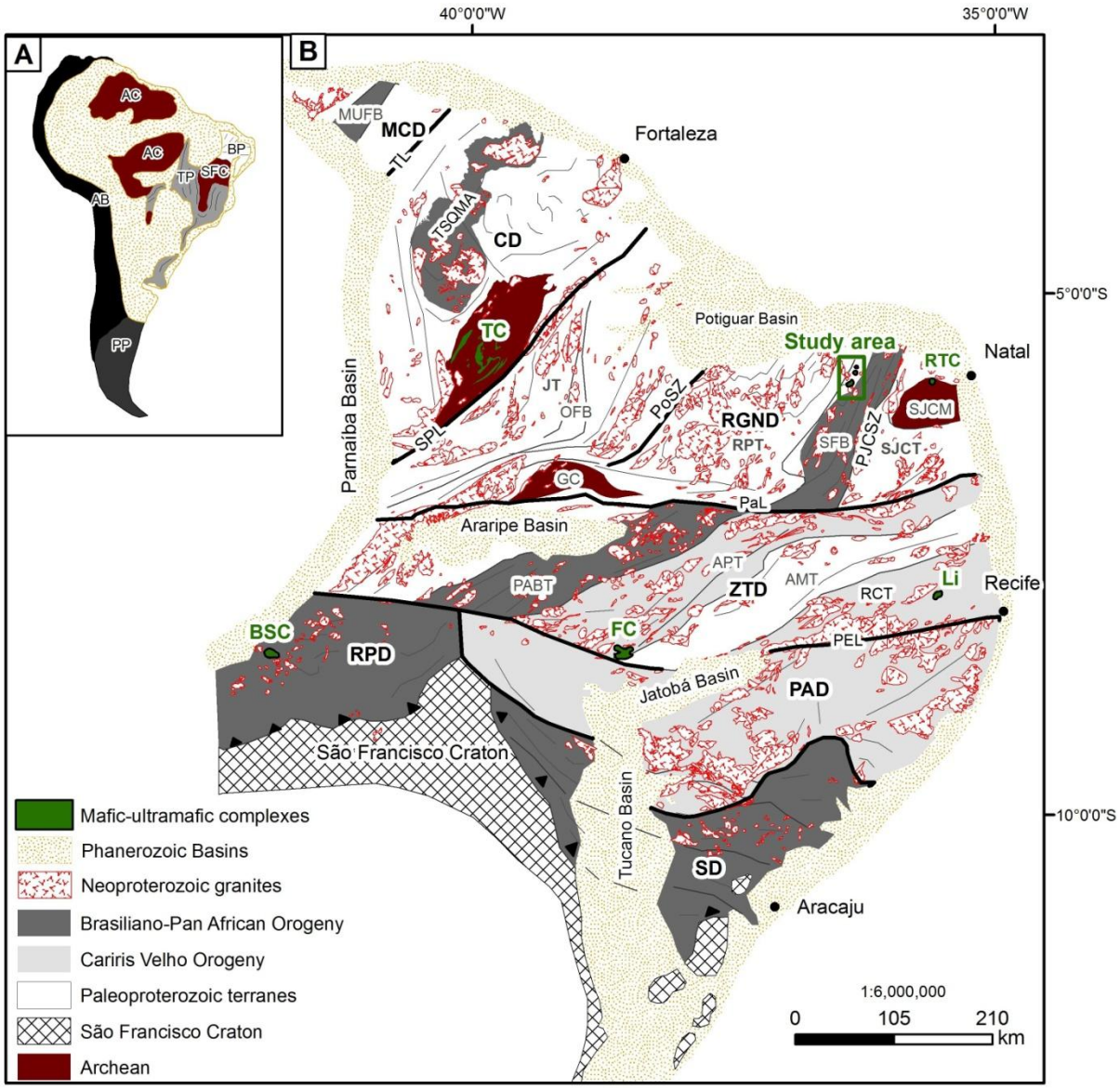

Figure 2. A) Geological outline of South America. AC = Amazonian craton; SFC = São Francisco craton; BP = Borborema Province; TP = Tocantins province; AB = Andean Belt, PP = Patagonia Province. B) Sketch showing the main shear zones that limit the domain subdivision of the Borborema province (modified from Van Schmus et al. 2011, Delgado et al. 2003 and Jardim de Sá, 1994). MUFB = Martinópolis-Ubajara fold belt; MCD = Médio Coreaú domain; CD = Ceará domain; TSQMA = Tamboril-Santa Quitéria magmatic arc; RGND = Rio Grande do Norte domain; JT = Jaguaribiano terrane; SJCT = São José do Campestre terrane; RPT = Rio Piranhas terrane OFB = Orós fold felt (1.8Ga); SFB = Seridó fold belt; GC = Granjeiro complex; SJCM = São José do Campestre massif; ZTD = Zona de Tranversal Domain; PABT = Piancó-Alto Brígida terrane; APT = Alto Pajeú terrane; AMT = Alto Moxoto terrane; RCT = Rio Capibaribe terrane; PAD = Pernambuco-Alagoas domain; SD = Sergipano domain and RPD = Riacho do Pontal domain. TL = Transbrasiliano lineament; SPL = Senador Pompeu lineament; PoSZ = Portalegre shear zone; PJCSZ = Picuí-João Câmara shear zone; PaL = Patos lineament; LPE = Pernambuco lineament. TC = Tróia complex; RTC = Riacho da Telha Complex; Li = Limoeiro (Ni-Cu-PGE); FC = Floresta complex and BSC = Brejo Seco Complex.

2.3 Material and Methods

2.3.1 Geological Mapping and Petrography

Detailed geological mapping (1: 25,000 scale) in the Lajes region from 2012 to 2015 occurred during the exploration program for iron ore. Geological interpretations were supported by geochemical and geophysical surveys, limited diamond drilling on iron ore targets and petrographic studies (22 thin-polished sections). The latter were developed in the Microscopy Laboratory of the Geoscience Institute of the University of Brasília (Brazil).

2.3.2 Mineral Chemistry

All mineral analyses were performed on polished thin sections using a fully automated SX-50 Electron Microprobe at the Geosciences Institute, University of Brasília (Brazil). Wavelength dispersive (WDS) analyses were performed at an accelerating voltage of 15 kV and a beam current of 25 nA. Background counting time was set to half of the peak counting time. Both synthetic and natural mineral Standards were used for the analyses and the same standards and procedure were retained throughout. Fe^{3+} contents were estimated using site and charge balance calculations on cation-normalized analyses (Droop, 1987). Systematic analyses of olivine (62 analyses), orthopyroxene (32 analyses), clinopyroxene (38), plagioclase (51 analyses) and amphiboles (78 analyses) were obtained from 16 representative samples from outcrops of the Lajes region intrusions.

2.3.3 Lithogeochemistry

Lithogeochemical analyses were performed in 18 representative samples of mafic-ultramafic rocks of Lajes-RN region. Sample preparation was accomplished at the Geochronology Laboratory of the University of Brasília. Analyses of major, minor and trace elements were carried out by ACME Analytical Laboratories Ltd (Vancouver - Canada) and a complete description of analytical methods is available in ACME home page (www.acmelab.com). The abundances major and minor elements were obtained by X-ray fluorescence (XRF) after fusion of the sample with lithium tetraborate. The abundances of major and trace elements were determined from melting 0.2g of the sample with lithium metaborate/tetraborate, diluted nitric acid

digestion and ICP-OES finish. The loss on ignition (LOI) was given by weight difference after fusion at 100° C. Precious metals and base metals were determined after 0.5 g of sample digestion with Acqua Regia with ICP-MS finish.

2.3.4 Sm-Nd isotopes

Sm–Nd isotopic analyses followed the method described by Gioia and Pimentel (2000) and were carried out at the Geochronology Laboratory of the University of Brasília. Whole-rock powders (~50 mg) of 11 representative samples of mafic-ultramafic rocks were mixed with ^{149}Sm–^{150}Nd spike solution and dissolved in Savillex capsules. Sm and Nd extraction of whole-rock samples followed conventional cation exchange techniques, with Teflon columns containing LN-Spec resin (HDEHP –diethylhexil phosphoric acid supported on PTFE powder). Sm and Nd samples were loaded on Re evaporation filaments of double filament assemblies, and the isotopic measurements were carried out on a multicollector Finnigan MAT 262 mass spectrometer in static mode. Uncertainties of Sm/Nd and $^{143}Nd/^{144}Nd$ ratios were better than ±0.1% (1σ) and ±0.0015% (1σ), respectively, according to repeated analyses of international rock standards BHVO-1 and BCR-1. $^{143}Nd/^{144}Nd$ ratios were normalized to $^{146}Nd/^{144}Nd$ 0.7219, and the decay constant used was (λ) 6.54 x 10^{-12}. The TDM values were calculated using DePaolo's (1981) model.

2.3.5 U-Pb isotopes

Mineral concentrates (zircon) were extracted from ca. 15 kg rock samples using conventional gravimetric and magnetic (Frantz isodynamic separator) techniques at the Geochronology Laboratory of the University of Brasília. Final purification was achieved by hand picking through a binocular microscope. For U–Pb analyses, fractions were dissolved in concentrated HF and HNO3 (HF:HNO3 = 4:1) using microcapsules in Parr-type bombs. A mixed ^{205}Pb–^{235}U spike was used. Chemical extraction followed a standard anion exchange technique, with Teflon microcolumns and following procedures modified from Bühn et al. (2009). Pb and U were loaded together onto single Re filaments with H3PO4 and silica gel, and isotopic analyses were carried out at the Geochronology Laboratory of the University of Brasília on a Finnigan MAT-262 multicollector mass spectrometer equipped with secondary electron multiplier ion counting. Procedure blanks for Pb, at the time of

analyses, were better than 20 pg. For correction of deviations the pattern GJ (Jackson et al., 2004) and 91500 (Wiedenbeck et al., 1995) were used. For data reduction and age calculation, PBDAT (Ludwig, 1993) and ISOPLOT-Ex (Ludwig, 2001) were used. Errors for isotopic ratios were 2σ.

2.4 Results

2.4.1 Local Geology

The geology of the region where mafic-ultramafic intrusions were identified is provided in Figure 3B. These intrusions are hosted by orthogneiss and migmatite of the paleoproterozoic Rio Piranhas terrain of the RGND (Fig. 2B and 3A). Orthogneiss close to the mafic-ultramafic intrusions are mainly medium-grained massive or banded gneiss with granoblastic texture. Gneissic rocks have darker bands with abundant biotite and hornblende, as well as minor associated augen gneiss with coarse-grained K-feldspar and migmatites. These rocks consist mainly of quartz, K-feldspar (perthitic microcline), plagioclase, biotite and hornblende. Frequent accessory minerals consist of titanite, magnetite, allanite and zircon. Minor amphibolite and supracrustal occur as up to several meters thick bands associated with orthogneiss. Metamorphic parageneses of banded orthogneiss, consisting of microcline-quartz-plagioclase-hornblende, indicate amphibolite facies of metamorphism associated. Minor retrometamorphic reactions are indicated by muscovite (after K-feldspar), chlorite (after biotite and hornblende) and epidote-group minerals (after plagioclase).

The mafic-ultramafic intrusions occur as small lensoid bodies (< 500 meters long) outcropping in a 32 km long NNE-SSW trend (Fig. 3B and 3C). This trend is parallel to Neoproterozoic (Brasiliano Cycle) steep dipping shear zones (55-80° W or E). These intrusions are characterized by medium- to coarse-grained texture, where primary magmatic features and igneous minerals are preserved, and medium-to fine-grained massive to foliated texture where metamorphic fabric and minerals prevail (Fig. 3C). These domains occur at the outcrop scale (i.e. few meters) up to intrusions (i.e. few hundred meters) consisting of a core with magmatic fabric and a transformed rim close to the contacts with host rocks (e.g. intrusion 3, Fig. 3C). The complete transition from magmatic to metamorphic fabric is reported in all of the investigated intrusions. The mafic-ultramafic rocks in the contact with host rocks have amphibolite

facies parageneses and prominent foliation parallel to the regional trend. Table 1 summarizes the petrographic features of the mafic-ultramafic intrusions.

Younger neoproterozoic metasediments of the Seridó Fold Belt (Fig. 3A) outcrop in the southeastern portion of the mapped area (Fig. 3B). These rocks occur in the Feiticeiro ridge and consist of interlayered quartzite, mica schist, marble and paragneiss with greenschist facies metamorphic assemblages (Archanjo and Salim, 1986; Carvalho, 1990). The metasedimentary rocks were thrusted westward over their basement paleoproterozoic terrane. Large neoproterozoic granitic plutons intrude both the paleoproterozoic terrane and Seridó Folded Belt in the south and southwest of the mapped area (Fig. 3B) (Hollanda et al., 2003; Nascimento et al., 2008; 2014). Phanerozoic mafic magmatism is indicated in the mapped area by tholeitiic dykes from two distinct magmatic events associated with the Atlantic rift (143 Ma and 126-113 Ma; Araújo et al., 2001) and alkaline dykes and volcanic necks (26 Ma; Araújo et al., 2001; Silveira, 2006; Knesel et al., 2011). The latter is illustrated by the Cabugi peak volcanic neck (Fig. 3B).

Table 1. Petrographic and mineralogical characteristics of mafic-ultramafic intrusions. Mineral abbreviations follow Whitney and Evans (2010).

Intrusion	extension	Rock	Cumulus mineral	Intercumulus mineral	Recrystallized and alteration mineral	Sulfide
1	250 x 80 m	Clinopyroxenite	Cpx + Chr		Tr + Act + Mag + Srp + Tlc + Chl	
2	500 x 120m 400 x 80m	Wehrlite and hornblendite	Ol + Chr+ Cpx	Opx + Pl	Mg-Hbl + Mg-Hst + Ts + Ep Mag + Srp + Tlc + Chl	Py + Po + Pn
3	200 x 120m	Clinopyroxenite and hornblendite	Cpx		Mg-Hbl + Mg-Hst + Ts + Act + Cum + Mag + Srp + Tlc + Chl	
4	250 x 60m	Troctolite and tschermakite	Ol + Pl	Cpx	Ts + Mg-Hst + Mg-Hbl + Mag	Py + Po + Ccp + Pn

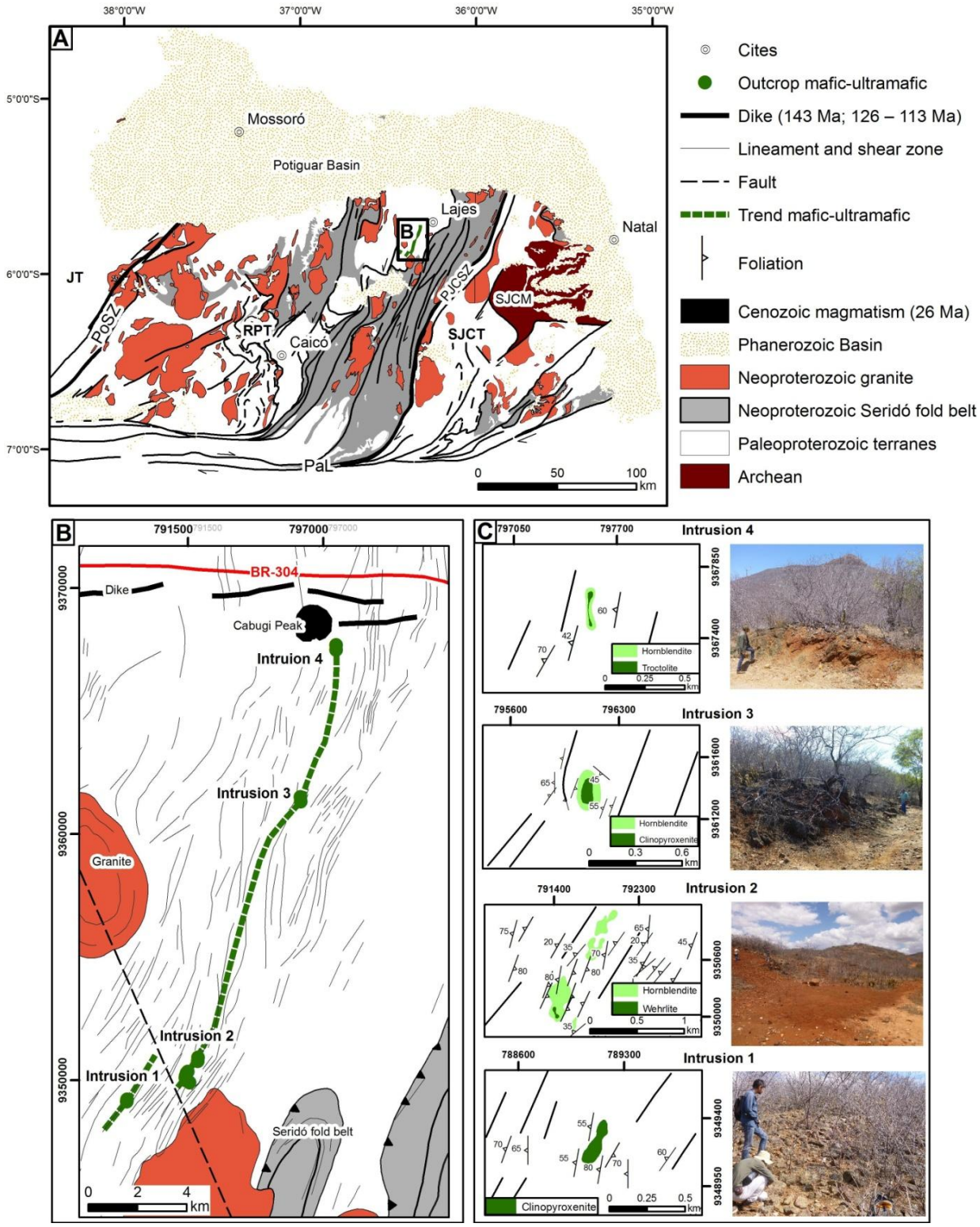

Figure 3. A) Geological framework of the Rio Grande do Norte Domain (modified after Jardim de Sá, 1994 and Angelim et al., 2006). SJCM = São José de Campestre massif; SJCT = São José de Campestre terrane; PJCSZ = Picuí-João Câmara shear zone, RPT = Rio Piranhas terrane; PaSZ = Portalegre Shear Zone. B) Local geological map. C) Geological map and photos of the mafic-ultramafic intrusions and adjacent host rocks.

2.4.1.1 Intrusion 1

This ~ 300 meters long ultramafic body follow the NNE-SSW orientation of the host orthogneiss (Fig. 3C). The intrusion is located close to the São José da Passagem village and consists mainly of massive tremolitite with variable proportions of chlorite, talc, serpentine and magnetite. Primary coarse-grained magmatic texture is preserved in the central portion of the intrusion, where oikocrysts (up to few centimeters) of Cpx (extensively replaced by tremolite/actinolite) are associated with medium-grained olivine pseudomorphs (replaced by fine-grained aggregates of serpentine, chlorite and magnetite) and tiny euhedral chromite (highly replaced by magnetite). Coarse-grained rocks with large Cpx pseudomorphs predominate in the core of the body, whereas highly transformed fine-grained tremolitite predominate in the outer contact of the intrusion. Intrusion 1 is interpreted to result of extensive replacement of wehrlite and olivine clinopyroxenite. Host rocks are foliated (Sn+1 55/285 to 80/270) orthogneiss.

2.4.1.2 Intrusion 2

Intrusion 2 consists of a ~ 1,000 meters long cluster of irregular ultramafic bodies (Fig. 3C). This intrusion, located close to the Pedra Branca village, is subdivided into a southern body and a northern body (Fig. 3C, Table 1), possibly as the result of tectonic fragmentation of an originally larger intrusion. Both bodies form lensoid structures following the NNE-SSW foliation of the host gneiss. The southern body consists of domains of wehrlite with primary igneous fabric and domains of amphibole-rich rocks where primary features are just eventually preserved. Wehrlite is a coarse- to medium-grained mesocumulate rock consisting mainly of cumulus olivine and clinopyroxene (Fig. 4 D-E-F), and variable proportions of intercumulus orthopyroxene and plagioclase. Cumulus chromite occurs as accessory tiny euhedral crystals (up to 1 vol %). Amphibole-rich rocks (hornblendite) are fine- to medium-grained granoblastic rocks consisting mainly of hornblende associated with variable proportions of chlorite, talc, serpentine and magnetite. The transition from wehrlite to massive or foliated hornblendite is frequent in the southern body. In partialy transformed rocks, interstitial plagioclase is partially to completely replaced by a chlorite and talc rich aggregate (Fig. 4 F-G-H). Along discrete shear zones wehrlite and hornblendite are replaced by a fine-grained aggregate of low temperature minerals consisting of serpentine, chlorite, talc, carbonate and vermiculate. The

northern body consists mainly of amphibole-rich rocks (hornblendite) similar to those described for the southern body. Primary igneous minerals in the northern body are restricted to extensively replaced Cpx crystals and accessory chromite partially replaced by magnetite. Hornblendite of the southern and northern bodies have chemical composition similar to wehrlite (see lithogeochemistry in the following section), thus supporting the interpretation that all hornblendites are transformed wehrlite. Host rocks are foliated (Sn+1 35/280 to 80/100) orthogneiss.

2.4.1.3 Intrusion 3

This ~ 300 meters long ultramafic body follows the NNE-SSW orientation of the host rocks (Fig. 3C). The intrusion, located close to the Cacimba de Cima ranch, is hosted by augen orthogneisses and migmatites, with minor associated magnetite-biotite gneiss, biotite schist and turmalinites (possibly metasediments). Intrusion 3 consists mainly of coarse-grained clinopyroxenite and chlorite-diopside hornblendite (Table 1). Clinopyroxenite has adcumulate primary texture but magmatic minerals (Cpx and chromite) are extensively replaced. Bands of coarse-grained clinopyroxenite are eventually preserved within domains of foliated fine-grained diopside hornblendite (Fig. 4 J) with granoblastic texture (Fig. 4 K-L).

2.4.1.4 Intrusion 4

This ~ 200 meters long mafic body follows the NNE-SSW orientation of host biotite gneiss (Fig. 3C). The intrusion, located close to the Cabugi peak, consists mainly of troctolite and hornblendite (Table 1). The troctolite has medium-grained mesocumulate primary texture (Fig. 4 M-N-O) consisting of cumulus olivine and plagioclase with variable amounts of intercumulus clinopyroxene. Reaction coronae are developed in the contact of olivine and plagioclase, consisting of one layer lamellar orthopyroxene (close to olivine) and another of symplectitic intergrowth of clinopyroxene and spinel (adjacent to plagioclase). Disseminated sulfides (up to 1 vol %) were identified in samples of troctolite. Sulfides are interstitial to cumulus minerals and consist of fine-grained aggregates of pyrrhotite, pentlandite and chalcopyrite. pentlandite also occurs as exsolution flames in pyrrhotite crystals. Blocks and boulders of hornblendite closely associated with troctolite in Intrusion 4 are interpreted as highly transformed troctolites. These rocks consist of medium- to fine-grained of hornblende, chlorite and magnetite.

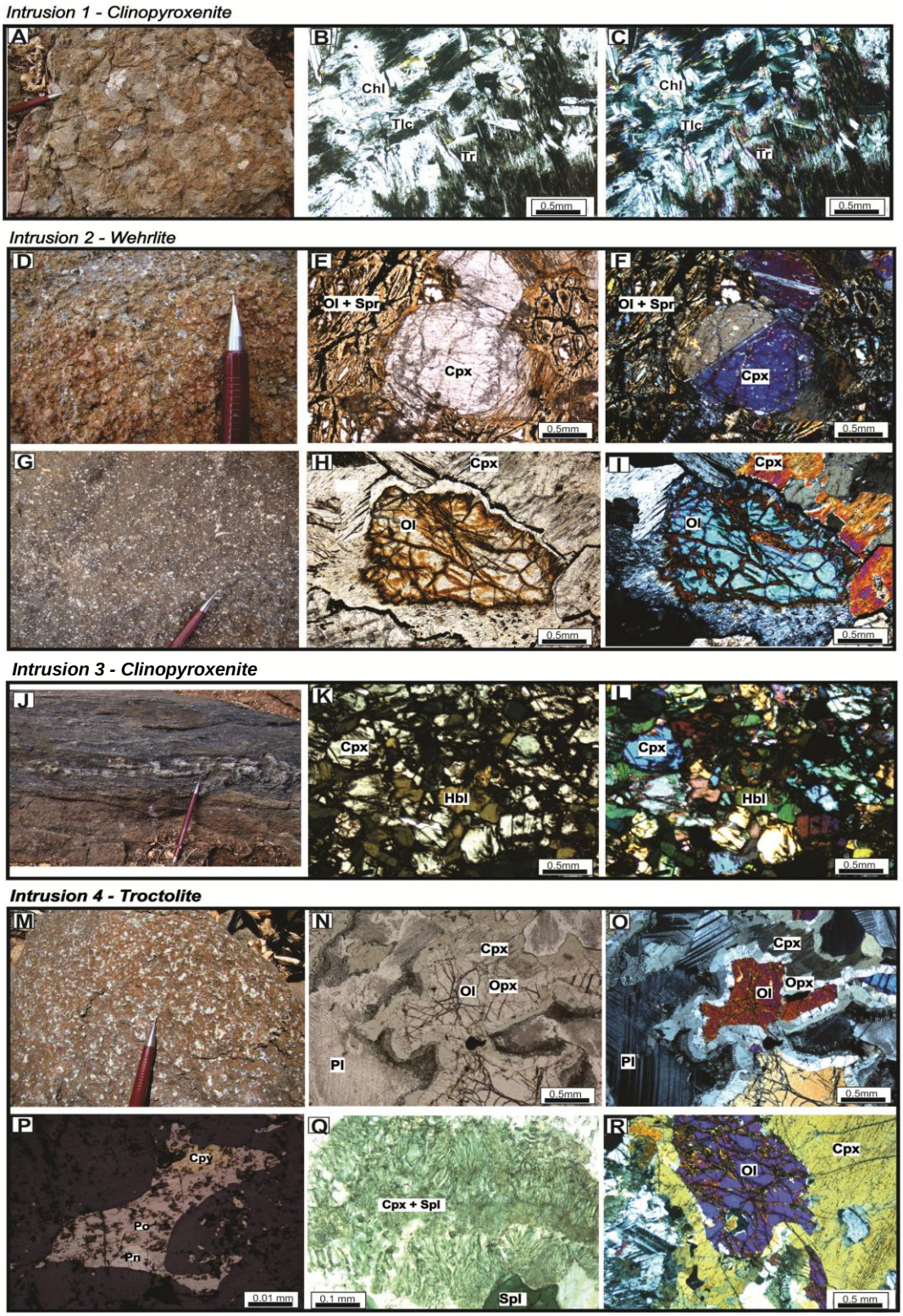

Figure 4. Petrographic features of typical mafic-ultramafic rocks. A) Clinopyroxenite with coarse-grained adcumulate texture. B-C) Photomicrograph of clinopyroxenite with tremolite, actinolite and talc. D) Medium-grained wehrlite. E-F) Photomicrograph of wehrlite with cumulus olivine (partially replaced by serpentine and magnetite) and twinned Cpx. G) Wehrlite with interstitial (intercumulus) plagioclase (white color). H-I) Photomicrograph of partially replaced wehrlite. J) Domain of massive coarse-grained clinopyroxenite within medium-grained diopside hornblendite. K-L) Photomicrograph of diopside hornblendite with granoblastic texture. M) Partially weathered surface of troctolite. N-O) Photomicrograph of cumulus olivine and plagioclase in troctolite. Note intercumulus Cpx and reaction coronae. P) Photomicrograph of interstitial sulfide in wehrlite. Q) symplectitic intergrowth of clinopyroxene and spinel. R) Photomicrograph of cumulus olivine and Cpx.

2.4.2 Mineral chemistry

Systematic electron microprobe analyses of olivine, clinopyroxene, orthopyroxene and plagioclase were performed in unweathered samples of mafic-ultramafic rocks with primary magmatic minerals and texture. Additional systematic analyses of amphiboles were performed in partially to extensively transformed samples. Few analyses of spinel, chromite, sulfides, chlorite and micas were performed to support the petrographic descriptions.

Olivine compositions were obtained in four samples of wehrlite from Intrusion 2 and two samples of troctolite from Intrusion 4 (see Table 2 for representative analyses). Olivine in Intrusion 2 range from $Fo_{80.6}$ to $Fo_{68.2}$ with Ni contents ranging from ~ 2000-500 ppm; whereas olivine in Intrusion 4 range from $Fo_{69.9}$ to $Fo_{67.6}$ with Ni contents ranging from ~ 1300-100 ppm (Fig. 5). Olivine compositions range from moderately primitive to fractionated in Intrusion 2 but has a narrow range of fractionated compositions in Intrusion 4.

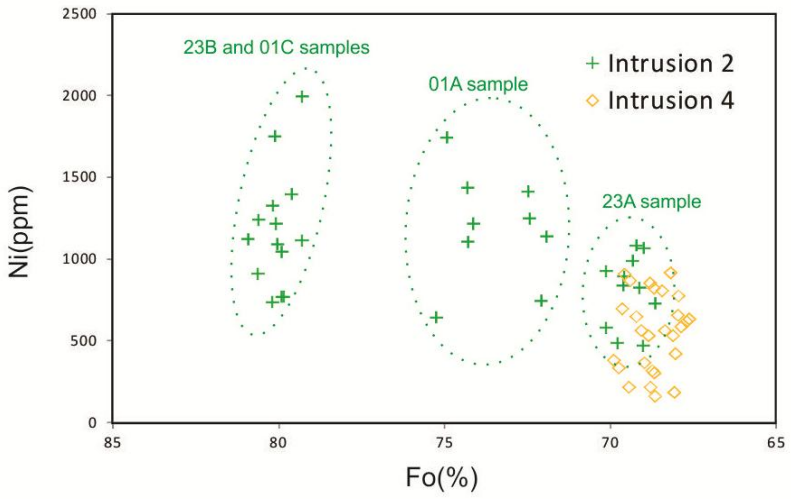

Figure 5. Plot of Fo vs Ni content of olivine (n=62).

Table 2.Representative analyses of olivine.

	Intrusion 2												Intrusion 4					
Rock	Wehrlite												Troctolite					
Sample	A-01C	A-01C	A-01C	A-01A	A-01A	A-01A	A-23B	A-23B	A-23B	A-23A	A-23A	A-23A	A-38D	A-38D	A-38D	A-38B	A-38B	A-38B
SiO_2	38.293	37.953	38.321	37.424	37.135	38.034	38.883	38.610	38.725	36.856	36.994	36.577	36.594	36.790	36.911	37.727	37.373	37.157
Al_2O_3	0.000	0.001	0.017	0.000	0.000	0.007	0.013	0.009	0.000	0.012	0.003	0.356	0.000	0.043	0.003	0.007	0.000	0.021
Cr_2O_3	0.052	0.000	0.092	0.001	0.000	0.001	0.067	0.000	0.053	0.063	0.038	0.089	0.000	0.059	0.000	0.000	0.000	0.023
MgO	42.041	41.855	42.849	36.654	36.681	38.498	43.127	42.220	42.484	34.878	35.577	35.384	35.265	35.454	34.790	33.953	33.794	33.887
MnO	0.315	0.327	0.268	0.532	0.610	0.444	0.231	0.241	0.260	0.353	0.456	0.476	0.342	0.282	0.235	0.222	0.137	0.328
FeO	19.557	19.104	18.372	25.298	26.266	22.958	18.470	18.921	18.828	27.765	27.003	26.867	27.384	27.395	27.565	28.367	28.505	28.362
NiO	0.142	0.178	0.158	0.095	0.215	0.222	0.116	0.133	0.155	0.105	0.074	0.118	0.089	0.043	0.083	0.024	0.075	0.162
Total	100.40	99.42	100.08	100.00	100.91	100.16	100.91	100.13	100.51	100.03	100.15	99.87	99.67	100.07	99.59	100.30	99.88	99.94
Si	0.9751	0.9749	0.9739	0.9867	0.9732	0.9901	0.9797	0.9829	0.9829	0.9820	0.9810	0.9725	0.9762	0.9753	0.9865	1.0077	1.0027	0.9965
Al	0.0000	0.0000	0.0005	0.0000	0.0000	0.0002	0.0004	0.0003	0.0000	0.0004	0.0001	0.0112	0.0000	0.0013	0.0001	0.0002	0.0000	0.0007
Cr	0.0010	0.0000	0.0018	0.0000	0.0000	0.0000	0.0013	0.0000	0.0011	0.0013	0.0008	0.0019	0.0000	0.0012	0.0000	0.0000	0.0000	0.0005
Mg	1.5960	1.6027	1.6235	1.4407	1.4331	1.4940	1.6200	1.6024	1.6076	1.3853	1.4065	1.4025	1.4025	1.4012	1.3861	1.3520	1.3517	1.3549
Mn	0.0068	0.0071	0.0058	0.0119	0.0135	0.0098	0.0049	0.0052	0.0056	0.0080	0.0102	0.0107	0.0077	0.0063	0.0053	0.0050	0.0031	0.0074
Fe^{2+}	0.4165	0.4104	0.3905	0.5578	0.5756	0.4998	0.3892	0.4028	0.3997	0.6186	0.5988	0.5974	0.6109	0.6074	0.6161	0.6337	0.6396	0.6361
Ni	0.0029	0.0037	0.0032	0.0020	0.0045	0.0046	0.0024	0.0027	0.0032	0.0023	0.0016	0.0025	0.0019	0.0009	0.0018	0.0005	0.0016	0.0035
Total	2.9983	2.9988	2.9992	2.9992	2.9999	2.9986	2.9979	2.9963	3.0000	2.9979	2.9990	2.9986	2.9993	2.9937	2.9959	2.9992	2.9987	2.9996
Fo	79.30	79.62	80.61	72.09	71.34	74.93	80.63	79.91	80.09	69.13	70.14	70.13	69.66	69.76	69.23	68.09	67.88	68.05

Cpx compositions were obtained in two samples of wehrlite from Intrusion 2, one sample of diopside hornblendite from Intrusion 3 and one sample of troctolite from Intrusion 4 (see Table 3 for representative analyses). Compositions of cumulus Cpx (see Fig. 4E and 4F) in wehrlite from intrusion 2 have higher En content (49-44 %) and higher TiO_2, Cr_2O_3 and Al_2O_3 contents compared with granoblastic metamorphic diopside (see Fig. 4K and 4L) in Intrusion 2 (En 34-36 %). Compositions of intercumulus Cpx in troctolite from Intrusion 4 have En content ranging from 44-46 % and very low Cr_2O_3 contents (< 0.01 wt. %). Cpx compositions highlight chemical differences of cumulus Cpx from moderately primitive wehrlite, intercumulus Cpx of fractionated troctolite and metamorphic diopside from extensively recristallized wehrlite (Fig. 6).

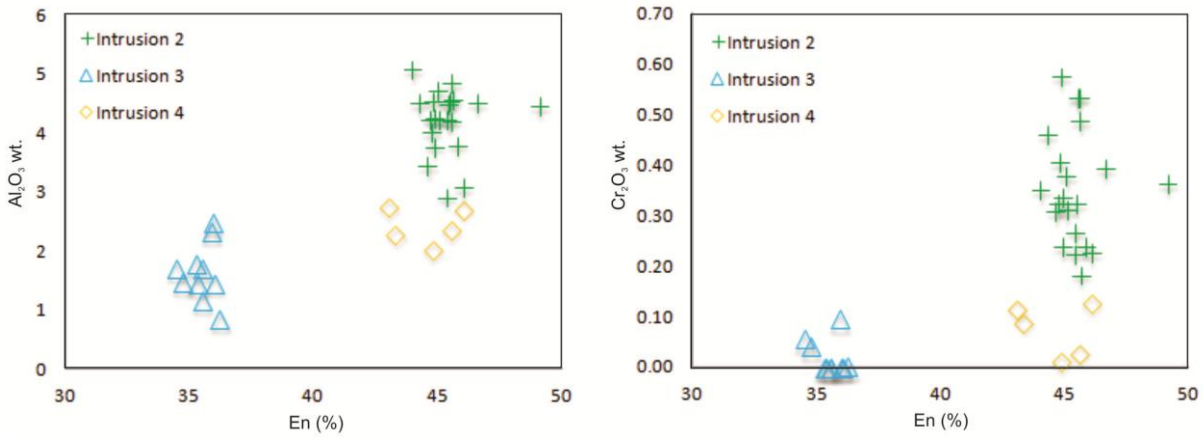

Figure 6. Plot of En vs Al2O3 and En vs Cr2O3 content of Cpx (n=38).

Opx compositions were obtained in two samples of wehrlite from Intrusion 2 and two samples of troctolite from Intrusion 4 (see Table 3 for representative analyses). Opx occurs as an intercumulus mineral in Intrusion 2 with En content ranging from 80.1-81.6 %. In Intrusion 4 Opx occurs as a subsolidus mineral formed from reaction of cumulus olivine and plagioclase. They have En content in the range of 72.3-75.1 %.

Table 3: Representative analyses of Cpx and Opx.

	Intrusion 2					Intrusion 3				Intrusion 4			
Rock	Wehrlite					Clinopyroxenite				Troctolite			
Sample	A-01C	A-01C	A-01C	A-23B	A-23B	A-44	A-44	A-44	A-44	A-38B	A-38B	A-38B	A-38D
SiO_2	51.0230	50.3850	53.8350	51.4790	55.0440	51.5050	51.9820	51.9290	51.5380	52.7840	52.4770	53.5730	53.3180
TiO_2	0.4420	0.4630	0.0950	0.1910	0.0000	0.0870	0.0000	0.0680	0.1580	0.1890	0.1990	0.0000	0.0560
Al_2O_3	4.4570	4.2360	2.9710	4.5490	0.7380	1.4690	1.7990	0.8620	1.4860	2.7510	2.2860	2.5080	1.8890
Cr_2O_3	0.3630	0.3230	0.0860	0.5740	0.0750	0.0000	0.0000	0.0010	0.0410	0.1170	0.0900	0.0000	0.0350
MgO	17.1500	15.5090	29.6900	15.3640	31.3250	12.4780	11.9800	12.7170	11.9480	15.2230	15.3030	26.1290	27.3670
CaO	21.0430	23.3780	0.1890	22.8230	0.1900	23.5650	22.9240	23.7300	23.6130	23.7770	23.5580	0.2930	0.2540
MnO	0.1330	0.1270	0.1840	0.1170	0.2170	1.0310	0.7190	0.8150	0.8700	0.1260	0.0500	0.1380	0.2890
FeO	4.7180	4.2270	11.9630	4.4930	12.3080	9.3610	9.8550	9.5260	9.8600	5.4500	5.5270	16.8180	16.3010
NiO	0.0000	0.0000	0.0500	0.0410	0.0020	0.0000	0.0620	0.0000	0.0350	0.0660	0.0000	0.0920	0.0600
Na2O	0.1640	0.2430	0.0230	0.2800	0.0000	0.5010	0.6520	0.4280	0.5920	0.2900	0.2110	0.0000	0.0300
Total	99.49	98.89	99.09	99.91	99.90	100.00	99.97	100.08	100.14	100.77	99.70	99.55	99.60
Si	1.8655	1.8616	1.9193	1.8849	1.9424	1.9284	1.9484	1.9431	1.9319	1.9245	1.9338	1.9472	1.9266
Ti	0.0122	0.0129	0.0025	0.0053	0.0000	0.0025	0.0000	0.0019	0.0045	0.0052	0.0055	0.0000	0.0015
Al	0.1920	0.1844	0.0807	0.1963	0.0307	0.0648	0.0795	0.0380	0.0656	0.1182	0.0993	0.0528	0.0734
Cr	0.0105	0.0094	0.0024	0.0166	0.0021	0.0000	0.0000	0.0000	0.0012	0.0034	0.0026	0.0000	0.0010
Mg	0.9348	0.8543	1.5780	0.8387	1.6479	0.6965	0.6694	0.7094	0.6677	0.8275	0.8407	1.4158	1.4743
Ca	0.8242	0.9254	0.0072	0.8953	0.0072	0.9452	0.9205	0.9513	0.9483	0.9288	0.9301	0.0114	0.0098
Mn	0.0041	0.0040	0.0056	0.0036	0.0065	0.0184	0.0228	0.0177	0.0087	0.0039	0.0016	0.0042	0.0088
Fe^{2+}	0.0912	0.0532	0.3264	0.0812	0.2807	0.0000	0.0093	0.0000	0.0000	0.0469	0.0533	0.5112	0.4293
Ni	0.0000	0.0000	0.0014	0.0012	0.0001	0.0000	0.0019	0.0000	0.0011	0.0019	0.0000	0.0027	0.0017
Na	0.0116	0.0174	0.0016	0.0199	0.0000	0.0364	0.0474	0.0310	0.0430	0.0205	0.0151	0.0000	0.0021
Total	3.9462	3.9226	3.9253	3.9429	3.9175	3.6922	3.6992	3.6924	3.6720	3.8807	3.8820	3.9454	3.9286
%Wo	43.31	48.44	0.37	47.84	0.36	48.85	48.48	48.56	49.26	48.31	47.91	0.59	0.50
%En	49.11	44.72	81.26	44.81	81.65	36.00	35.25	36.22	34.68	43.04	43.31	73.04	74.58
%Fs	7.58	6.84	18.37	7.35	18.00	15.15	16.27	15.22	16.06	8.64	8.78	26.37	24.92
Mineral	Aug	Di	En	Di	En	Di	Di	Di	Di	Di	Di	En	En

Plagioclase compositions were obtained in two samples of troctolite from Intrusion 4 (see Table 4 for representative analyses). Plagioclase crystals are well preserved (e.g. Fig. 4N and 4O) except for minor but widespread saussuritization, as indicated by tiny inclusions of zoisite. Analyses of plagioclase which partially incorporated zoisite crystals, characterized by higher CaO contents and An values, were disregarded. Plagioclase compositions are similar in both samples and have An content in the range of 79.9-89.0 %.

Table 4. Representative analyses of plagioclase.

					Intrusion 4					
Rock					Troctolite					
Sample	38D	A-38B	A-38B	A-38B	38B	A-38D	38D	38D	38D	38D
Na_2O	2.20	2.10	1.64	1.85	1.11	1.91	2.21	2.05	1.62	1.49
K_2O	0.03	0.02	0.01	0.02	0.03	0.02	0.03	0.06	0.03	0.04
SiO_2	46.78	46.20	46.28	45.88	44.88	46.47	46.82	46.88	45.93	45.43
Al_2O_3	34.00	33.72	33.94	34.40	34.42	33.29	33.03	33.38	34.02	34.59
FeO	0.08	0.08	0.03	0.05	0.08	0.02	0.11	0.07	0.05	0.05
CaO	15.98	16.08	17.06	16.34	18.37	16.47	16.65	16.84	17.27	18.05
Total	99.07	98.18	98.95	98.54	98.90	98.18	98.85	99.26	98.93	99.65
Na	0.197	0.189	0.147	0.166	0.100	0.172	0.198	0.183	0.146	0.133
K	0.002	0.001	0.001	0.001	0.002	0.001	0.002	0.003	0.002	0.002
Si	2.156	2.149	2.144	2.131	2.086	2.166	2.165	2.161	2.129	2.090
Al	1.846	1.849	1.853	1.883	1.885	1.829	1.800	1.813	1.858	1.875
Fe^{2+}	0.000	0.000	0.000	0.000	0.000	0.000	0.000	0.000	0.000	0.000
Ca	0.789	0.802	0.847	0.813	0.915	0.823	0.825	0.831	0.858	0.890
Total	4.990	4.990	4.992	4.994	4.988	4.991	4.991	4.991	4.992	4.991
% An	79.90	80.84	85.14	82.90	89.94	82.58	80.46	81.68	85.32	86.79

Amphibole compositions were obtained in fourteen samples from all four investigated intrusions (see Table 5 for representative analyses). These samples include foliated fine- to medium-grained hornblendite and diopside hornblendite with granoblastic texture (e.g., Fig. 4 K-L), troctolite with intercumulus Cpx and minor amphibole, as well as fine-grained tremolitite consisting of aggregates of colorless amphibole and variable proportions of serpentine, chlorite and magnetite (e.g., Fig. 4B and 4C). These rocks have Ca-amphiboles with highly variable compositions that fit into three major groups (see Fig. 7, Fig. 8 and Table 5 for normalization parameters and representative analyses). Tremolite occurs is samples with low temperature assemblages (i.e., serpentine, chlorite, talc) and is indicated by $Al^{+4} < 0.1$ and $Na^{+} < 0.3$. Mg-hastingsite is characteristic of late-magmatic interstitial amphibole in troctolite with igneous mineralogy and texture, indicated by high

contents of Al^{+4} (1.81-2.04) and Na^{+} (0.61-0.77). Amphibole in metamorphic rocks with granoblastic textures and amphibolite facies mineral assemblages (e.g., hornblende + plagioclase; Cpx + hornblende) have variable compositions including Mg-hornblende, Mg-hastingite and tschermakite. These amphiboles have highly variable Al^{+4} (0.56-1.88) and Na^{+} (0.15-0.60) contents, as well as Mg and Fe contents.

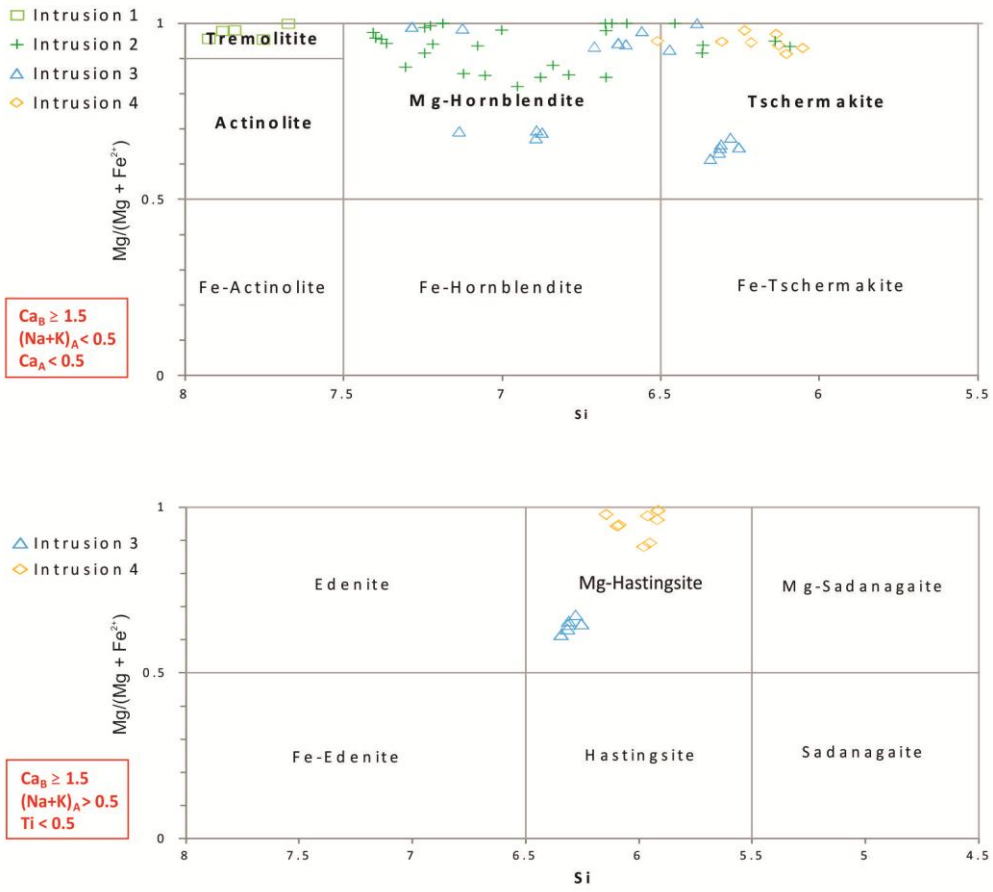

Figure 7. Classification of amphiboles (n=78). Based on Leake et al. (1997).

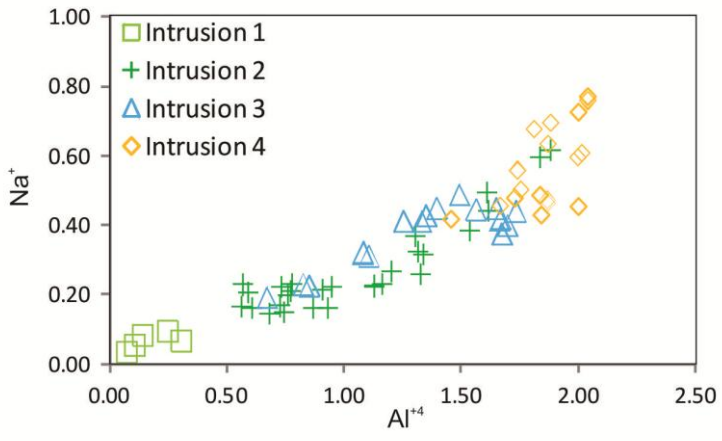

Figure 8. Plot of Al^{+4} and Na^{+} for amphiboles (n=78). See Table 5 for normalization parameters.

Table 5. Representative analyses of amphiboles.

	Intrusion 1		Intrusion 2						Intrusion 3				Intrusion 4			
Rock	Clinopyroxenite		Wehrlite			Hornblendite			Clinopyroxenite		Hornblendite		Troctolite		Hornblendite	
Sample	A-19	A-19	A-01A	A-01B	A-23A	A-22	A-25	A-26	A-44C	A-44C	A-44	A-44	A-38B	A-38D	A-38E	A-38E
SiO_2	58.02	57.30	44.24	50.33	53.54	51.40	52.17	52.37	46.64	50.92	41.76	42.62	41.65	43.01	43.37	42.48
TiO_2	0.00	0.19	0.12	0.50	0.06	0.36	0.30	0.28	0.18	0.03	0.45	0.49	0.63	0.07	0.38	0.80
Al_2O_3	0.98	1.54	12.57	7.23	4.54	4.81	5.53	5.04	10.17	6.22	11.14	11.38	15.51	14.40	13.81	14.16
FeO	2.50	2.90	8.93	8.46	5.10	7.74	6.29	6.35	9.07	7.82	17.30	17.05	8.40	9.13	9.44	10.05
MnO	0.14	0.30	0.05	0.13	0.06	0.15	0.07	0.11	0.20	0.18	0.56	0.70	0.04	0.04	0.15	0.20
MgO	23.99	23.81	15.83	18.25	20.53	18.91	20.34	19.98	16.68	18.69	11.11	11.07	15.58	15.60	15.19	14.79
CaO	12.43	12.47	12.31	11.64	12.81	12.85	12.26	12.61	12.04	11.98	12.09	11.85	11.78	11.64	12.01	12.08
Na_2O	0.33	0.37	1.77	0.82	0.78	0.55	0.86	0.63	1.48	0.85	1.52	1.44	2.60	2.43	1.81	1.69
K_2O	0.04	0.05	0.46	0.12	0.13	0.25	0.17	0.12	0.26	0.15	1.48	1.48	0.33	0.09	0.20	0.71
Cl	0.00	0.02	0.20	0.06	0.02	0.03	0.04	0.02	0.04	0.02	0.07	0.04	0.03	0.03	0.14	0.08
Cr_2O_3	0.01	0.03	0.00	0.10	0.43	0.00	0.00	0.21	0.00	0.05	0.00	0.03	0.05	0.00	0.10	0.00
V_2O_3	0.00	0.00	0.00	0.00	0.02	0.09	0.01	0.00	0.00	0.02	0.05	0.01	0.05	0.00	0.03	0.06
NiO	0.05	0.06	0.04	0.04	0.09	0.04	0.05	0.08	0.00	0.02	0.00	0.00	0.00	0.00	0.00	0.00
SrO	0.01	0.01	0.07	0.00	0.25	0.04	0.00	0.00	0.01	0.04	0.02	0.00	0.00	0.00	0.00	0.00
Total	98.49	99.03	96.58	97.67	98.34	97.22	98.08	97.82	96.76	96.97	97.55	98.15	96.65	96.44	96.61	97.08
Si	7.859	7.753	6.392	7.056	7.409	7.260	7.226	7.277	6.672	7.176	6.269	6.338	6.004	6.193	6.250	6.136
Al^{+4}	0.141	0.246	1.608	0.944	0.591	0.740	0.774	0.723	1.328	0.824	1.731	1.662	1.996	1.807	1.750	1.864
Total	8	8	8	8	8	8	8	8	8	8	8	8	8	8	8	8
Al^{+3}	0.016	0.000	0.532	0.250	0.150	0.061	0.127	0.103	0.386	0.208	0.239	0.332	0.639	0.635	0.595	0.546
Ti	0.000	0.018	0.013	0.052	0.006	0.038	0.031	0.029	0.019	0.003	0.051	0.054	0.068	0.007	0.041	0.086
Fe^{3+}	0.090	0.101	0.609	0.570	0.221	0.460	0.488	0.482	0.619	0.546	0.732	0.651	0.624	0.687	0.707	0.694
V	0.000	0.000	0.000	0.000	0.002	0.010	0.001	0.000	0.000	0.002	0.006	0.002	0.006	0.000	0.003	0.006
Cr	0.001	0.003	0.000	0.011	0.047	0.000	0.000	0.024	0.000	0.006	0.000	0.003	0.006	0.000	0.012	0.000
Mg	4.844	4.804	3.410	3.814	4.235	3.981	4.200	4.140	3.557	3.926	2.486	2.453	3.348	3.349	3.262	3.184
Ni	0.006	0.006	0.005	0.005	0.010	0.004	0.006	0.009	0.000	0.003	0.000	0.000	0.000	0.000	0.000	0.000

	Intrusion 1		Intrusion 2						Intrusion 3				Intrusion 4			
Rock	Clinopyroxenite		Wehrlite			Hornblendite			Clinopyroxenite		Hornblendite		Troctolite		Hornblendite	
Sample	A-19	A-19	A-01A	A-01B	A-23A	A-22	A-25	A-26	A-44C	A-44C	A-44	A-44	A-38B	A-38D	A-38E	A-38E
Fe^{2+}	0.043	0.068	0.432	0.297	0.329	0.447	0.147	0.213	0.419	0.307	1.440	1.469	0.309	0.321	0.380	0.482
Mn	0.000	0.000	0.000	0.000	0.000	0.000	0.000	0.000	0.000	0.000	0.045	0.035	0.000	0.000	0.000	0.000
Total	5.000	5.000	5.000	5.000	5.000	5.000	5.000	5.000	5.000	5.000	5.000	5.000	5.000	5.000	5.000	5.000
Ca	1.804	1.806	1.905	1.748	1.899	1.945	1.820	1.878	1.845	1.808	1.944	1.888	1.819	1.796	1.854	1.868
Na	0.086	0.096	0.494	0.224	0.209	0.151	0.231	0.170	0.412	0.232	0.441	0.415	0.727	0.677	0.505	0.474
K	0.007	0.009	0.085	0.021	0.022	0.044	0.030	0.021	0.047	0.026	0.284	0.281	0.060	0.017	0.036	0.130
Total	1.896	1.911	2.484	1.993	2.130	2.140	2.080	2.069	2.304	2.066	2.669	2.584	2.606	2.490	2.395	2.473
Mineral	Tr	Tr	Ts	Mg-Hbl	Mg-Hbl	Mg-Hbl	Mg-Hbl	Mg-Hbl	Mg-Hbl	Mg-Hbl	Mg-Hst	Mg-Hst	Mg-Hst	Mg-Hst	Ts	Ts

2.4.3 Lithogeochemistry

2.4.3.1 Major and minor elements

Whole-rock chemical compositions of representative samples of the investigated mafic-ultramafic rocks are listed in Table 6. Variable amounts of loss on ignition reflect the degree of alteration and/or different alteration minerals for distinct rock types. Hence, in the following discussion and diagrams, major and minor elements will be quoted as weight percent oxide from analyses (see Table 6) normalized to 100% on an anhydrous basis. The plot of major element oxides against MgO (Fig. 9) suggests that bulk compositions are mainly controlled by different amounts of olivine, clinopyroxene and plagioclase in the original igneous rock. This suggestion is supported by comparing major element compositions with the composition of cumulus minerals described in the previous section (Fig. 9). Rocks from intrusions 1, 2 and 3 have compositions consistent with variable proportions of cumulus olivine and clinopyroxene and minor intercumulus plagioclase, as indicated by petrographic features. Rocks from Intrusion 4 have compositions consistent with variable proportions of cumulus olivine and plagioclase and abundant intercumulus clinopyroxene, as also indicated by petrographic features described in these samples. Chemical compositions of samples where primary igneous minerals and textures are preserved are similar to highly transformed samples from the same intrusion, thus supporting that the metamorphic recrystallization did not promoted a significant change in major element composition.

Cr_2O_3 contents for mafic-ultramafic rocks from Intrusion 1 (up to 0.47 wt. %) and Intrusion 2 (up to 0.38 wt. %) are higher than contents for mafic-ultramafic rocks from intrusions 3 and 4 (< 0.02 wt. %) (Table 6; Fig. 9). These results are consistent with the occurrence of relicts of cumulus chromite just in wehrlite and clinopyroxenite from intrusions 1 and 2. Distinct contents for Cr_2O_3 and Mg# (Table 6) are consistent with intrusions located in the south (Intrusions 1 and 2) crystallized from relatively primitive (Mg# between 73.3 and 80.5) chromite saturated magmas, while intrusions located in the north crystallized from more fractionated magmas (Mg# between 57.0 and 68.7).

Table 6. Chemical composition of mafic-ultramafic rocks.

		Intrusion 1		Intrusion 2									Intrusion 3		Intrusion 4		
Rock		Clinopyroxenite		Wehrlite					Hornblendite				Clinopyroxenite		Troctolite	Hornblendite	
Sample		A-19A	A-19B	A-01A	A-23A	A-23B	A-24A	A-24B	A-21	A-22	A-25	A-26	A-44A	A-44B	A-38B	A-38A	A-38C
SiO_2	wt. %	45.50	45.05	43.37	43.47	42.47	46.89	49.34	51.27	51.57	48.02	50.25	41.58	35.54	42.34	40.63	40.05
Al_2O_3		6.57	6.39	9.10	7.66	8.57	7.67	6.90	7.50	5.07	7.26	6.86	9.83	9.78	14.53	11.99	12.53
Fe_2O_3		11.04	10.91	13.12	12.65	11.25	9.22	9.17	9.04	7.51	10.12	8.60	17.43	24.66	15.21	16.01	15.93
MnO		0.20	0.16	0.16	0.19	0.16	0.12	0.16	0.15	0.18	0.16	0.13	0.19	0.19	0.16	0.16	0.17
MgO		23.96	25.24	20.29	23.12	21.29	21.18	14.57	14.14	17.31	23.39	18.08	21.50	18.34	17.66	19.18	18.20
CaO		4.08	3.77	7.60	6.92	8.27	8.49	13.37	14.00	14.37	4.15	11.59	3.03	3.95	8.18	5.91	6.13
Na_2O		0.14	0.12	0.63	0.46	0.56	0.40	0.42	0.69	0.47	0.15	0.76	0.23	0.33	0.78	0.64	0.66
K_2O		0.05	0.02	0.14	0.09	0.06	0.05	0.30	0.22	0.29	0.02	0.14	0.04	0.05	0.06	0.07	0.16
P_2O_5		0.06	0.17	<0.01	<0.01	<0.01	0.04	0.07	0.09	0.02	0.02	0.01	0.01	0.02	<0.01	0.02	<0.01
TiO_2		0.43	0.34	0.13	0.11	0.11	0.15	0.66	0.59	0.28	0.14	0.27	0.10	0.99	0.09	0.08	0.12
Cr_2O_3		0.43	0.47	0.13	0.14	0.14	0.20	0.25	0.20	0.03	0.16	0.38	0.01	0.02	0.02	0.01	0.01
LOI		6.9	6.8	4.9	4.7	6.7	5.2	4.4	1.7	2.5	5.9	2.5	5.6	5.7	0.5	4.9	5.6
Total		99.36	99.44	99.57	99.51	99.58	99.61	99.61	99.59	99.60	99.49	99.57	99.55	99.57	99.53	99.60	99.56
Mg#		79.46	80.48	73.38	76.52	77.14	80.37	73.91	73.60	80.43	80.47	78.94	68.74	57.00	67.42	68.11	67.07
Sc	ppm	13	9	16	15	15	18	40	44	39	15	38	8	8	8	7	7
V		88	68	59	50	47	61	185	188	133	49	130	37	467	35	31	51
Cr		2907	3222	882	971	951	1334	1696	1334	219	1074	2613	89	157	130	62	68
Co		119.3	73.8	117.2	119.3	115.4	92.8	62.1	55.0	59.7	91.5	83.7	120.8	125.6	135.8	120.2	128.3
Ni		830	743	571	586	540	412	418	333	298	563	398	539	258	343	434	347
Cu		17.0	22.7	6.7	1.5	3.7	20.8	9.6	0.7	61.9	16.6	0.5	54.8	98.6	49.4	38.3	73.2
Zn		24	19	33	35	15	8	17	2	18	11	7	21	38	4	21	29
Ga		7.5	7.0	6.4	5.6	5.9	7.6	11.4	8.9	5.6	6.5	6.7	5.8	10.9	7.4	6.7	8.0
Rb		3.0	0.7	2.0	1.0	1.6	0.3	6.4	3.8	4.5	0.2	0.6	1.1	0.8	1.3	1.0	6.0
Sr		69.5	54.8	150.4	62.3	211.7	36.7	95.4	209.6	34.3	12.7	64.6	68.0	57.2	545.1	148.3	274.9
Y		9.7	10.8	4.9	3.6	2.9	5.0	9.9	9.8	10.2	4.2	9.4	1.2	2.8	1.4	2.0	1.8

		Intrusion 1		Intrusion 2									Intrusion 3		Intrusion 4		
Rock		Clinopyroxenite		Wehrlite					Hornblendite				Clinopyroxenite		Troctolite	Hornblendite	
Sample		A-19A	A-19B	A-01A	A-23A	A-23B	A-24A	A-24B	A-21	A-22	A-25	A-26	A-44A	A-44B	A-38B	A-38A	A-38C
Zr		36.7	47.1	8.8	8.5	7.1	23.6	60.4	50.1	15.8	20.5	23.3	6.3	8.7	3.1	4.0	3.2
Nb		3.8	4.2	0.3	0.4	0.5	1.0	1.9	3.6	0.4	1.4	1.0	0.2	0.6	<0.1	<0.1	<0.1
Cs		<0.1	<0.1	<0.1	<0.1	<0.1	<0.1	0.1	0.5	0.2	<0.1	<0.1	0.1	<0.1	<0.1	<0.1	<0.1
Ba		283	39	53	23	39	30	130	40	85	2	7	18	23	142	26	47
Hf		0.9	1.4	0.3	0.4	0.3	0.6	1.7	1.5	0.7	0.6	0.8	0.2	0.2	0.1	0.1	0.2
Ta		<0.1	0.4	<0.1	<0.1	<0.1	<0.1	0.1	0.4	<0.1	0.1	<0.1	<0.1	<0.1	0.1	<0.1	<0.1
Pb		1.0	0.8	3.4	0.5	0.4	6.2	1.2	1.9	2.2	1.0	0.4	2.3	1.2	0.4	0.2	0.4
Th		2.1	2.2	0.4	0.6	<0.2	1.2	1.3	2.1	0.4	4.0	0.4	0.7	1.3	<0.2	<0.2	<0.2
U		0.6	0.5	0.3	0.2	<0.1	0.5	0.3	0.4	0.2	0.3	0.1	0.2	0.6	<0.1	<0.1	<0.1
La		40.4	33.1	5.5	2.6	1.9	6.4	17.7	16.3	10.5	5.3	5.0	3.2	6.1	2.1	4.3	4.4
Ce		101.6	51.7	5.8	4.7	4.8	21.5	30.2	36.8	14.9	8.3	13.9	4.1	9.2	2.8	4.0	6.5
Pr		7.11	6.69	1.01	0.68	0.65	2.05	4.01	4.07	2.52	1.39	1.87	0.42	1.28	0.37	0.66	0.72
Nd		25.1	24.3	4.2	2.8	2.9	7.5	16.4	16.2	10.5	5.9	7.9	1.4	4.8	1.5	2.5	3.4
Sm		3.77	3.64	0.90	0.74	0.76	1.33	3.26	3.36	2.34	1.08	1.98	0.36	0.71	0.29	0.48	0.45
Eu		0.85	0.76	0.31	0.24	0.27	0.36	0.91	0.92	0.47	0.17	0.60	0.13	0.31	0.26	0.23	0.27
Gd	ppm	3.31	2.91	1.06	0.75	0.70	1.29	2.88	2.70	2.42	0.95	2.05	0.35	0.72	0.40	0.47	0.40
Tb		0.39	0.38	0.15	0.11	0.10	0.18	0.41	0.38	0.36	0.14	0.32	0.04	0.09	0.05	0.05	0.05
Dy		1.94	2.02	0.82	0.65	0.62	1.10	1.96	2.04	1.92	0.89	1.92	0.32	0.42	0.27	0.38	0.29
Ho		0.36	0.35	0.15	0.12	0.14	0.19	0.38	0.35	0.43	0.17	0.39	0.04	0.09	0.04	0.06	0.05
Er		0.90	0.93	0.47	0.31	0.35	0.55	1.05	1.01	1.07	0.46	1.03	0.16	0.24	0.13	0.18	0.17
Tm		0.13	0.14	0.06	0.04	0.05	0.07	0.15	0.14	0.15	0.07	0.14	0.02	0.03	0.02	0.02	0.03
Yb		0.84	0.89	0.42	0.26	0.27	0.51	0.83	0.86	0.98	0.43	0.91	0.13	0.22	0.11	0.15	0.15
Lu		0.12	0.13	0.07	0.04	0.03	0.08	0.11	0.13	0.14	0.06	0.14	0.03	0.03	0.02	0.02	0.03
(La/Sm)N		6.92	5.87	3.95	2.27	1.61	3.11	3.51	3.13	2.90	3.17	1.63	5.74	5.55	4.67	5.78	6.31
(Gd/Yb)N		3.26	2.70	2.09	2.39	2.14	2.09	2.87	2.60	2.04	1.83	1.86	2.23	2.71	3.01	2.59	2.21

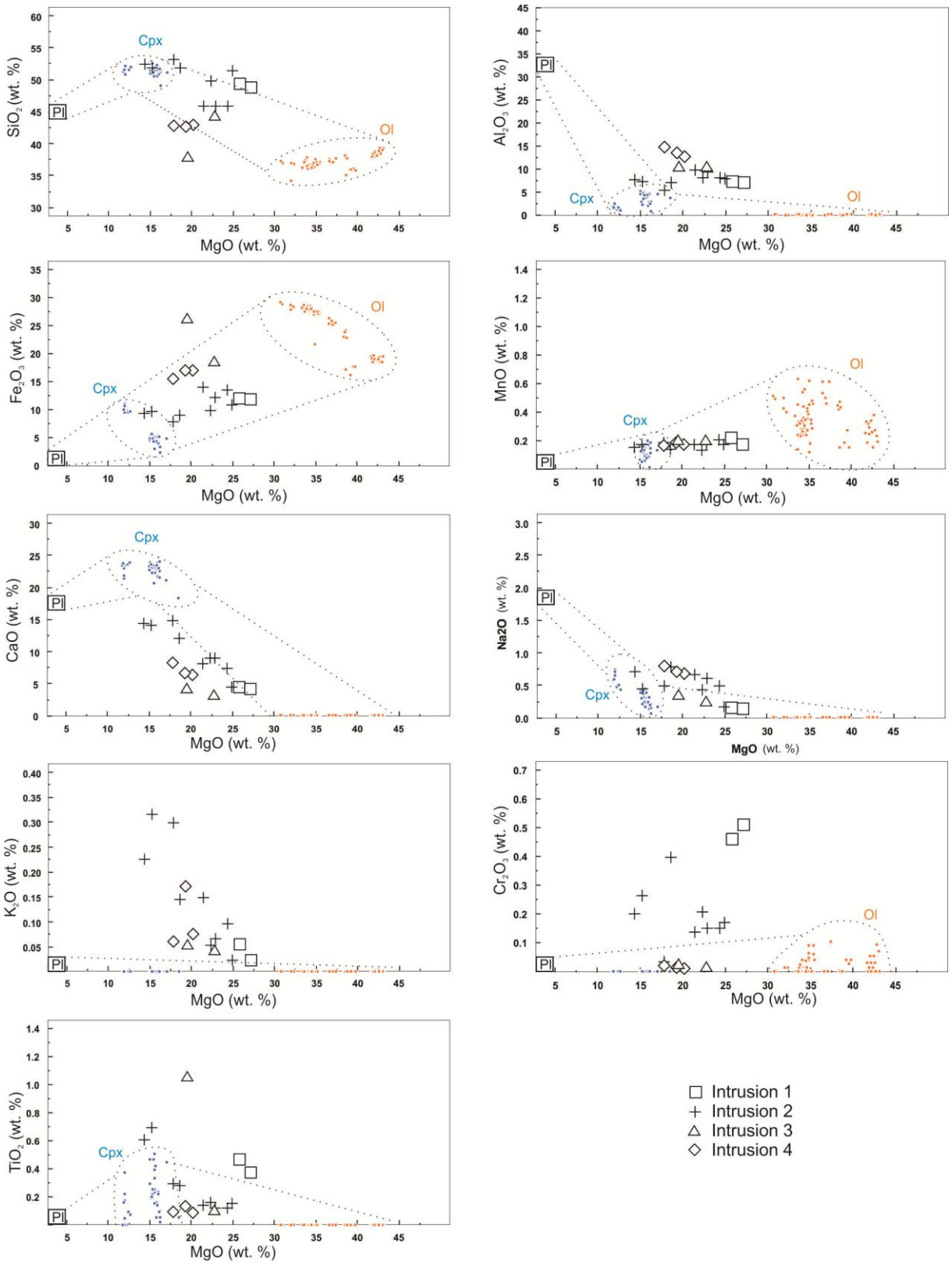

Figure 9. Plot of MgO versus major oxides and selected minor elements for mafic-ultramafic rocks. See Table 6 for chemical analyses. The compositions indicated for olivine, clinopyroxene and plagioclase correspond to electron microprobe analyses reported in this study.

2.4.3.2 Trace elements

The studied mafic-ultramafic rocks have relatively low contents of incompatible trace elements (Table 6), as expected for olivine, clinopyroxene and plagioclase cumulates. Rare earth element (REE) contents are variable (Table 6) but provide remarkably similar chondrite-normalized REE profiles for different mafic-ultramafic rocks from all the four intrusions investigated (Fig. 10). REE profiles are characterized by distinctively positive slopes for LREE (e.g., progressive enrichment toward lighter REE) and slightly positive slope for HREE. These profiles reflect distinct chondrite-normalized La/Sm (1.61 to 6.92; average 4.08) and Gd/Yb (1.83 to 3.26; average 2.29) ratios. Troctolites (Pl + Ol cumulates) and hornblendite from Intrusion 4 have distinctively positive Eu anomalies (Fig. I0J) compared with rocks from other intrusions. Very similar REE profiles for troctolite and closely associated hornblendite in Intrusion 4 support the interpretation that the later result from metamorphic recrystallization of troctolite.

Chondrite-normalized trace element profiles of mafic-ultramafic rocks are fractionated, as indicated by relative enrichment in large ion lithophile elements (LILE) and relative depletion high field strength elements (HFSE) (Fig. 10). Several samples have pronounced negative Nb and Ta anomalies, a feature that becomes more evident when Nb and Ta are compared with adjacent alteration-resistant elements (e.g., Th and La). Trace-element profiles are similar for different intrusions excepting Intrusion 4. The later has pronounced positive Eu and Sr anomalies, likely to be associated with their origin through accumulation of plagioclase (i.e., Pl cumulates).

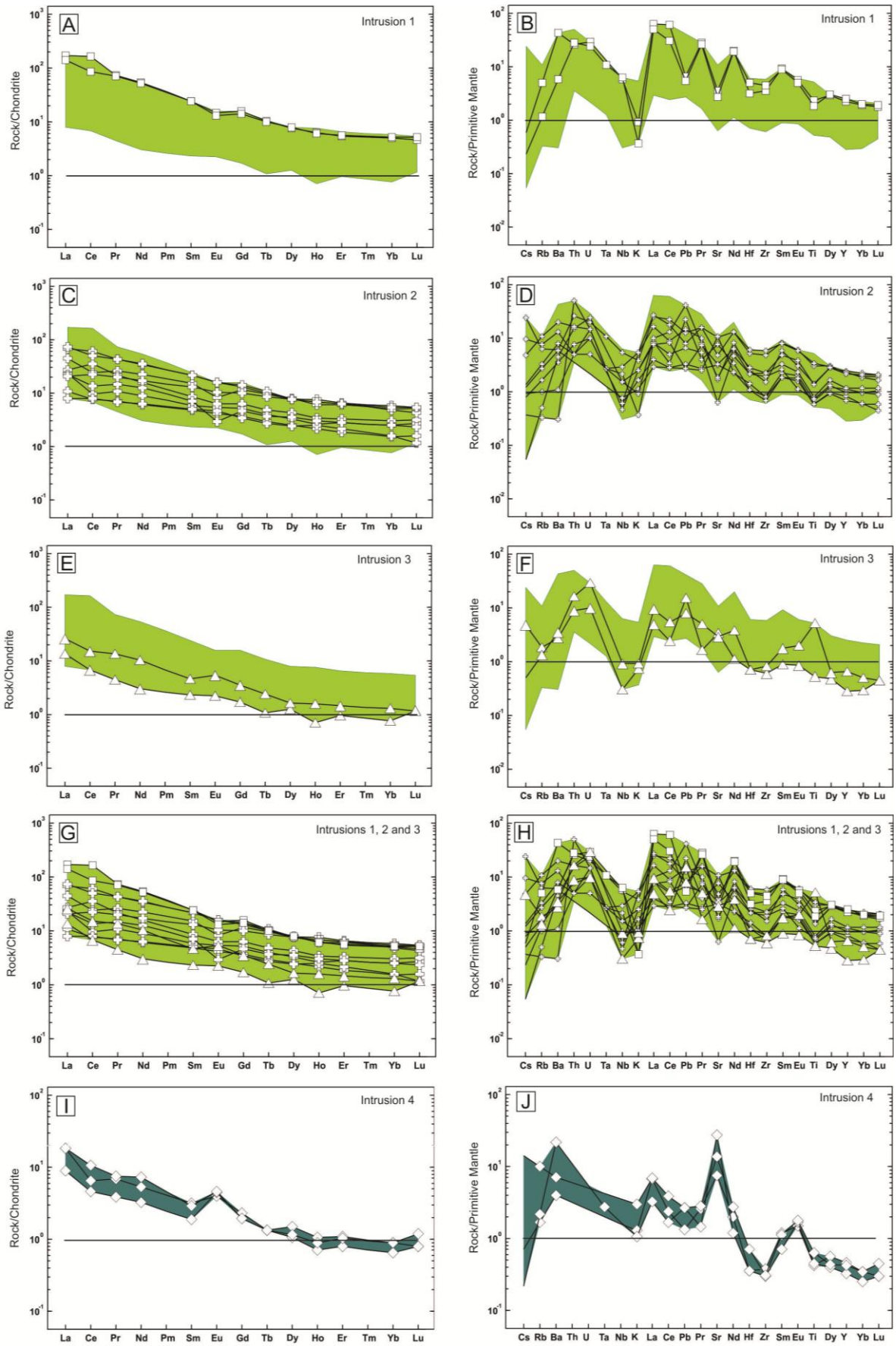

Figure 10. Chondrite-normalized REE and trace elements profiles for mafic-ultramafic rocks. Data from Table 6. Chondrite and Primitive Mantle normalization values are from Sun and McDonough (1989;1995).

2.4.4 U-Pb isotopes

From a total of 20 large (~ 15 Kg) samples of mafic-ultramafic rocks collected in the four investigated intrusions, four samples returned a concentrate with an appropriate amount of zircons for systematic U-Pb isotope studies. These samples include a clinopyroxenite from Intrusion 1 (sample 1-19B), two hornblendites from Intrusion 2 (Sample A-21 and A-25) and a clinopyroxenite from Intrusion 3 (sample A-44). From these three intrusions four representative samples of adjacent host rocks were also collected for U-Pb studies in zircons. These samples include three orthogneisses (sample A-10 located close to Intrusion 1; sample A-18 and A-28 located close to Intrusion 2) and a magnetite-biotite gneiss (sample A-41 located close to Intrusion 3). Analytical U-Pb results for zircons from these samples are provided in Table 7 and Figure 11.

Zircon crystals from mafic-ultramafic intrusions and host rocks have distinct morphological features (Fig. 11). In mafic-ultramafic rocks subhedral prismatic zircon crystals (100 to 350μm) or fragmented grains predominate. Several crystals have varied degrees of rounding or absorbed borders, similar to features described in zircons from mafic-ultramafic intrusions in high-grade terrains (e.g., Corfu et al., 2003; Pimentel et al., 2006; DellaGiustina et al., 2011). These zircon crystals are colorless or reddish (sample A-44, Intrusion 3) with well defined oscillatory zoning typical of magmatic zircons (e.g., Vavra, 1990). The host rocks have colorless euhedral zircon crystals with elongated prismatic habit (150 to 250μm). These zircons usually have well defined oscillatory zoning with darker core.

U-Pb results for the investigated mafic-ultramafic samples are similar and render a cluster of concordant to variably discordant spot analyses for each sample. There is no systematic difference for results from analyses of core and rim of the same zircon crystal (Table 7). These results define Discordia lines with upper intercept ages for each sample of 2198.4±7.7 Ma (Fig. 11A; sample A-19B from Intrusion 1), 2192.3±9.8 Ma (Fig. 11C; sample A-21 from Intrusion 2), 2191±15 Ma (Fig. 11E; sample A-25 from Intrusion 2) and 2201.6±8.6 Ma (Fig. 11G; sample A-44 from Intrusion 3). The ages indicated for all samples are very close and overlap at ca. 2.195 Ma (2190.7 to 2201.6 Ma). These results support the interpretation that mafic-ultramafic intrusions crystallized from mafic-ultramafic magmas at ca. 2195±5 Ma.

U-Pb results for three samples of orthogneiss hosting the mafic-ultramafic intrusions are similar and render a cluster of concordant to variably discordant spot analyses for each sample. These results define Discordia lines with upper intercept ages for each sample of 2231±11 Ma (Fig. 11B, host rock of Intrusion 1), 2216±10 Ma (Fig. 11D, host rock of Intrusion 2) and 2230±10 Ma (Fig. 11F; host rock of Intrusion 2). The ages indicated for these three orthogneiss are close and overlap at ca. 2220-2230 Ma. These results support the interpretation that the most common rock type hosting the mafic-ultramafic intrusions crystallized from felsic magmas at ca. 2220-2230 Ma. U-Pb results for a biotite gneiss associated with host rocks of Intrusion 3 render a highly variable array of spot analyses. A group of 17 concordant to variably discordant spot analyses define a Discordia age of 2479±18 Ma (Fig. 11H; sample A-41). Several analyses from this sample provide Neoarchean $^{207}Pb/^{236}U$ ages (2.50-2.71 Ma). This result support the interpretation that host rocks also include an older component of Neoarchean sialic crust.

Table 7. U–Pb LA-MC-ICPMS data. c = core; r = rim; n = number of spot analyses.

Zircon	Site	$^{232}Th/^{238}U$	207Pb*/206Pb* Ratio	±1s	207Pb*/235U Ratio	±1s	206Pb*/238U Ratio	±1s	Rhor	207Pb*/206Pb* age	±1s	207Pb*/235U age	±1s	206Pb*/238U age	±1s	Conc (%) 6/8 - 7/6	Conc (%) 6/8 - 7/5
Intrusion 1 (Sample A-19B - Clinopyroxenite - n=29)																	
Z-2	c	0.142	0.134	0.434	6.465	1.115	0.349	1.027	0.91	2103.763	7.838	2041.136	9.807	1931.594	17.147	91.8	94.6
Z-3	c	0.166	0.137	0.372	6.909	0.831	0.367	0.744	0.88	2136.132	6.692	2099.760	7.374	2012.978	12.856	94.2	95.9
Z-3	r	0.250	0.135	0.363	6.218	1.043	0.335	0.978	0.93	2109.765	6.544	2007.000	9.124	1862.023	15.817	88.3	92.8
Z-4	c	0.192	0.136	0.558	6.424	1.308	0.343	1.183	0.90	2123.919	10.059	2035.551	11.495	1901.999	19.489	89.6	93.4
Z-5	c	0.483	0.139	0.735	7.441	1.066	0.389	0.772	0.70	2161.759	12.759	2165.867	9.498	2118.141	13.930	98.0	97.8
Z-6	c	0.315	0.131	0.562	6.547	1.070	0.362	0.910	0.84	2062.054	10.208	2052.207	9.421	1992.970	15.596	96.6	97.1
Z-7	c	0.475	0.136	0.485	7.076	0.969	0.377	0.838	0.85	2128.151	8.741	2120.991	8.618	2062.702	14.800	96.9	97.3
Z-8	c	0.345	0.136	0.420	7.155	0.779	0.381	0.656	0.81	2131.314	7.570	2130.889	6.940	2079.194	11.656	97.6	97.6
Z-9	c	0.192	0.136	0.968	6.915	1.228	0.370	0.757	0.58	2122.804	17.441	2100.542	10.897	2027.712	13.166	95.5	96.5
Z-9	c	0.217	0.135	0.574	6.668	1.058	0.358	0.889	0.82	2116.819	10.353	2068.415	9.346	1971.185	15.103	93.1	95.3
Z-10	c	0.162	0.137	0.463	7.266	0.789	0.386	0.639	0.77	2133.952	8.334	2144.644	7.042	2104.054	11.468	98.6	98.1
Z-11	c	0.584	0.141	0.466	7.859	0.741	0.404	0.576	0.72	2191.344	8.342	2215.024	6.673	2187.232	10.675	99.8	98.7
Z-12	c	0.272	0.136	0.856	7.028	1.512	0.375	1.247	0.82	2126.620	15.416	2115.019	13.443	2052.413	21.919	96.5	97.0
Z-13	c	0.223	0.135	0.512	6.890	0.881	0.370	0.717	0.78	2114.190	9.245	2097.355	7.812	2030.013	12.480	96.0	96.8
Z-14	c	0.198	0.136	0.361	7.145	0.935	0.381	0.862	0.91	2128.772	6.509	2129.710	8.328	2079.422	15.327	97.7	97.6
Z-15	c	0.569	0.136	0.347	6.715	0.791	0.359	0.711	0.88	2122.958	6.258	2074.625	6.993	1977.181	12.107	93.1	95.3
Z-16	c	0.578	0.136	0.381	6.810	0.800	0.363	0.704	0.86	2128.389	6.858	2087.068	7.086	1995.926	12.083	93.8	95.6
Z-16	r	0.553	0.137	0.456	7.028	0.861	0.372	0.731	0.82	2137.786	8.209	2114.956	7.658	2041.098	12.785	95.5	96.5
Z-17	c	0.172	0.135	0.652	7.315	1.032	0.393	0.799	0.75	2114.369	11.767	2150.598	9.215	2136.303	14.534	101.0	99.3
Z-18	r	0.148	0.136	0.483	7.101	1.176	0.379	1.072	0.91	2124.422	8.704	2124.215	10.469	2072.878	19.011	97.6	97.6
Z-19	c	0.647	0.065	0.913	0.797	1.459	0.089	1.138	0.77	718.004	19.949	595.285	6.571	548.381	5.981	76.4	92.1
Z-20	c	0.174	0.135	0.344	6.874	0.798	0.369	0.721	0.88	2116.836	6.206	2095.336	7.078	2023.429	12.513	95.6	96.6
Z-21	c	0.302	0.138	0.506	7.315	0.885	0.385	0.726	0.79	2151.372	9.093	2150.683	7.903	2098.310	12.997	97.5	97.6
Z-22	c	0.243	0.136	0.413	6.827	0.845	0.365	0.737	0.85	2123.855	7.437	2089.238	7.484	2004.596	12.704	94.4	95.9
Z-23	c	0.404	0.140	0.715	6.635	1.136	0.345	0.883	0.76	2173.614	12.819	2064.000	10.026	1908.364	14.583	87.8	92.5
Z-24	c	0.173	0.135	0.547	6.762	1.053	0.363	0.900	0.84	2114.014	9.869	2080.738	9.318	1997.734	15.465	94.5	96.0
Z-25	c	0.383	0.063	1.310	0.794	1.873	0.092	1.338	0.70	637.140	29.008	593.368	8.415	566.305	7.254	88.9	95.4

Zircon	Site	$^{232}Th/^{238}U$	207Pb*/206Pb* Ratio	±1s	207Pb*/235U Ratio	±1s	206Pb*/238U Ratio	±1s	Rhor	207Pb*/206Pb* age	±1s	207Pb*/235U age	±1s	206Pb*/238U age	±1s	Conc (%) 6/8 - 7/6	Conc (%) 6/8 - 7/5
Z-26	c	0.488	0.134	0.444	7.037	0.948	0.382	0.837	0.87	2094.922	8.036	2116.055	8.426	2086.462	14.922	99.6	98.6
Z-27	c	0.352	0.135	0.431	7.034	0.837	0.379	0.717	0.83	2109.547	7.776	2115.759	7.439	2071.070	12.707	98.2	97.9
Intrusion 2 (Sample A-21 - Hornblendite - n=26)																	
Z-1	c	0.337	0.134	0.763	6.778	1.303	0.367	1.056	0.80	2097.913	13.787	2082.803	11.526	2017.587	18.292	96.2	96.9
Z-2	c	0.800	0.136	1.038	6.757	1.701	0.360	1.347	0.78	2128.627	18.693	2080.146	15.042	1982.308	22.993	93.1	95.3
Z-3	c	0.299	0.134	0.867	6.417	1.266	0.346	0.923	0.71	2105.345	15.660	2034.544	11.123	1917.615	15.305	91.1	94.3
Z-4	c	0.406	0.130	0.702	6.016	1.170	0.336	0.937	0.78	2043.857	12.764	1978.170	10.189	1869.142	15.195	91.5	94.5
Z-5	c	0.508	0.135	1.134	7.066	1.729	0.378	1.306	0.75	2120.546	20.436	2119.792	15.383	2067.993	23.105	97.5	97.6
Z-6	c	0.653	0.129	1.208	5.766	1.702	0.324	1.199	0.69	2036.293	21.995	1941.346	14.728	1808.126	18.897	88.8	93.1
Z-7	c	0.574	0.132	1.674	6.966	2.522	0.384	1.886	0.74	2070.244	30.351	2107.046	22.389	2093.395	33.707	101.1	99.4
Z-8	c	0.388	0.127	1.208	6.382	2.245	0.366	1.892	0.84	1999.873	22.080	2029.734	19.703	2009.439	32.659	100.5	99.0
Z-9	c	0.494	0.123	1.117	3.897	2.949	0.229	2.729	0.92	1956.058	20.516	1613.036	23.825	1328.817	32.769	67.9	82.4
Z-11	c	0.452	0.137	1.391	7.398	2.282	0.392	1.808	0.79	2139.584	25.034	2160.768	20.408	2130.811	32.806	99.6	98.6
Z-13	c	0.368	0.135	0.864	6.984	1.473	0.374	1.193	0.80	2119.964	15.570	2109.366	13.082	2047.913	20.933	96.6	97.1
Z-14	c	0.488	0.136	1.653	6.837	2.179	0.364	1.420	0.64	2131.919	29.756	2090.502	19.303	1999.124	24.416	93.8	95.6
Z-15	c	0.270	0.134	1.377	6.075	2.082	0.330	1.562	0.74	2094.801	24.892	1986.673	18.153	1838.295	24.983	87.8	92.5
Z-16	c	0.707	0.132	0.884	6.203	1.361	0.340	1.034	0.74	2079.470	16.014	2004.894	11.899	1886.144	16.916	90.7	94.1
Z-17	c	0.386	0.138	0.799	7.631	1.282	0.401	1.002	0.77	2152.524	14.356	2188.520	11.505	2173.927	18.488	101.0	99.3
Z-18	c	0.439	0.122	0.995	3.982	1.599	0.236	1.252	0.77	1939.976	18.318	1630.614	12.978	1366.152	15.410	70.4	83.8
Z-19	c	0.442	0.135	0.868	6.916	1.192	0.371	0.818	0.66	2117.230	15.649	2100.674	10.577	2033.512	14.261	96.0	96.8
Z-20	c	0.358	0.136	0.757	7.208	1.120	0.385	0.826	0.71	2123.498	13.646	2137.501	9.989	2100.403	14.801	98.9	98.3
Z-21	c	0.364	0.137	1.837	7.019	2.776	0.372	2.081	0.75	2137.693	33.057	2113.813	24.674	2038.941	36.383	95.4	96.5
Z-22	c	0.439	0.134	0.866	6.842	1.188	0.369	0.814	0.66	2106.446	15.634	2091.163	10.526	2025.539	14.145	96.2	96.9
Z-23	c	0.304	0.125	1.530	4.382	2.185	0.255	1.560	0.71	1972.810	28.059	1708.859	18.067	1464.105	20.436	74.2	85.7
Z-24	c	0.390	0.127	1.200	4.562	2.464	0.261	2.152	0.87	2001.254	21.928	1742.438	20.524	1496.482	28.745	74.8	85.9
Z-25	c	0.288	0.135	0.727	6.780	1.113	0.365	0.843	0.73	2110.871	13.125	2083.092	9.850	2005.396	14.525	95.0	96.3
Z-26	c	0.236	0.137	0.782	8.029	1.340	0.424	1.089	0.80	2142.898	14.059	2234.266	12.102	2279.960	20.907	106.4	102.0
Z-28	c	0.403	0.129	0.807	5.052	1.615	0.284	1.399	0.86	2034.763	14.692	1828.143	13.690	1611.159	19.945	79.2	88.1
Z-29	c	0.280	0.135	0.781	6.646	1.193	0.357	0.901	0.73	2115.140	14.093	2065.411	10.528	1967.035	15.282	93.0	95.2

Zircon	Site	$^{232}Th/^{238}U$	207Pb*/206Pb* Ratio	±1s	207Pb*/235U Ratio	±1s	206Pb*/238U Ratio	±1s	Rhor	207Pb*/206Pb* age	±1s	207Pb*/235U age	±1s	206Pb*/238U age	±1s	Conc (%) 6/8 - 7/6	Conc (%) 6/8 - 7/5
Intrusion 2 (Sample A-25 - Hornblendite - n=28)																	
Z-1	c	0.386	0.137	0.632	7.352	1.324	0.390	1.163	0.87	2134.130	11.384	2155.107	11.830	2124.987	21.048	99.6	98.6
Z-2	c	0.411	0.125	1.780	5.554	2.678	0.321	2.000	0.77	1983.756	31.351	1909.050	22.784	1795.837	31.274	90.5	94.1
Z-3	c	0.568	0.136	0.762	7.735	1.385	0.413	1.157	0.83	2123.313	13.726	2200.670	12.456	2230.310	21.818	105.0	101.3
Z-4	c	0.592	0.135	0.845	7.449	1.254	0.400	0.927	0.72	2113.440	15.251	2166.933	11.228	2170.713	17.077	102.7	100.2
Z-5	c	0.375	0.136	0.765	7.836	1.218	0.417	0.948	0.76	2130.607	13.770	2212.394	10.970	2247.074	17.994	105.5	101.6
Z-6	c	0.465	0.137	0.944	7.594	1.423	0.404	1.065	0.73	2133.462	16.989	2184.189	12.769	2185.172	19.744	102.4	100.0
Z-7	c	0.498	0.136	1.043	7.577	1.571	0.406	1.175	0.74	2120.689	18.805	2182.094	14.096	2194.381	21.862	103.5	100.6
Z-8	c	0.030	0.137	0.992	7.283	1.517	0.385	1.148	0.74	2143.868	17.833	2146.667	13.546	2097.948	20.564	97.9	97.7
Z-9	c	0.513	0.137	0.910	7.494	1.606	0.395	1.323	0.82	2145.239	16.354	2172.228	14.383	2148.228	24.172	100.1	98.9
Z-10	c	0.525	0.138	0.891	7.653	1.276	0.401	0.913	0.69	2157.316	16.007	2191.129	11.460	2174.223	16.853	100.8	99.2
Z-11	c	0.385	0.136	0.731	7.338	1.158	0.390	0.898	0.76	2132.263	13.167	2153.455	10.347	2123.573	16.243	99.6	98.6
Z-12	c	0.370	0.137	0.735	7.825	1.260	0.415	1.023	0.80	2138.558	13.230	2211.135	11.340	2235.822	19.320	104.5	101.1
Z-13	c	0.383	0.140	0.734	7.513	1.428	0.389	1.226	0.85	2177.454	13.144	2174.556	12.800	2119.397	22.137	97.3	97.5
Z-13	r	0.357	0.134	1.051	7.240	1.606	0.392	1.215	0.75	2102.246	18.335	2141.413	14.231	2130.165	22.001	101.3	99.5
Z-14	c	0.619	0.166	0.895	9.639	1.425	0.422	1.109	0.78	2467.826	15.029	2400.932	13.022	2267.747	21.161	91.9	94.5
Z-15	c	0.428	0.137	0.671	7.633	1.029	0.404	0.780	0.73	2141.860	12.064	2188.709	9.237	2185.606	14.462	102.0	99.9
Z-16	c	0.432	0.133	1.002	7.241	1.359	0.394	0.917	0.65	2092.243	18.127	2141.553	12.122	2140.802	16.711	102.3	100.0
Z-17	c	0.310	0.135	0.718	7.464	1.106	0.402	0.841	0.74	2109.571	12.953	2168.687	9.900	2178.401	15.548	103.3	100.4
Z-18	c	0.675	0.134	0.739	7.230	1.279	0.392	1.044	0.80	2098.767	13.351	2140.228	11.409	2131.349	18.950	101.6	99.6
Z-19	c	0.407	0.137	0.761	7.783	1.230	0.413	0.966	0.77	2135.127	13.698	2206.195	11.065	2229.167	18.205	104.4	101.0
Z-20	c	0.480	0.136	0.906	7.259	1.450	0.386	1.132	0.77	2132.367	16.315	2143.824	12.939	2104.030	20.318	98.7	98.1
Z-21	c	0.386	0.141	0.864	8.199	1.541	0.423	1.276	0.82	2186.756	15.460	2253.269	13.945	2272.037	24.433	103.9	100.8
Z-21	r	0.112	0.139	0.828	8.077	1.470	0.422	1.214	0.82	2163.189	14.853	2239.658	13.279	2269.126	23.228	104.9	101.3
Z-22	c	0.313	0.136	0.814	7.264	1.400	0.387	1.139	0.80	2128.662	14.661	2144.424	12.494	2109.042	20.487	99.1	98.4
Z-23	c	0.432	0.135	0.727	7.035	1.111	0.379	0.841	0.73	2108.304	13.121	2115.850	9.881	2072.508	14.903	98.3	98.0
Z-24	c	0.396	0.143	0.953	9.049	1.358	0.458	0.967	0.69	2219.918	16.997	2342.983	12.417	2428.595	19.576	109.4	103.7
Z-24	r	0.479	0.132	0.779	6.155	1.675	0.338	1.483	0.88	2077.416	14.116	1998.056	14.633	1875.284	24.132	90.3	93.9
Z-25	c	0.087	0.141	0.832	7.932	1.345	0.408	1.057	0.77	2189.290	14.893	2223.315	12.132	2206.557	19.753	100.8	99.2

Zircon	Site	$^{232}Th/^{238}U$	207Pb*/206Pb* Ratio	±1s	207Pb*/235U Ratio	±1s	206Pb*/238U Ratio	±1s	Rhor	207Pb*/206Pb* age	±1s	207Pb*/235U age	±1s	206Pb*/238U age	±1s	Conc (%) 6/8 - 7/6	Conc (%) 6/8 - 7/5
Intrusion 3 (Sample A-44 - Clinopyroxenite - n=26)																	
Z-1	c	0.028	0.140	1.051	8.429	1.709	0.436	1.348	0.78	2179.304	18.828	2278.315	15.517	2333.838	26.397	107.1	102.4
Z-2	c	0.026	0.141	1.008	9.078	1.594	0.466	1.235	0.76	2194.514	18.019	2345.894	14.578	2464.877	25.297	112.3	105.1
Z-4	c	0.024	0.138	0.990	8.839	1.529	0.465	1.166	0.75	2151.219	17.788	2321.570	13.950	2461.241	23.848	114.4	106.0
Z-5	c	0.026	0.140	1.046	8.507	1.654	0.440	1.281	0.76	2178.483	18.744	2286.679	15.027	2352.859	25.248	108.0	102.9
Z-6	c	0.030	0.133	1.047	6.060	1.998	0.330	1.702	0.85	2089.983	18.936	1984.459	17.415	1838.617	27.227	88.0	92.7
Z-7	c	0.016	0.138	1.164	7.557	1.762	0.397	1.322	0.74	2152.119	20.913	2179.800	15.796	2156.480	24.233	100.2	98.9
Z-8	c	0.021	0.140	1.211	8.513	1.935	0.441	1.510	0.77	2177.219	21.698	2287.334	17.585	2355.713	29.787	108.2	103.0
Z-9	c	0.032	0.141	1.099	9.148	1.724	0.470	1.329	0.76	2192.120	19.649	2352.935	15.782	2483.519	27.390	113.3	105.5
Z-11	c	0.032	0.141	1.238	8.912	2.100	0.460	1.697	0.80	2185.203	22.161	2329.056	19.176	2438.221	34.449	111.6	104.7
Z-13	c	0.031	0.137	0.964	8.185	1.461	0.435	1.097	0.74	2133.564	17.363	2251.642	13.219	2327.537	21.438	109.1	103.4
Z-14	c	0.022	0.141	1.070	9.071	1.610	0.466	1.202	0.74	2193.423	19.145	2345.205	14.722	2464.619	24.623	112.4	105.1
Z-15	c	0.023	0.139	1.133	8.364	1.657	0.435	1.209	0.72	2169.095	20.326	2271.259	15.030	2330.091	23.639	107.4	102.6
Z-16	c	0.018	0.135	1.178	7.331	1.702	0.393	1.229	0.71	2116.054	21.252	2152.575	15.211	2138.581	22.365	101.1	99.3
Z-17	c	0.026	0.139	1.113	8.409	1.742	0.440	1.340	0.76	2159.050	19.974	2276.199	15.808	2352.088	26.413	108.9	103.3
Z-18	c	0.013	0.137	0.932	7.420	1.500	0.393	1.175	0.77	2137.045	16.779	2163.415	13.423	2138.825	21.391	100.1	98.9
Z-18	r	0.020	0.141	0.932	8.645	1.344	0.446	0.969	0.70	2185.486	16.679	2301.286	12.232	2376.692	19.252	108.7	103.3
Z-19	c	0.014	0.134	0.911	6.524	1.263	0.352	0.874	0.67	2104.126	16.453	2049.153	11.116	1946.504	14.688	92.5	95.0
Z-19	r	0.028	0.140	0.908	8.585	1.393	0.444	1.057	0.74	2182.087	16.256	2294.956	12.671	2366.762	20.936	108.5	103.1
Z-20	c	0.022	0.141	0.948	8.748	1.461	0.451	1.111	0.75	2185.519	16.972	2312.094	13.311	2400.343	22.271	109.8	103.8
Z-21	c	0.033	0.141	0.978	8.618	1.520	0.443	1.163	0.75	2191.191	17.501	2298.413	13.825	2363.923	23.008	107.9	102.9
Z-22	c	0.058	0.138	0.898	7.998	1.439	0.419	1.124	0.77	2156.480	16.125	2230.802	12.987	2257.747	21.415	104.7	101.2
Z-23	c	0.027	0.140	0.874	8.339	1.373	0.432	1.059	0.76	2178.460	15.653	2268.584	12.445	2313.855	20.579	106.2	102.0
Z-24	c	0.029	0.141	0.895	8.719	1.444	0.450	1.133	0.77	2184.513	16.026	2309.073	13.154	2394.861	22.665	109.6	103.7
Z-25	c	0.014	0.136	0.885	6.878	1.372	0.366	1.049	0.75	2132.426	15.928	2095.864	12.167	2009.048	18.113	94.2	95.9
Z-26	c	0.020	0.137	1.045	7.542	1.549	0.399	1.143	0.73	2140.497	18.791	2177.957	13.885	2164.919	21.026	101.1	99.4
Z-27	c	0.023	0.136	0.955	6.950	1.545	0.371	1.215	0.78	2126.248	17.198	2105.079	13.718	2033.193	21.193	95.6	96.6
Host of intrusion 1 (Sample A-10B - Ortho augen gneiss - n=17)																	
Z-2	r	0.074	0.140	1.084	8.317	1.695	0.432	1.303	0.76	2174.584	19.429	2266.197	15.362	2313.064	25.318	106.4	102.1

Zircon	Site	$^{232}Th/^{238}U$	207Pb*/206Pb* Ratio	±1s	207Pb*/235U Ratio	±1s	206Pb*/238U Ratio	±1s	Rhor	207Pb*/206Pb* age	±1s	207Pb*/235U age	±1s	206Pb*/238U age	±1s	Conc (%) 6/8 - 7/6	Conc (%) 6/8 - 7/5
Z-4	c	0.032	0.139	0.914	8.408	1.611	0.437	1.327	0.82	2170.371	16.391	2276.057	14.623	2339.014	26.032	107.8	102.8
Z-5	c	0.218	0.139	0.994	8.236	1.517	0.429	1.146	0.74	2166.419	17.822	2257.328	13.734	2303.162	22.197	106.3	102.0
Z-7	r	0.279	0.142	1.208	7.846	1.827	0.401	1.371	0.74	2200.250	21.581	2213.472	16.451	2174.558	25.297	98.8	98.2
Z-8	c	0.034	0.138	1.455	5.625	2.794	0.295	2.385	0.85	2157.728	26.124	1919.972	24.085	1665.287	35.000	77.2	86.7
Z-9	c	0.068	0.140	1.213	7.480	2.038	0.386	1.638	0.80	2183.264	21.714	2170.592	18.253	2105.417	29.417	96.4	97.0
Z-10	c	0.072	0.138	1.195	7.691	1.769	0.404	1.305	0.73	2154.549	21.458	2195.572	15.895	2186.305	24.188	101.5	99.6
Z-11	c	0.030	0.141	0.892	8.611	1.520	0.444	1.231	0.80	2186.898	15.958	2297.707	13.828	2367.275	24.389	108.2	103.0
Z-13	c	0.090	0.144	1.590	8.086	2.397	0.408	1.795	0.74	2222.014	28.339	2240.725	21.665	2207.368	33.547	99.3	98.5
Z-14	c	0.095	0.141	1.281	8.646	2.016	0.446	1.557	0.77	2185.872	22.927	2301.406	18.352	2376.512	30.955	108.7	103.3
Z-14	r	0.108	0.143	1.523	7.520	2.541	0.381	2.034	0.80	2215.369	27.170	2175.407	22.775	2081.980	36.196	94.0	95.7
Z-16	c	0.073	0.139	0.714	7.604	1.184	0.396	0.944	0.78	2167.094	12.800	2185.340	10.623	2152.069	17.281	99.3	98.5
Z-18	c	0.012	0.136	0.944	5.983	1.503	0.318	1.170	0.77	2131.448	16.990	1973.372	13.077	1781.225	18.211	83.6	90.3
Z-19	c	0.030	0.123	2.111	4.953	3.789	0.293	3.147	0.85	1943.255	37.273	1811.372	31.517	1656.807	45.810	85.3	91.5
Z-20	c	0.068	0.141	1.030	7.762	1.406	0.401	0.957	0.66	2184.196	18.439	2203.793	12.647	2171.757	17.645	99.4	98.5
Z-21	c	0.015	0.140	0.922	8.430	1.703	0.436	1.432	0.83	2181.191	16.504	2278.416	15.454	2331.935	28.012	106.9	102.3
Z-22	c	0.245	0.140	0.929	8.100	1.696	0.419	1.419	0.83	2179.006	16.642	2242.274	15.331	2257.325	27.028	103.6	100.7
Host of intrusion 2 (Sample A-18 - Bt Hbl orthogneiss - n=25)																	
Z-1	c	0.047	0.142	0.802	6.799	1.674	0.347	1.469	0.88	2202.760	13.866	2085.600	14.710	1921.087	24.358	87.2	92.1
Z-2	c	0.074	0.140	0.743	8.576	1.653	0.443	1.476	0.89	2181.053	13.300	2294.042	15.029	2365.946	29.239	108.5	103.1
0Z-3	c	0.070	0.139	0.786	8.389	1.625	0.439	1.423	0.87	2161.050	14.107	2273.953	14.747	2344.960	27.969	108.5	103.1
Z-4	c	0.171	0.140	0.814	7.816	1.532	0.405	1.298	0.84	2179.297	14.574	2210.102	13.792	2189.940	24.105	100.5	99.1
Z-5	c	0.074	0.141	0.695	7.749	1.279	0.400	1.074	0.83	2183.907	12.442	2202.269	11.506	2168.942	19.785	99.3	98.5
Z-6	c	0.076	0.144	0.943	8.979	1.523	0.453	1.196	0.77	2223.542	16.806	2335.868	13.917	2408.677	24.045	108.3	103.1
Z-7	c	0.119	0.159	1.814	9.427	2.654	0.430	1.938	0.73	2395.451	31.750	2380.494	24.365	2307.148	37.578	96.3	96.9
Z-8	c	0.118	0.142	0.917	6.713	1.721	0.344	1.456	0.84	2199.022	16.384	2074.331	15.206	1903.566	24.000	86.6	91.8
Z-9	r	0.084	0.136	1.136	8.444	1.873	0.449	1.489	0.79	2133.074	20.448	2279.928	17.001	2389.731	29.730	112.0	104.8
Z-10	c	0.209	0.133	0.990	6.383	1.926	0.349	1.652	0.86	2082.006	17.319	2029.978	16.769	1931.057	27.510	92.7	95.1
Z-11	c	0.058	0.138	1.312	8.400	2.248	0.441	1.825	0.81	2154.382	23.569	2275.209	20.398	2355.212	36.013	109.3	103.5
Z-12	c	0.056	0.139	1.558	8.242	3.031	0.431	2.600	0.86	2161.714	27.965	2258.010	27.445	2309.853	50.467	106.9	102.3

Zircon	Site	$^{232}Th/^{238}U$	207Pb*/206Pb* Ratio	±1s	207Pb*/235U Ratio	±1s	206Pb*/238U Ratio	±1s	Rhor	207Pb*/206Pb* age	±1s	207Pb*/235U age	±1s	206Pb*/238U age	±1s	Conc (%) 6/8 - 7/6	Conc (%) 6/8 - 7/5
Z-13	c	0.030	0.141	1.046	9.045	1.865	0.464	1.543	0.82	2194.734	18.712	2342.558	17.048	2457.155	31.529	112.0	104.9
Z-14	c	0.068	0.134	0.911	7.568	1.413	0.410	1.080	0.76	2099.296	15.908	2181.089	12.594	2215.059	20.221	105.5	101.6
Z-15	c	0.223	0.139	0.796	7.679	1.333	0.400	1.069	0.79	2169.424	14.278	2194.184	11.977	2167.693	19.684	99.9	98.8
Z-16	c	0.201	0.132	0.970	8.385	1.433	0.462	1.055	0.73	2070.777	16.994	2273.535	12.917	2447.071	21.440	118.2	107.6
Z-17	c	0.105	0.137	0.946	7.636	1.706	0.405	1.421	0.83	2135.523	17.020	2189.107	15.321	2193.157	26.408	102.7	100.2
Z-19	c	0.063	0.141	1.039	8.310	1.336	0.427	0.840	0.60	2190.310	18.580	2265.371	12.105	2293.796	16.208	104.7	101.3
Z-20	c	0.067	0.142	1.043	7.749	1.374	0.395	0.893	0.63	2206.213	18.635	2202.265	12.353	2145.400	16.302	97.2	97.4
Z-20	r	0.092	0.139	0.846	7.336	1.447	0.382	1.174	0.80	2168.433	15.171	2153.243	12.931	2085.957	20.923	96.2	96.9
Z-22	c	0.119	0.142	1.046	7.950	2.234	0.405	1.974	0.88	2206.767	18.674	2225.385	20.150	2192.086	36.686	99.3	98.5
Z-23	c	0.077	0.140	1.130	7.131	1.895	0.371	1.521	0.80	2171.585	20.266	2127.925	16.874	2032.738	26.514	93.6	95.5
Z-24	c	0.054	0.137	0.997	7.808	1.488	0.413	1.104	0.73	2143.459	17.929	2209.149	13.390	2226.374	20.787	103.9	100.8
Z-25	c	0.097	0.139	1.177	6.960	1.748	0.362	1.292	0.73	2169.021	21.113	2106.390	15.516	1993.407	22.146	91.9	94.6
Host of intrusion 2 (Sample A-28 - Bt Hbl Orthogneiss - n=25)																	
Z-1	c	0.193	0.134	1.340	5.546	2.054	0.299	1.557	0.75	2106.270	24.196	1907.827	17.671	1687.881	23.121	80.1	88.5
Z-2	c	0.586	0.141	0.882	8.014	1.328	0.412	0.993	0.73	2190.193	15.783	2232.612	11.993	2224.904	18.689	101.6	99.7
Z-3	c	0.068	0.130	0.915	5.365	1.619	0.299	1.336	0.82	2050.175	16.621	1879.310	13.856	1685.846	19.816	82.2	89.7
Z-4	c	0.334	0.141	1.001	7.754	1.530	0.399	1.158	0.74	2189.581	17.905	2202.901	13.762	2164.233	21.281	98.8	98.2
Z-5	c	0.187	0.139	0.895	5.352	1.648	0.280	1.384	0.83	2160.582	16.056	1877.289	14.100	1591.431	19.520	73.7	84.8
Z-6	c	0.462	0.127	1.151	4.887	1.932	0.279	1.551	0.80	2009.220	21.014	1799.936	16.280	1584.335	21.788	78.9	88.0
Z-7	c	0.474	0.144	1.492	8.218	2.558	0.415	2.078	0.81	2221.940	26.594	2255.362	23.158	2237.872	39.295	100.7	99.2
Z-8	c	0.404	0.144	1.682	7.693	2.378	0.387	1.680	0.70	2227.853	29.977	2195.793	21.366	2109.734	30.230	94.7	96.1
Z-9	c	0.446	0.142	1.948	7.962	2.849	0.406	2.079	0.73	2205.797	34.793	2226.712	25.699	2195.861	38.682	99.5	98.6
Z-13	c	0.213	0.136	1.185	8.525	2.186	0.454	1.837	0.84	2127.990	21.355	2288.626	19.868	2414.761	36.997	113.5	105.5
Z-14	c	0.538	0.139	1.063	8.327	1.711	0.435	1.342	0.78	2164.800	19.062	2267.230	15.514	2326.222	26.197	107.5	102.6
Z-15	c	0.493	0.140	0.949	7.772	1.524	0.402	1.192	0.77	2180.881	16.998	2204.912	13.711	2177.571	22.035	99.8	98.8
Z-16	c	0.552	0.141	0.896	8.297	1.285	0.428	0.921	0.70	2186.430	16.034	2263.980	11.644	2295.141	17.789	105.0	101.4
Z-17	c	0.500	0.141	0.890	8.131	1.300	0.419	0.947	0.71	2187.187	15.931	2245.739	11.754	2255.672	18.030	103.1	100.4
Z-18	c	0.334	0.138	0.908	7.717	1.463	0.405	1.147	0.77	2154.026	16.310	2198.624	13.152	2193.167	21.327	101.8	99.8
Z-19	c	0.376	0.141	1.015	7.957	1.486	0.408	1.085	0.72	2194.148	18.157	2226.108	13.401	2207.122	20.270	100.6	99.1

Zircon	Site	$^{232}Th/^{238}U$	207Pb*/206Pb* Ratio	±1s	207Pb*/235U Ratio	±1s	206Pb*/238U Ratio	±1s	Rhor	207Pb*/206Pb* age	±1s	207Pb*/235U age	±1s	206Pb*/238U age	±1s	Conc (%) 6/8 - 7/6	Conc (%) 6/8 - 7/5
Z-20	c	0.600	0.140	0.896	8.062	1.438	0.417	1.124	0.77	2179.702	16.052	2238.039	12.986	2247.656	21.330	103.1	100.4
Z-21	c	0.572	0.143	1.118	8.278	1.545	0.419	1.067	0.67	2218.192	19.933	2261.966	13.999	2255.809	20.311	101.7	99.7
Z-23	c	0.042	0.140	1.465	7.829	1.998	0.406	1.358	0.67	2177.347	26.253	2211.551	17.987	2195.012	25.260	100.8	99.3
Z-24	c	0.436	0.141	1.462	7.786	1.845	0.401	1.125	0.59	2186.740	26.173	2206.532	16.604	2174.676	20.773	99.4	98.6
Z-25	c	0.062	0.139	1.034	7.644	1.639	0.399	1.271	0.77	2165.214	18.549	2190.089	14.715	2163.750	23.369	99.9	98.8
Z-26	c	0.346	0.139	1.031	7.569	1.487	0.395	1.071	0.71	2166.648	18.494	2181.214	13.337	2144.135	19.544	99.0	98.3
Z-27	c	0.315	0.139	1.069	7.969	1.470	0.416	1.009	0.67	2162.839	19.177	2227.532	13.261	2243.936	19.123	103.7	100.7
Z-28	c	0.516	0.140	0.959	8.128	1.429	0.422	1.059	0.73	2172.910	17.194	2245.403	12.918	2270.616	20.264	104.5	101.1
Z-29	c	0.026	0.128	1.141	5.152	1.793	0.291	1.384	0.76	2023.839	20.789	1844.746	15.249	1648.204	20.127	81.4	89.3
Bt gneiss basemente and host intrusion 3 (Sample A-41 - n=24)																	
Z-1	c	0.525	0.164	0.666	10.118	1.175	0.447	0.968	0.81	2449.648	11.592	2445.642	10.856	2383.393	19.283	97.3	97.5
Z-2	c	0.327	0.187	0.715	13.062	1.080	0.507	0.810	0.72	2667.027	12.190	2684.144	10.189	2644.426	17.561	99.2	98.5
Z-3	c	0.211	0.151	0.720	7.974	1.238	0.383	1.007	0.80	2309.568	12.722	2228.087	11.170	2089.070	17.968	90.5	93.8
Z-4	c	0.215	0.174	0.618	10.978	1.107	0.457	0.919	0.81	2550.379	10.650	2521.265	10.302	2426.963	18.577	95.2	96.3
Z-5	c	0.238	0.162	0.656	9.237	1.311	0.414	1.135	0.86	2428.007	11.444	2361.828	12.013	2231.550	21.414	91.9	94.5
Z-6	c	0.170	0.175	0.787	9.243	1.239	0.383	0.956	0.75	2557.378	13.553	2362.415	11.348	2091.725	17.084	81.8	88.5
Z-9	c	0.348	0.184	0.684	12.121	1.134	0.478	0.904	0.78	2641.732	11.686	2613.841	10.637	2517.917	18.851	95.3	96.3
Z-10	c	0.422	0.159	0.822	9.705	1.336	0.442	1.054	0.77	2398.008	14.378	2407.202	12.301	2361.095	20.836	98.5	98.1
Z-11	c	0.149	0.158	0.690	9.376	1.308	0.432	1.111	0.84	2380.494	12.093	2375.529	11.997	2313.700	21.593	97.2	97.4
Z-12	c	0.325	0.162	0.649	10.130	1.125	0.454	0.918	0.80	2425.859	11.331	2446.679	10.394	2413.769	18.490	99.5	98.7
Z-13	c	0.239	0.162	0.669	9.781	1.170	0.438	0.959	0.81	2427.510	11.666	2414.368	10.773	2342.198	18.843	96.5	97.0
Z-14	c	0.189	0.157	0.620	7.501	1.435	0.346	1.294	0.90	2379.308	10.873	2173.057	12.853	1913.703	21.421	80.4	88.1
Z-15	c	0.257	0.162	0.683	9.886	1.048	0.443	0.795	0.73	2427.487	11.914	2424.181	9.662	2363.211	15.723	97.4	97.5
Z-16	c	0.205	0.162	0.621	9.964	0.991	0.447	0.772	0.75	2426.373	10.841	2431.478	9.142	2380.211	15.359	98.1	97.9
Z-18	c	0.259	0.161	0.665	9.570	1.061	0.432	0.826	0.76	2414.444	11.612	2394.255	9.750	2314.536	16.072	95.9	96.7
Z-20	c	0.390	0.187	0.843	12.477	1.207	0.483	0.863	0.69	2671.182	14.365	2641.006	11.342	2541.277	18.124	95.1	96.2
Z-21	c	0.049	0.140	0.869	7.336	1.413	0.381	1.114	0.78	2173.681	15.584	2153.188	12.630	2080.485	19.814	95.7	96.6
Z-22	c	0.401	0.182	0.898	12.098	1.246	0.483	0.864	0.67	2619.383	15.369	2612.004	11.689	2541.956	18.159	97.0	97.3
Z-23	c	0.172	0.160	0.651	9.809	1.083	0.445	0.866	0.78	2406.525	11.374	2416.974	9.981	2372.188	17.188	98.6	98.1

Zircon	Site	$^{232}Th/^{238}U$	207Pb*/206Pb* Ratio	±1s	207Pb*/235U Ratio	±1s	206Pb*/238U Ratio	±1s	Rhor	207Pb*/206Pb* age	±1s	207Pb*/235U age	±1s	206Pb*/238U age	±1s	Conc (%) 6/8 - 7/6	Conc (%) 6/8 - 7/5
Z-24	c	0.188	0.158	0.596	9.708	1.021	0.446	0.829	0.79	2383.553	10.451	2407.477	9.400	2378.529	16.488	99.8	98.8
Z-26	c	0.327	0.162	0.680	10.157	1.163	0.454	0.944	0.79	2431.249	11.864	2449.178	10.753	2412.814	18.993	99.2	98.5
Z-27	c	0.271	0.161	1.134	9.467	1.694	0.425	1.258	0.73	2422.383	19.802	2384.389	15.560	2284.719	24.209	94.3	95.8
Z-28	c	0.219	0.171	0.935	10.779	1.361	0.457	0.989	0.71	2521.417	16.153	2504.275	12.644	2424.933	19.990	96.2	96.8
Z-29	c	0.523	0.164	1.212	10.520	1.644	0.466	1.111	0.66	2447.831	21.105	2481.692	15.247	2464.237	22.754	100.7	99.3

Pb* indicates the radiogenic Pb isotopes.

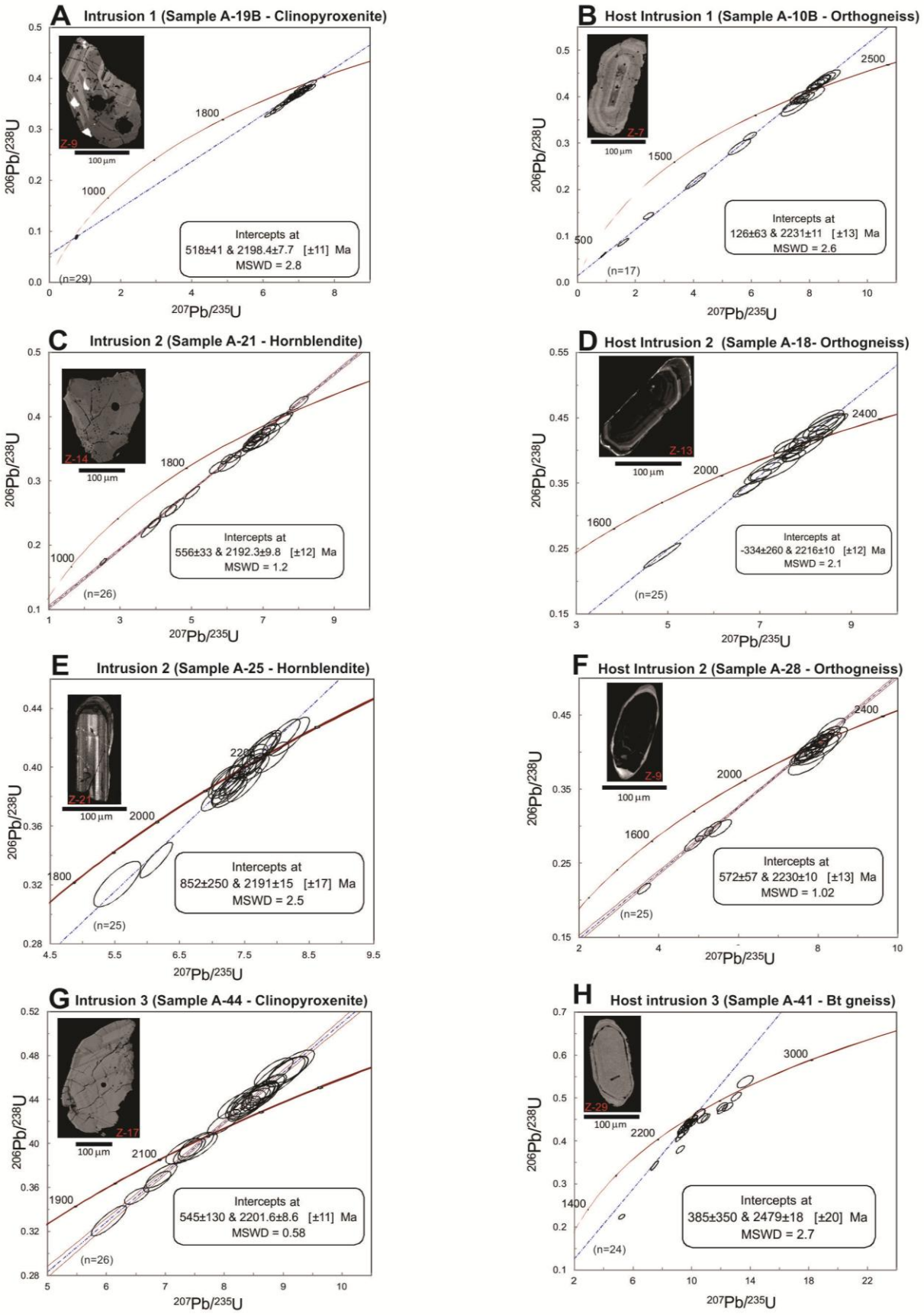

Figure 11. LA-MC-ICPMS U-Pb plots. Data from Table 7. Photomicrographs are true color cathodo-luminecence images of representative zircon crystals.

2.4.5 Sm-Nd isotopes

The Sm-Nd isotopic data of mafic-ultramafic intrusions and host rocks are listed in Table 8. Nd isotopic data obtained for mafic and ultramafic rocks render Nd T_{DM} model ages between 2.26 and 2.82 Ga, with variably negative (up to -4.45) and positive (up to +2.21) $\varepsilon_{Nd\ (T)}$ values. The Sm–Nd data for mafic-ultramafic rocks of different mafic-ultramafic intrusions are similar and suggest that they all share the same Nd isotopic signature. Nd isotopic data obtained for orthogneiss hosting the mafic-ultramafic intrusions render Nd model ages between 2.49 and 2.63 Ga, with variably negative (-1.15 to -2.99) $\varepsilon_{Nd\ (T)}$ values. Nd isotopic data obtained for one sample of biotite gneiss associated with host rocks of the mafic-ultramafic intrusions has and older model age (3.10 Ga) and the most negative $\varepsilon_{Nd\ (T)}$ value (- 3.10 Ga). Depleted mantle model ages (Fig. 12) overlap at ca. 2.2 to 2.8 Ga for mafic-ultramafic rocks and hosting orthogneiss, indicating an enriched component in these rocks.

Table 8. Sm–Nd isotopic data for mafic-ultramafic intrusions and host rocks. The εNd (T) values were calculated considering U-Pb zircon ages obtained for each group of rocks considered (see section 4.4 for U-Pb zircon ages).

Sample	Rock	Sm(ppm)	Nd(ppm)	$^{147}Sm/^{144}Nd$	$^{143}Nd/^{144}Nd$	± 2σ	$\varepsilon_{Nd\ (0)}$	$\varepsilon_{Nd\ (t)}$	$T_{DM\ (Ga)}$
Intrusion 1									
A-19A	Clinopyroxenite	4.161	24.923	0.1009	0.511090	± 16	-30.19	-3.13	2.63
A-19B	Clinopyroxenite	3.901	22.836	0.1033	0.511195	± 14	-28.15	-1.75	2.54
Intrusion 2									
A-01A	Wehrlite	1.054	4.902	0.1300	0.511666	± 73	-18.95	-0.11	2.50
A-01C	Wehrlite	0.952	4.510	0.1275	0.511664	± 5	-19.01	0.57	2.43
A-23A	Wehrlite	6.478	39.722	0.0986	0.511225	± 23	-27.56	0.17	2.40
A-24A	Wehrlite	1.669	8.916	0.1132	0.511278	± 16	-26.53	-2.94	2.67
A-24B	Wehrlite	3.619	17.780	0.1230	0.511573	± 18	-20.78	0.06	2.46
A-21	Hornblendite	6.587	34.256	0.1162	0.511367	± 3	-24.79	-2.05	2.62
A-22	Hornblendite	2.505	11.592	0.1307	0.511743	± 13	-17.45	1.21	2.38
A-25	Hornblendite	1.264	6.496	0.1177	0.511287	± 13	-26.35	-4.04	2.79
A-26	Hornblendite	2.220	9.192	0.1460	0.511831	± 18	-15.73	-1.42	2.73
Intrusion 3									
A-44B	Clinopyroxenite	0.840	5.195	0.0977	0.511283	± 14	-26.42	1.56	2.30
A-44A	Hornblendite	0.420	2.156	0.1176	0.511265	± 27	-26.78	-4.45	2.82
A-44D	Hornblendite	8.883	39.071	0.1374	0.511587	± 18	-20.50	-3.76	2.92
Intrusion 4									
A-38A	Hornblendite	0.621	3.059	0.1226	0.511419	± 19	-23.77	-2.85	2.72
A-38B	Troctolite	0.515	2.368	0.1316	0.511806	± 9	-16.22	2.19	2.28
A-38C	Hornblendite	0.574	3.329	0.1042	0.511410	± 12	-23.96	2.21	2.26
Host									
A-10B	Orthogneiss	4.176	29.763	0.0848	0.510927	± 13	-33.37	-1.32	2.49
A-18	Orthogneiss	4.460	36.400	0.0741	0.510718	± 18	-37.45	-2.33	2.53

Sample	Rock	Sm(ppm)	Nd(ppm)	$^{147}Sm/^{144}Nd$	$^{143}Nd/^{144}Nd$	± 2σ	$\varepsilon_{Nd\ (0)}$	$\varepsilon_{Nd\ (t)}$	$T_{DM\ (Ga)}$
A-28	Orthogneiss	11.436	67.493	0.1024	0.511119	± 16	-29.62	-2.99	2.63
A-35A	Orthogneiss	10.722	52.363	0.1238	0.511523	± 10	-21.75	-1.15	2.57
A-41	Bt gneiss	3.898	17.469	0.1349	0.511452	+/-8	-23,13	-3.53	3.10

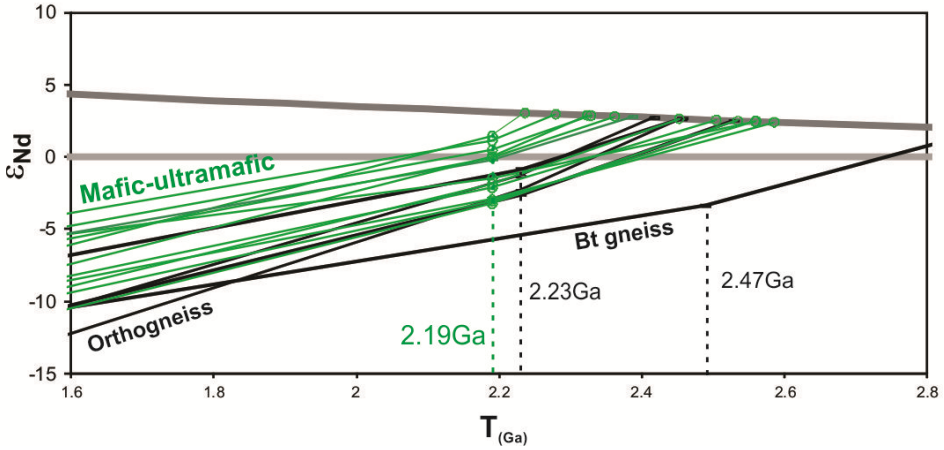

Figure 12. Nd isotope compositions of rocks from mafic-ultramafic intrusions and host rocks.

2.5 Discussion

2.5.1 Age of mafic-ultramafic magmatism and country rocks

The U-Pb zircon ages presented in topic 2.4.3 provides a geochronological framework for the following discussions of this study. A summary of key implications of the geochronological results is presented to introduce the discussions regarding the composition of the parental magma of mafic-ultramafic intrusions, the regional tectonic setting for this magmatism, as well as the implication of this magmatic event for mineral exploration.

Geochronological results (Table 7, Fig. 11) support the interpretation that mafic-ultramafic intrusions crystallized from mafic-ultramafic magmas at ca. 2195±5 Ma. The ages indicated for samples from three intrusions overlap at ca. 2195 Ma, thus suggesting that the NNE-SSW trend array of mafic-ultramafic intrusions are associated with an specific Paleoproterozoic magmatic event. Age dating together with similar Nd isotopes and lithogeochemical results for these intrusions support the interpretation that they are part of a plutonic suite. Therefore, the discussion regarding the composition of parental magma and fractionation may be integrated for this cluster of mafic-ultramafic intrusions. U-Pb zircon dating (Table 7, Fig. 11) also supports the interpretation that mafic-ultramafic rocks intruded orthogneiss that crystallized from felsic magmas at ca. 2220-2230 Ma. The results also indicate that

host rocks have an older component of Neoarchean sialic crust (2.50-2.68 Ga), as reported by U-Pb ages of a biotite gneiss associated with orthogneiss. These results provide important constraints for the regional tectonic setting of the mafic-ultramafic magmatism.

2.5.2 Fractionation and composition of the parental magma

The composition of the parental magma of these mafic-ultramafic intrusions cannot be constrained by common approaches used to define their composition in well-exposed and unaltered intrusions (e.g., chilled margin, bulk composition, extrusive equivalents, related dykes, and melt inclusions). Therefore, the composition of the parental magma may be just inferred from the crystallization sequences of the intrusions and the geochemistry of cumulus minerals and cumulate rocks.

The investigated intrusions are poorly exposed small bodies of partially to extensively metamorphosed cumulate rocks, thus hampering a detailed description of the crystallization sequence as commonly reported for well exposed layered intrusions (e.g., Skaergaard intrusion, McBirney, 1989; Niquelândia Complex, Ferreira Filho et al., 1998, 2010). Based upon the samples with the best preserved igneous minerals and textures, Ol+Cpx+Chr and Cpx cumulates prevail in Intrusions 1-2-3, whereas Ol+Pl cumulates occur in Intrusion 4. These cumulates indicate fractionation through Ol-Cpx-Pl crystallization, thus following a sequence different from silica saturated magmas where Opx precedes Cpx (Eales and Cawthorn, 1996).

The compositional range of cumulus Ol crystals from Intrusion 2 ($Fo_{80.6\text{-}68.2}$) and Intrusion 4 ($Fo_{69.9}$ to $Fo_{67.6}$) is consistent with a moderately primitive (or moderately MgO-rich) to fractionated compositions for the parental magma of these rocks. The composition of the most primitive cumulus Ol ($Fo_{80.6}$) is comparable with those reported for the Ni-Cu mineralized Permian Kalatongke mafic intrusions in northwest China (Fo_{80}; Zhang et al., 2009) and for troctolites of the Permo-Jurassic Longwood Complex in New Zealand (Fo_{82}; Price et al., 2011). The compositional range of cumulus plagioclase coexisting with cumulus olivine in Intrusion 4 is characterized by very high An content ($An_{89.0}$ to $An_{79.9}$). The coexisting Ol-Pl compositional range of Intrusion 4 is unusual for tholeiitic layered intrusions, which follow a trend of concomitant fractionation of olivine and plagioclase (Fig. 13). Results of coexisting Ol-Pl for Intrusion 4 are similar to the compositional range of arc-type gabbroic rocks (e.g. Phanerozoic Longwood Complex in New Zealand, Price

et al., 2011; Proterozoic Rymmen-Eriksberg gabbros in Sweden, Claeson and Meurer, 1984). Relatively high An contents of plagioclase coexisting with olivine occur in tholeiitic magma composition that is both aluminous and have high water content, as described in subduction-related magmatic arc (e.g., Claeson and Meurer, 1984; Price et al., 2011).

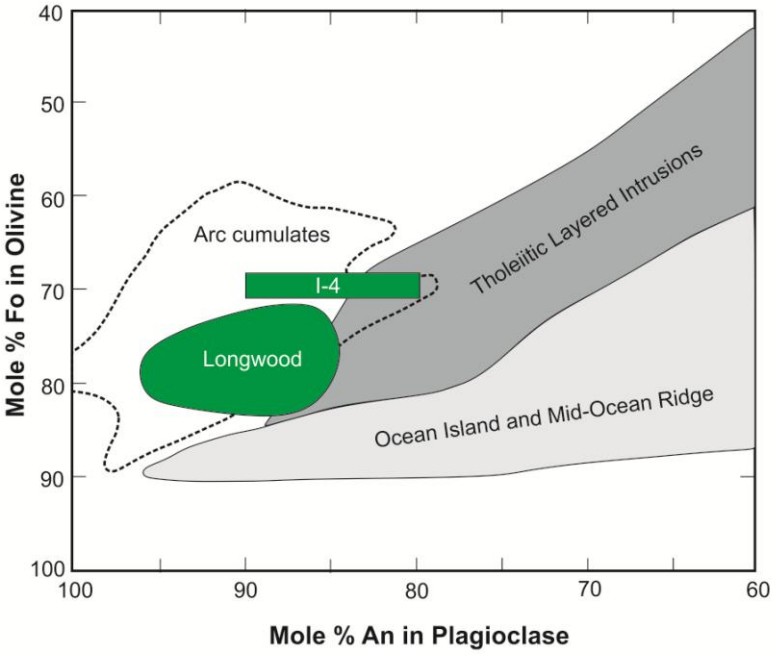

Figure 13. Compositions of coexisting olivine and plagioclase from Intrusion 4 (I-4). Field for tholeiitic layered intrusions is from Beard (1986). Field for the Longwood Igneous Complex is from Price et al. (2011).

Chondrite-normalized trace element profiles of mafic-ultramafic rocks are fractionated, as indicated by relative enrichment in LREE and Th, with negative Nb and Ta anomalies (Fig. 10). Nd isotopic data obtained for mafic and ultramafic rocks render Nd model ages between 2.26 and 2.82 Ga, with variably negative (up to -4.45) and positive (up to +2.21) $\varepsilon_{Nd\ (T)}$ values (Table 8; Fig. 12). Trace element data together with Nd isotopic compositions of mafic-ultramafic rocks suggest that older crust was recycled during magmatic processes that formed the intrusive rocks. These results are consistent with crustal contamination during emplacement of a moderately primitive mantle melt (e.g., Naldrett, 2004; Pirajno et al., 2009; Teixeira et al., 2015), as well as the result of melting an old lithospheric mantle (e.g., Maier and Groves, 2011; Price et al., 2011; Kamenetsky et al., 2013). The interpretation of lithogeochemical and isotopic data of cumulate rocks is not straightforward and, therefore, the evaluation of the tectonic setting where the primary magmas that fed the mafic-ultramafic intrusions originated will be considered together with the regional

tectonic setting. The discussion will be focused on constraints provided by lithogeochemical and Nd isotopic data for the interpretation of the mafic-ultramafic intrusions into the orogenic environments of the Rio Grande do Norte Domain.

2.5.3 Petrotectonic setting of mafic-ultramafic intrusions

The Paleoproterozic is characterized by important events of continental growth (Taylor & McLennan, 1985; Martin, 1993, 1994; Reddy and Evans, 2009), particularly significant during the siderian and riacian periods (Condie, 2000; Brito Neves, 2011). In the Borborema Province these events of crustal growth are documented at ca. 2.4-2.2 Ga in the Médio Coreaú, Rio Grande do Norte an Zona Transversal domains (Fetter et al., 2000; Santos et al., 2009; Dantas et al., 2008; Hollanda et al., 2011; Medeiros et al., 2012; Santos et al., 2014). The mafic-ultramafic intrusions investigated in this study occur in the paleoproterozoic Rio Piranhas terrain of the RGND (Fig. 2 and 3). The later consists mainly of calc-alkaline quartz-feldspathic rocks (generally ascribed as orthogneiss and migmatite) interpreted to be formed in a ca. 2.15-2.25 magmatic arc (Souza et. al. 2007; Hollanda et al., 2011) which partially recycled older crustal segments (Fetter et al., 2000; Dantas et al., 2008).

U-Pb zircon ages presented in this study indicate that mafic-ultramafic intrusions crystallized from moderately primitive to fractionated parental magmas at ca. 2195±5 Ma. Our results also indicate that mafic-ultramafic rocks intruded orthogneiss that crystallized from felsic magmas at ca. 2220-2230 Ma, thus providing a narrow window of time (ca. 30 Ma) for the reported events of felsic and mafic plutonism. The age of host orthogneiss (i.e., 2.22 to 2.23 Ga) fits into the time span indicated for the calc-alkaline magmatism of the Rio Piranhas terrain, thus consistent with their emplacement associated with the ca. 2.15-2.25 Ga magmatic arc reported in previous studies (Souza et al., 2007; Hollanda et al., 2011). The older ages (ca. 2.50-2.68 Ga) reported in our study for a biotite gneiss associated with host orthogneiss is also consistent with previous studies indicating that older crustal components are reworked during arc-type magmatism of the Rio Piranhas terrain (Fetter et al., 2000; Dantas et al., 2008). This regional arc-related tectonic setting indicated for the mafic-ultramafic intrusions and their host rocks provides a framework to constraint the generation and evolution of the mafic-ultramafic magmas (Fig. 14).

The existence of a crustal component older than arc-related plutonic rocks (i.e., 2.50-2.71 Ga age of biotite gneiss; Fig. 11H) provides evidence that such rocks may have participated in processes associated with the mafic-ultramafic magmatism. This is consistent with lithogeochemical and Nd isotope data for mafic-ultramafic intrusions. Our results also indicate that mafic-ultramafic magmas intruded shortly after (i.e., ca. 20-30 Ma) the emplacement of calc-alkaline magmas at ca. 2220-2230 Ma, thus providing a narrow window of time (ca. 30 Ma) for the reported events of felsic and mafic plutonism. Therefore, the mafic-ultramafic magmatism is part of the magmatic arc evolution, possibly resulting from partial melting of mantle in final stages of the orogeny (Fig. 14). The composition of the mafic-ultramafic magma may result from a specific composition of the mantle wedge above subduction zones, which is expected to be affected by metasomatism from fluids released from subducted oceanic crust. The composition of coexisting plagioclase and olivine in troctolites is consistent with an origin associated with melting of metasomatic mantle (e.g., Claeson and Meurer, 1984; Price et al., 2011).

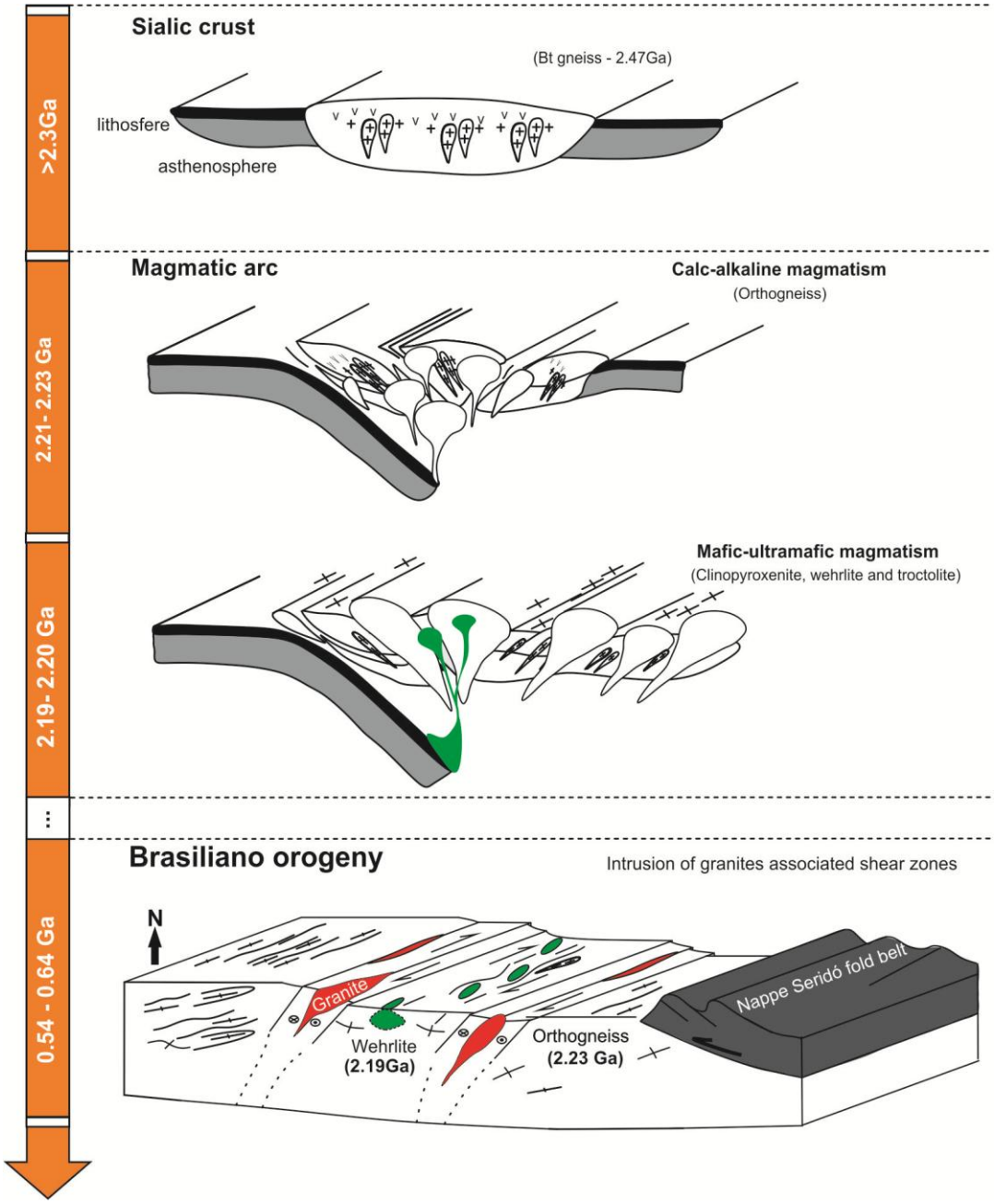

Figure 14. Schematic model for the evolution of the mafic-ultramafic intrusions and host rocks.

2.5.4 Potential for magmatic Ni-Cu-PGE deposits

World-class intrusion-related Ni–Cu-(PGE) sulfide deposits usually occur in extensional tectonics in the crust, including rifted continental crust or continental margins, such as Noril'sk-Talnakh (Russia), Voisey's Bay (Canada), Jinchuan (China) and Duluth Complex (USA) (Naldrett, 2004; Barnes and Lightfoot, 2005). Ni-Cu-(PGE) deposits associated with orogenic compressive tectonic settings are considered to be uncommon and usually of lesser economic importance (Naldrett, 2004). However, recent discoveries of sizeable Ni-Cu-(PGE) sulfide deposits in

orogenic belts of different ages suggest significant potential for exploration. Large Ni-Cu-(PGE) deposits associated with orogenic belts include, among others, the Katalogke deposit in central Asia orogenic belt (Song and Li, 2009), the Selebi-Phikwe deposit in Botswana (Maier et al., 2008) and the Aguablanca deposit in Spain (Tornos et al., 2001). In Brazil, the potential for exploration in orogenic belts is indicated by recent discoveries or development of Ni-Cu-(PGE) deposits in the Brasília belt (Americano do Brasil deposit, Mota-e-Silva et al., 2011), in the Itabuna-Salvador-Curaçá belt (Santa Rita deposit, Ferreira Filho et al., 2013) and in the Transversal Domain of the Borborema Province (Limoeiro deposit, Mota-e-Silva et al., 2013).

The mafic-ultramafic intrusions described in this study provides a new window for exploration in the Borborema Province. These ca. 2.190±5 Ma intrusions were identified in NNE-SSW trend following steep dipping shear zones. The regional tectonic setting suggest that primary magmas were partial melting of mantle in final stages of the orogeny. The primary magmatic structure of these intrusions, a key feature for mineral exploration, is not yet defined due to poor outcropping. A moderately primitive parental magma is indicated by olivine compositions from wehrlite (Fo content of up to 80.6 %; Ni content up to 2,000 ppm), providing a potentially fertile magma to segregate economic Ni-Cu-PGE deposits. Disseminated sulfides (up to 1 vol %) were identified in outcrops of troctolite in Intrusion 4. They have interstitial texture and composition (pyrrhotite, pentlandite and chalcopyrite) typical of magmatic sulfides segregated from immiscible sulfide liquids. This finding is significant as an indication that both sulfide-saturated and sulfide-unsaturated intrusions occur.

2.6 Conclusions

The principal conclusions of this study are as follows:

1. An array of mafic-ultramafic intrusions occur as small lensoid bodies (< 500 meters long) outcropping in a 32 km long NNE-SSW trend in the paleoproterozoic Rio Piranhas terrain of the Rio Grande do Norte domain (Borborema Province).

2. The mafic-ultramafic intrusions consist of variable proportions of wehrlite (Ol + Cpx ± Chr cumulate), clinopyroxenite (Cpx cumulate) and troctolite (Ol + Pl cumulate).

The primary igneous textures and mineralogy are partially replaced by amphibolite facies metamorphic assemblages and tectonic fabric.

3. The composition of the most primitive olivine indicate parental magmas with moderately primitive compositions ($Fo_{80.6}$ and ~ 2,000 ppm Ni). The compositional range of cumulus plagioclase coexisting with cumulus olivine in troctolites is characterized by very high An content ($An_{89.0}$ to $An_{79.9}$), similar to magma compositions described in subduction-related magmatic arcs.

4. U-Pb zircon ages indicate that mafic-ultramafic intrusions crystallized at ca. 2195±5 Ma. U-Pb zircon ages of host orthogneiss indicate that they crystallized from felsic magmas at ca. 2220-2230 Ma, thus providing a narrow window of time (ca. 30 Ma) for the reported events of felsic and mafic plutonism. U-Pb zircon ages of host rocks also include older ages (ca. 2.50-2.68 Ga) indicating that older crustal components are reworked during mafic and felsic magmatism.

5. Reported mafic-ultramafic and felsic (calc-alkaline) magmatism is correlated with the ca. 2.15-2.25 Ga magmatic arc reported in previous studies of the Rio Piranhas terrain of the Rio Grande do Norte domain.

6. The mafic-ultramafic magmatism is interpreted as originated in a magmatic arc, possibly resulting from partial melting of a mantle wedge above the subduction zone in final stages of the orogeny.

7. The cluster of mafic-ultramafic intrusions described in this study provides a new window for exploration for Ni-Cu-(PGE) deposits in the Borborema Province.

2.7 Acknowledgements

This study is part of the first author's (A.C.D. Ferreira) M.Sc. dissertation developed at the Instituto de Geociências (Universidade de Brasília). The authors are grateful to the Conselho Nacional de Ciência e Tecnologia (CNPq) for continuous support to field and laboratory work through research grants. Cesar F. Ferreira Filho is a Research Fellow of CNPq since 1996, and acknowledges the continuous support through research grants and scholarships for the "Metalogenênese de Depósitos Associados ao Magmatismo Máfico-Ultramáfico" Research Group.

2.8 References

Almeida, F. F. M., Hasui, Y., Brito Neves, B. B., Fuck, R. A., 1981. Brazilian structural provinces: an introduction. Earth Sci. Rev., v.17, pp. 1-29.

Angelim, L. A. A., Medeiros, V. C., Nesi, J. R., 2006. Programa Geologia do Brasil (PGB). Projeto Geologia e Recursos Minerais do Estado do Rio Grande do Norte. Mapa geológico do Estado do Rio Grande do Norte. Escala. 1:500.000. Recife: CPRM/FAPERN.

Araújo, M. G. de S., Brito Neves, B. B. De, Archanjo, C. J., 2001. Idades $^{40}AR/^{39}AR$ do magmatismo básico Meso-Cenozóico da Província Borborema oriental, Nordeste do Brasil. In: SIMPÓSIO DE GEOLOGIA DO NORDESTE. Natal: SBG. Núcleo Nordeste. Boletim do Núcleo Nordeste da SBG, 17, pp. 260-261.

Archanjo, C.J., Salim, J., 1986. Posição da Formação Seridó no Contexto Estratigráfico Regional (RN-PB). Atlas do XII Simpósio de Geologia do Nordeste, pp. 270-281.

Arthaud, M.H., Caby, R., Fuck, R.A., Dantas, E.L., Parente, C.V., 2008. Geology of the northern Borborema Province, NE Brazil and its correlation with Nigeria, NW Africa. In: Pankhurst, R.J., Trouw, R.A.J., Brito Neves, B.B., De Wit, M.J. (Eds.), West Gondwama: Pre-Cenozoic Correlations Across the South Atlantic Region, v. 294. Geological Society of London, Special Publications, pp. 49-67.

Barnes, S. J., Lightfoot P.C., 2005. Formation of magmatic nickel sulfide ore deposits and processes affecting their copper and platinum group element contents. In: Hedenquist JW, Thompson JFH, GoldfarbRJ, Richards JP (eds) Economic Geology, One Hundredth Anniversary Volume, pp. 179-214.

Beard, J.S., 1986. Characteristic mineralogy of arc-related cumulate gabbros: implications for the tectonic setting of gabbroic plutons and for andesite genesis. Geology 14, pp.848–851.

Bertrand, J. M., Jardim De Sá, E. F., 1990. Where are the Eburnean-Transamazonian collisional belts? Can. J. Earth Sci. 27, pp. 1382-1393.

Brito Neves, B. B., 1975. Regionalização geotectônica do Pré-Cambriano Nordestino. Tese de Doutorado. Inst. Geoc. USP, 198p.

Brito Neves, B. B., Van Schmus, W.R., Santos, E. J., Campos Neto, M. C., Kozuch, M., 1995. O Evento Cariris Velhos Na Província Borborema: Integração De Dados, Implicações E Perspectivas. Revista Brasileira de Geociências,v.25, pp. 279-296.

Brito Neves, B. B., Dos Santos, E. J., Van Schmus, W. R., 2000. Tectonic history of the Borborema Province, Northeastern Brazil. In: Cordani, U., Milani, E. J., Thomaz Filho, A., Campos, D. A., (Eds.). Tectonic evolution of South America. 31st International Geological Congress, Rio de Janeiro, Brazil, pp. 151–182.

Brito Neves, B.B., 2011. The Paleoproterozoic in the South-American continent: Diversity in the geologic time. Journal of South American Earth Sciences. v. 32, pp. 270–286.

Bühn, B. M., Pimentel, M, M., Matteini, M., Dantas, E.L., 2009. High spatial resolution analysis of Pb and U isotopes for geochronology by laser ablation multi-collector

inductively coupled plasma mass spectrometry (LA-MC-ICP-MS. Anais da Academina Brasileira de Ciências. v. 81, pp. 1-16.

Caby, R., 1989. Precambrian terranes of Benin-Nigeria, and Northeast Brazil and Late Proterozoic South Atlantic fit. Geol. Soc. America, Spec. Paper, v. 230, pp. 145-158.

Caby, R., Sial, A. N., Arthaud, M., Vauchez, A., 1991. Crustal evolution and the Brasiliano Orogeny in Northeast Brazil. In: DALLMEYER, R. D., LÉCORCHÉ, J. P. (Ed.). The West African Orogens and Circum-Atlantic Correlatives. Berlin: Springer-Verlag, pp. 373-397.

Claeson, D.T., Meurer, W.P., 2004. Fractional crystallisation of hydrous basaltic “arctype” magmas and the formation of amphibole-bearing gabbroic cumulates. Contributions to Mineralogy and Petrology, v. 147, pp. 288–304.

Carvalho, O. O., 1990. Geologia e Petroquímica de Uma Sequência Metavulcanossedimentar no Nordeste da Faixa Seridó, Sudoeste de Lajes, Rio Grande do Norte. Dissertação de Mestrado Nº61. Universidade de Brasília. Instituto de Geociências.

Corfu, F., Hanchar, J.M., Hoskin, P.O.W., Kinny, P., 2003. Atlas of zircon textures. In Zircon (eds Hanchar, J. M. & Hoskin, P.W.O.) 469–500 (Reviews in Mineralogy & Geochemistry, Vol. 53, Mineralogical Society of America and Geochemical Society.

Condie, K.C., 2000. Episodic continental growth models: afterthoughts and extensions. Tectonophysics, v. 322, pp. 153-162.

Da Costa, F.G., Rodrigues, J.B., Naleto, J.L.C., Vasconcelos, A.H., Barrueto, H.R. 2014. 2036 Ma SHRIMP U-Pb zircon age for PGE-bearing chromitite of the Tróia mafic-ultramafic complex, Ceará Central Domain, north Borborema Province. 9TH South American Symposium Isotope Geology, SSAGI, São Paulo, pp. 164.

Dantas, E. L., 1992. Evolução tectono-magmática do maciço polidiapírico São Vicente/Florânia - RN. 1992. 272 p. Dissertação (Mestrado) - Instituto de Geociências e Ciências Exatas, Universidade Estadual Paulista, Rio Claro.

Dantas, E.L., Negrão, M.M., Buhn, B., 2008. 2,3 Ga continental crust generation in the Rio Grande do norte terrane, NE-Brazil (VI SSAGI, San Carlos Bariloche, 2008). Book of Abstracts. In: VI South American Symposium on Isotope Geology. pp. 40. also in CD-rom.

Dantas E.L., Van Schmus W.R., Hackspacher P.C., Fetter A.H., Neves B.B.B., Cordani U.G., Nutman A.P., Williams S., 2004. The 3.4-3.5 São José do Campestre Massif, NE Brazil: remnants of the oldest crust in South America. Precambrian Research., v. 130, pp. 113-137.

Della Giustina, M.E.S., Pimentel, M.M., Ferreira Filho C.F., and Hollanda, M.H.B.M., 2011. Dating coeval mafic magmatism and ultrahigh-temperature metamorphism in the Anápolis-Itauçu Complex, Central Brazil: Lithos, v. 124, pp. 82−102.

Delgado, I.M., Souza, J.D., Silva, L.C., Silveira Filho, N.C., Santos, R.A., Pedreira, A.J., Guimarães, J,T, Angelim, L.A.A., Vasconcelos, A.M., Gomes, I.P., Lacerda Filho, J.V., Valente, C.R., Perrotta, M.P., Heineck, C.A., 2003. Geotectônica do Escudo

Atlântico. In: Bizzi, L.A., Schobbenhaus, C., Vidotti, R.M., Gonçalves, J.H., eds., 2003. Geologia, tectônica e recursos minerais do Brasil. Brasília, CPRM, pp. 259-291.

Depaolo, D. J., 1981. A neodymium and strontium isotopic study of the Mesozoic calc-alkaline granitic batholithys of the Sierra Nevada and Peninsular Ranges, California. Journal of Geophysical Research, v. 86, pp. 10470-10488.

Droop, G. T. R., 1987. A general equation for estimating Fe3+ concentrations in ferromagnesian silicates and oxides from microprobe analyses, using stoichiometric criteria. Mineralogical Magazine, v. 51, pp. 431-435.

Eales, H.V., Cawthorn, R.G., 1996. The Bushveld Complex. In: Cawthorn, R.G. (Ed.), Layered Intrusions. Elsevier, Amsterdam, pp. 181–229.

Ferreira Filho, C. F., Naldrett, A. J., Gorton, M.P., 1998. REE and pyroxene compositional variation across the Niquelândia layered intrusion, Brazil: petrological and metallogenetic implications. Trans Inst Min Metall (Applied Earth Sciences) 107:B1–B21.

Ferreira Filho, C.F., Pimentel, M.M., Araújo, S.M., Laux, J.H., 2010. Layered intrusions and volcanic sequences in Central Brazil: geological and geochronological constraints for Mesoproterozoic (1.25 Ga) and Neoproterozoic (0.79 Ga) igneous associations. Precambrian Research, v. 183, pp. 617–634.

Ferreira Filho, C. F., Cunha, J.C., Cunha, E.M. and Canela, J.H.C., 2013. Depósito de níquel, cobre sulfetado de Santa Rita, Itagibá, Bahia, Brasil. Série Arquivos Abertos, v. 39, Companhia Baiana de Pesquisa Mineral (CBPM), Salvador-Bahia, 59 pp.

Fetter, A. H., Van Schmus, W. R., Santos, T. J. S., Neto, J. A. N., Henriarthaud, M., 2000. U-Pb and Sm-Nd geochronological constraints on the crustal evolution and basement architecture of Ceará State, NW Borborema Province, NE Brazil: Implications for the existence of the Paleoproterozoic supercontinent Atlantica., v. 30, pp. 102-106.

Gioia, S. M. C. L., Pimentel, M. M., 2000. The Sm-Nd isotopic method in the Geochronology Laboratory of the University of Brasília. Anais Academia Brasileira de Ciências, v. 72, pp. 219-245.

Hackspacher, P.C., Van Schmus, W.R., Dantas, E.L., 1990. Um embasamento Transamazônico na Provincia Borborema. Congresso Brasileiro de Geologia, 36, Natal, Anais, v. 6, pp. 2683-2696.

Hollanda, M.H.B.M., Jardim De Sa´, E.F., Pimentel, M.M., Macedo, M.H.F., 1999. Sr–Nd isotopic evidence of an archaean source involved in the Brasiliano syntectonic alkaline magmatism (Serido´ Belt, Northeastern Brazil). II South American Symposium on Isotope Geology (Cordoba, Argentina) Proceedings, pp. 215–218.

Hollanda, M.H.B.M., Pimentel, M.M., Jardim De Sá, E.F., 2003. Paleoproterozoic subduction-related metasomatic signatures in the lithospheric mantle beneath NE Brazil: Inferences from trace element and Sr-Nd-Pb isotopic compositions of Neoproterozoic high-K igneous rocks. Journal of South American Earth Sciences, v. 15, pp. 885-900.

Hollanda, M. H. B. M., Archanjo, C. J., Souza, L. C., Dunyi, L., Armstrong, L., 2011. Long-lived Paleoproterozoic granitic magmatism in the Seridó-Jaguaribe domain, Borborema Province-NE Brazil. Journal of South American Earth Sciences, v. 32, pp. 287-300.

Hollanda, M.H.B.M., Archanjo, C. J., Bautista, J. R., Souza, L. C., 2015. Detrital zircon ages and Nd isotope compositions of the Seridó andLavras da Mangabeira basins (Borborema Province, NE Brazil): Evidence for exhumation and recycling associated with a major shiftin sedimentary provenance. Precambrian Research, v. 258, pp.186–207.

Jackson, S.E., Pearson, N. J., Griffin, W.L., Belousova, E.A., 2004. The application of laser ablation-inductively coupled plasma-mass spectrometry to in situ U-Pb zircon geochronology. Chemical Geology, v. 211, pp. 47-69.

Jardim de Sá, E.F., 1994. A Faixa Seridó (Província Borborema, Ne Brasil) e o seu Significado Geodinâmico na Cadeia Brasiliana/Pan-Africana. Unpublished Ph.D. Thesis, Universidade De Brasília, 803pp.

Jesus, B. A., 2011. Rochas Máficas e Ultramáficas do Complexo Riacho Da Telha, Maciço São José Do Campestre, Província Borborema, NE Do Brasil. Dissertação de Mestrado, IG-UnB, 80pp.

Kamenetsky, V.S., Maas, R., Fonseca, R.O.C., Balhaus, C., Heuser, A., Brauns, M., Norman, M.D., Woodhead, J.D., Rodemann, T., Kuzmin, D.V., Bonatti, E., 2013. Noble metals potential of sulfide-saturated melts from subcontinental lithosphere. Geology v.41, pp. 575-578.

Knesel, K.M., Souza, Z.S., Vasconcelos, P.M., Cohen, B.E., Silveira, F.V., 2011. 40Ar/39Ar geochronology reveals the youngest volcanism in mainland Brazil and no evidence for a plume trace on the continent. Earth and Planetary Sciences Letters, v. 302, pp. 38-50.

Lages, G.A., 2014. Os complexos máfico-ultrameaficos mineralizados (Fe-Ti±V±Cu±Cr) de Floresta e Bodocó na porção ocidental da Província Borborema e suas implicações geodinâmicas para a evolução da parte oeste da Zona Transversal. Dissertação de Mestrado, IG-UnB, 116 pp.

Leake, B.E., Wooley, A.R., Arps, C.E.S., Birch, W.D., Gilbert, M.C., Grice, J.D., Hawthorne, F.C., Kato, A., Kisch H.J., Krivovichev, V.G., Linthout, K., Laird, J., Mandarino, J.A., Maresch, W.V., Nickel, E.H., Schumacher, J., Smith, J.C., Stephenson, N.C. N., Ungaretti, L., Whittaker, E.J.W., Youzhi G., 1997. Nomenclature of Amphiboles: Report of the Subcommittee on Amphiboles of the International Mineralogical Association Commission on New Minerals and Mineral Names. Mineral. Mag., v. 61, pp.295-321.

Legrand, J. M., Dantas, E. L., Liegeois, J. P., 1997. Definição e caracterização do embasamento da porção Oeste da Faixa Seridó (Província Borborema, NE-Brasil). In: SIMPÓSIO DE GEOLOGIA DO NORDESTE, 17, Fortaleza. Resumos expandidos. Fortaleza: SBG. Núcleo Nordeste, 1997. 537pp. il. (Boletim do Núcleo Nordeste da SBG, 15) pp.50-55.

Legrand, J. M., Liegeois, J. P., Deutsch, S., 1991. Datação U/Pb e Rb/Sr das rochas pré-cambrianas da região de Caicó. Reavaliação da definição de um embasamento arqueano. In: SIMPÓSIO DE GEOLOGIA DO NORDESTE, 14, 1991, Recife. Atas. Recife: SBG. v. 12, pp. 276-279.

Lightfoot, P.C., Evans-Lamswood, D., 2014. Structural controls on the primary distribution of mafic–ultramafic intrusions containing Ni–Cu–Co–(PGE) sulfide mineralization in the roots of large igneous provinces. Ore Geology Reviews, v. 64, pp. 354–386.

Ludwig, K.R., 1993. PBDAT, a computer program for processing Pb–U–Th isotope data. USGS Open File Report, v. 88, 34pp.

Ludwig, K.R., 2001. User´s Manual for Isoplot/Ex version 2.47. A geochronological toolkit for Microsoft Excel. Berkeley Geochronology Center Special Publication 1a, 55 p.

Maier, W.D., Barnes, S-J., Chinyepi, G., Barton, Jr. JM., Eglington, B., Setshedi, I., (2008) The composition of magmatic Ni–Cu–(PGE) sulfide deposits in the Tati and Selebi-Phikwe belts of eastern Botswana. Miner Depos, v. 43, pp. 37–60.

Maier, W.D., Groves, D.I., 2011. Temporal and spatial controls on the formation of magmatic PGE and Ni-Cu deposits. Min. Depos., v. 46, pp. 841-857.

Martin, H., 1993. The mechanisms of petrogenesis of the Archean continental crust Comparison with modern processes. Lithos, v. 30, pp. 373-388.

Martin, H., 1994. The Archean grey gneiss and the genesis of continental crust. In: Condie, K. C. (ed) The Archean Crustal Evolution. Amsterdam: Elsevier, pp. 205-259.

McBirney, A.R., 1989. The Skaergaard Layered Series: I. Structure and average composition: Journal of Petrology, v. 30, pp. 363−397.

Mcdonough, W.F., Sun, S.S., 1995. The composion of the Earth, Chemical Geology, v. 120, pp. 228.

Medeiros, V.C., Nascimento, M. A. L., Galindo, A. C., Dantas, E. L., 2012. Augen gnaisses riacianos no Domínio Rio Piranhas-Seridó – Província Borborema, Nordeste do Brasil. Revista do Instituto de Geociências – USP. Geol. USP, Sér. cient., São Paulo, v. 12, pp. 3-14.

Mota-e-Silva, J., Ferreira Filho, C.F., Bühn, B., Dantas, E.L., 2011, Geology, petrology and geochemistry of the “Americano do Brasil” layered intrusion, central Brazil, and its Ni-Cu sulfide deposits: Mineralium Deposita, v. 46, pp. 57–90.

Mota-e-Silva, J., Ferreira Filho, C.F., Giustina, M.E.S., 2013. The Limoeiro deposit: Ni-Cu-PGE sulfide mineralization hosted within an Ultramafic tubular magma conduit in the Borborema Province, Northeastern Brazil. Econ Geol, v. 108, pp. 1753–1771.

Mota-e-Silva, J., Prichard, H.M., Ferreira Filho, C.F., Fisher, P.C., McDonald, I., 2015. Platinum-group minerals in the Limoeiro Ni–Cu–(PGE) sulfide deposit, Brazil: the effect of magmatic and upper amphibolite to granulite metamorphic processes on PGM formation. Miner Deposita, DOI 10.1007/s00126-015-0585-0.

Naldrett, A.J., 2004. Magmatic Sulfide Deposits – Geology, Geochemistry and Exploration. Germany, Springer Berlin, 724pp.

Nascimento, M.A.L., Medeiros, V.C., Galindo, A.C., 2008. Magmatismo Ediacarano a Cambriano no Domínio Rio Grande do Norte, Província Borborema, NE do Brasil. Estudos Geológicos, v. 18, pp. 4-29.

Nascimento, M.A.L., Galindo, A.C., Medeiros, V.C., 2014. Ediacaran to Cambrian magmatic suites in the Rio Grande do Norte domain, extreme Northeastern Borborema Province (NE of Brazil): Current knowledge. Journal of South American Earth Sciences, v. 58, pp. 281-299.

Pimentel, M.M.; Ferreira Filho, C.F.; Armele, A. 2006. Neoproterozoic age of the Niquelândia Complex, central Brazil: further ID-TIMS and Sm-Nd isotopic evidence. Journal of South American Earth Science, 21: 228-238.

Pirajno, F., Ernst, R.E., Borisenko, A.S., Fedoseev, G., Naumov, E.A., 2009, Intraplate magmatism in Central Asia and China and associated metallogeny. Ore Geology Reviews, v. 35, pp. 114–136.

Price, R., Sprandler, C., Arculus, R., Reay, A., 2011. The Longwood Igneous Complex, Southland, New Zealand: A Permo-Jurassic, intra-oceanic, subduction-related, I-type batholithic complex. Lithos, v. 126, pp. 1–21.

Reddy, S. M., Evans, D.A.D., 2009. Paleoproterozoic supercontinents and global evolution: Correlations from core to atmosphere. In: Reddy, S.M., Mazunder, R., Evans, D.A.D., Collins, A.S. (eds) Paleoproterozoic Supercontinents and Global Evolution.

Sá, J.M., Mcreath, I., Letterrier, J., 1995. Petrology, geochemistry and geodynamic setting of Proterozoic igneous suites of the Orós fold belt (Borborema Province, Northeast Brazil). J. South Amer. Earth Sc., v. 8, pp 299-314.

Sá, J. M., Souza, L. C., Legrand, J. M., Galindo, A. C., Maia, H. N., Fillippi, R. R., 2014. U-Pb and Sm-Nd data of the Rhyacian and Statherian Orthogneisses from Rio Piranhas-Seridó and Jaguaribeano Terranes, Borborema Province, Northeast of Brazil. Geol. USP, Sér. cient, v.14, pp. 97-110.

Santos, L.C.M.L., Dantas E. L., Santos, E. J., Lima, H. M., 2014. Early to Late Paleoproterozoic magmatism in NE Brazil: The Alto Moxoto Terrane and its tectonic implications for the Pre-West Gondwana assembly. Journal of South American Earth Sciences, v. 58, pp. 188-209.

Santos, E.J., 1996. Ensaio preliminar sobre terrenos e tectônica acrescionária na Província Borborema. In 39º Congresso Brasileiro de Geologia, v 1, pp. 47-50.

Santos, E.J., Van Schmus,W.R., Kozuch, M., Brito Neves, B.B., 2010. The Cariris Velhos tectonic event in northeast Brazil. Journal of South American Earth Sciences, v. 29, pp. 61-76.

Salgado, S.S., Ferreira Filho C.F., Uhlein A., Caxito F. A., 2014. Geologia, Estratigrafia e Petrografia do Complexo de Brejo Seco, Faixa Riacho do Pontal, sudeste do Piauí. Revista Geonomos, v. 22.

Silveira, F.V., 2006. Magmatismo Cenozóico da Porção Central do Rio Grande do Norte, NE do Brasil. Ph.D. Thesis n°15 / PPGG, Universidade Federal do Rio Grande do Norte, 220pp.

Song, X.Y., Li, X.R., 2009, Geochemistry of the Kalatongke Ni-Cu-(PGE) sulfide deposit, NW China: Implications for the formation of magmatic sulfide mineralization in a postcollisional environment. Mineralium Deposita, v. 44, pp. 303−327.

Souza, Z. S., Martin, H., Macedo, M. H., Peucat, J. J., Jardim de Sá, E. F., 1993. Un segment de croûte continentale juvénile d'àge protérozoique inférieur: le Complexe de Caicó (Rio Grande do Norte, NE-Brésil). Comptes Rendus de l'Académie de Sciences, v. 316, pp. 201-208.

Souza, Z. S., Martin, H., Peucat, J. J., Jardim De Sá, E. F., Macedo, M. H. F., 2007. Calc-Alkaline Magmatism At The Archean-Proterozoic Transition: The Caicó Complex Basement (Ne Brasil). Jounal of Petrology, v. 48, pp. 2149-2185.

Su, B.X., Qin, K.Z., Sakyi, P.A, Li, X.H., Yang, Y.H., Sun, H., Tang, D.M., Liu, P.P., Xiao, Q.H., Malaviarachchi, S.P.K., 2011. U–Pb ages and Hf–O isotopes of zircons from Late Paleozoic mafic–ultramafic units in southern Central Asian Orogenic Belt: tectonic implications and evidence for an Early-Permian mantle plume. Gondwana Res., v. 20, pp. 516–531.

Sun, S. S., McDonough, W.F., 1989. Chemical and isotopic systematics of oceanic basalts: implications for mantle composition and processes. In: Saunders, A.D., Norry, M.J. Eds., Magmatism in Ocean Basins. Geol. Soc. Spec. Publ., London, pp. 313–345.

Taylor, S. R., McLennan, S. M., 1985. The Continental Crust: its Composition and Evolution. Oxford: Blackwell, 312 pp.

Teixeira, A.S., Ferreira Filho, C.F., Della Giustina, M.E.S., Araujo, S.M., Silva, H.H.A.B., 2015. Geology, petrology and geochronology of the Lago Grande layered complex: Evidence for a PGE-mineralized magmatic suite in the Carajas Mineral Province, Brazil. Journal of South American Earth Sciences, v. 64, pp. 116-138.

Tornos, F., Casquet, C., Galindo, C., Velasco, F., Canales, A., (2001) A new style of Ni–Cu mineralization related to magmatic breccia pipes in a transpressional magmatic arc, Aguablanca, Spain. Miner Deposita, v. 36, pp. 700–706.

Van Schmus, W. R., Dantas, E., Fetter, A., Brito Neves, B. B.; Hackspacher, P. C., Babinsk, M., 1995. Neoproterozoic Age for Seridó Group, NE Borborema Province, Brazil. Anais do XXXIX Cong. Bras. Geol., v. 6, pp.152-155.

Van Schmus, W. R., Brito Neves, B.B., Williams, I. S., Hackspacher, P. C., Fetter, A. H., Dantas, E. L., Babinski, M., 2003. The Seridó Group of NE Brazil, a late Neoproterozoic pre-to syn-collisional basin in West Gondwana: insights form SHRIMP U-Pb detrital zircon ages and Sm-Nd crustal residence (TDM) ages. Precambrian Research, v. 127, pp. 287-327.

Van Schmus, W.R., Oliveira, E.P, Silva Filho, A.F., Toteu, S.F., Penaye, J., Guimarães, I. P., 2008. Proterozoic links between the Borborema Province, NE Brazil, and the Central African Fold Belt. In: Pankhurst R.J., Trouw R.A.J., Brito Neves B.B & De Wit M.J. (eds.) West Gondwana: Pre-Cenozoic correlations across the South Atlantic region. Geological Society, London, Special Publication, v. 294, pp. 69-99.

Van Schmus, W.R., Kozuch, M., Brito Neves, B.B. 2011. Precambrian history of theZona Transversal of the Borborema Province, NE Brazil: insights from Sm–Ndand U–Pb geochronology. J. S. Am. Earth Sci. v. 31, pp. 227–252.

Vavra, G., 1990. On the kinematics of zircon growth and its petrogenetic significance: a cathodoluminescence study. Contributions to Mineralogy and Petrology, v. 106, pp. 90–99.

Whitney, D.L., Evans, B.W., 2010. Abbreviations for names of rock-forming minerals. American Mineralogist, v. 95,pp. 185-187.

Wiedenbeck, M., AllÉ, P., Corfu, F., Griffin, W.L., Meier, M., Oberli, F., Quadt, A.V., Roddick, J.C., Spiegel, W., 1995. Three natural zircon standards for U–Th–Pb, Lu–Hf, trace element and REE analyses. Geostand. Newsl., v. 19, pp. 1–23.

Zhang, Z.C., Mao, J.W., Chai, F.M., Yan, S.H., Chen, B.L., and Pirajno, F., 2009. Geochemistry of the Permian Kalatongke mafic intrusions, North Xinjiang, Northwest China: Implications for the genesis of magmatic Ni-Cu sulfide deposits: ECONOMIC GEOLOGY, v. 104, pp. 185−203.

3. CONCLUSÕES

As principais conclusões desse estudo são as seguintes:

1. Intrusões máfica-ultramáficas afloram sob a forma de corpos lenticulares (<500 metros de comprimento) ao longo de trend de mais de 30 km de direção NNE-SSW no Terreno Rio Piranhas, porção central do Domínio Rio Grande do Norte.

2. As rochas máfica-ultramáficas são constituídas por proporções variádas de wehrlitos (Ol + Cpx ± Chr cúmulus), clinopiroxenitos (Cpx cúmulos) e troctolitos (Ol + Pl cúmulos). A mineralogia e a textura ígnea primária são parcialmente substituídas por assembleia metamórfica do fácies anfibolito e trama tectônica.

3. A composição das olivinas mais primitivas indicam magmas parentais com composições moderadamente primitiva ($Fo_{80,6}$ e ~ 2000 ppm de Ni). A composição dos plagioclásios em equílibrio com olivina cúmulus em troctolitos é caracterizada por elevados teores da anortita ($An_{89,0}$ para $An_{79,9}$). Este campo de variação de Fo e An é correlacionável a composições de magma descritos em ambientes de arcos magmáticos relacionados a subdução.

4. Idades sistemáticas U-Pb em zircão apotam idade de 2195 ± 5 Ma para a cristalização das intrusões máfica-ultramáficas. As encaixantes ortognáissicas apresentam idades U-Pb em zircão magmáticos entre 2220-2230 Ma. Assim, têm-se uma estreita janela de tempo (cerca de 30 Ma) entre os eventos plutonicos félsico e máficos. Datação U-Pb em zircões obtida em rocha encaixante (biotita gnaisse) revelou idade sideriana de 2,47 Ga, com zirções herdados de 2,50-2,71Ga indicando que componentes crustais neoarqueanos foram retrabalhados durante magmatismo máfico e félsico riaciano.

5. Magmatismo máfico-ultramáfico é interpretado como originado em um ambiente de arco magmático, possivelmente resultante da fusão parcial de uma cunha do manto acima da zona de subducção em fases finais do orogênese.

6. Magmatismo máfico-ultramáfico e félsico (cálcioalcalino) pode ser correlacionado a atuação de arcos magmáticos de 2,15 - 2,25 Ga relatado em estudos anteriores no Domínio Rio Grande do Norte.

7. As intrusões máfica-ultramáficas descritas neste estudo abrem uma nova janela para a exploração dos depósitos de Ni-Cu (PGE) na Província Borborema.

4. ANEXOS

Tabela 9 – Química mineral das olivinas estudadas.

Rocha	Amostra	SiO_2	Al_2O_3	Cr_2O_3	MgO	MnO	FeO	NiO	Total	Si	Al	Cr	Mg	Mn	Fe^{2+}	Ni	Total	Fo
Intrusão 2 Wehrlito	A-01A	36.96	0.00	0.00	37.05	0.50	25.78	0.15	100.4	0.97	0.00	0.00	1.45	0.01	0.57	0.00	3.00	71.9
		37.42	0.00	0.00	36.65	0.53	25.30	0.10	100.0	0.99	0.00	0.00	1.44	0.01	0.56	0.00	3.00	72.1
		37.10	0.02	0.00	37.08	0.46	25.15	0.16	100.0	0.98	0.00	0.00	1.45	0.01	0.55	0.00	3.00	72.4
		37.55	0.02	0.10	37.47	0.61	25.36	0.18	101.3	0.98	0.00	0.00	1.45	0.01	0.55	0.00	3.00	72.5
		36.97	0.00	0.00	35.10	0.62	27.33	0.11	100.1	0.98	0.00	0.00	1.39	0.01	0.61	0.00	3.00	69.6
		37.14	0.00	0.00	36.68	0.61	26.27	0.22	100.9	0.97	0.00	0.00	1.43	0.01	0.58	0.00	3.00	71.3
		37.67	0.00	0.00	38.67	0.47	24.05	0.16	101.0	0.97	0.00	0.00	1.49	0.01	0.52	0.00	3.00	74.1
		38.05	0.00	0.00	38.59	0.42	23.78	0.18	101.0	0.98	0.00	0.00	1.49	0.01	0.51	0.00	3.00	74.3
		37.58	0.00	0.00	38.82	0.43	22.75	0.08	99.7	0.98	0.00	0.00	1.51	0.01	0.50	0.00	3.00	75.3
		38.03	0.01	0.00	38.50	0.44	22.96	0.22	100.2	0.99	0.00	0.00	1.49	0.01	0.50	0.00	3.00	74.9
Intrusão 2 Wehrlito	A-01C	37.98	0.00	0.03	42.15	0.29	18.65	0.22	99.3	0.97	0.00	0.00	1.61	0.01	0.40	0.00	3.00	80.1
		38.11	0.01	0.01	42.44	0.34	18.68	0.09	99.7	0.97	0.00	0.00	1.62	0.01	0.40	0.00	3.00	80.2
		37.82	0.00	0.03	41.77	0.25	19.44	0.25	99.6	0.97	0.00	0.00	1.60	0.01	0.42	0.01	3.00	79.3
		38.29	0.00	0.05	42.04	0.32	19.56	0.14	100.4	0.98	0.00	0.00	1.60	0.01	0.42	0.00	3.00	79.3
		37.48	0.00	0.00	34.97	0.39	21.56	0.14	94.5	1.04	0.00	0.00	1.44	0.01	0.50	0.00	2.99	74.3
		37.95	0.00	0.00	41.86	0.33	19.10	0.18	99.4	0.97	0.00	0.00	1.60	0.01	0.41	0.00	3.00	79.6
		38.29	0.00	0.01	41.98	0.19	18.50	0.17	99.1	0.98	0.00	0.00	1.61	0.00	0.40	0.00	3.00	80.2
		38.32	0.02	0.09	42.85	0.27	18.37	0.16	100.1	0.97	0.00	0.00	1.62	0.01	0.39	0.00	3.00	80.6
Intrusão 2 Wehrlito	A-23A	36.12	0.00	0.09	34.82	0.41	26.86	0.06	98.4	0.98	0.00	0.00	1.40	0.01	0.61	0.00	3.00	69.8
		36.61	0.04	0.03	29.76	0.48	28.75	0.13	95.8	1.04	0.00	0.00	1.26	0.01	0.68	0.00	2.99	64.9
		36.77	0.00	0.01	32.37	0.40	28.31	0.10	98.0	1.01	0.00	0.00	1.32	0.01	0.65	0.00	3.00	67.1
		36.86	0.01	0.06	34.88	0.35	27.77	0.11	100.0	0.98	0.00	0.00	1.39	0.01	0.62	0.00	3.00	69.1
		36.95	0.01	0.04	34.83	0.42	27.47	0.13	99.8	0.99	0.00	0.00	1.39	0.01	0.61	0.00	3.00	69.3
		36.99	0.00	0.04	35.58	0.46	27.00	0.07	100.1	0.98	0.00	0.00	1.41	0.01	0.60	0.00	3.00	70.1
		37.11	0.02	0.01	33.76	0.45	27.47	0.09	98.9	1.00	0.00	0.00	1.36	0.01	0.62	0.00	3.00	68.7

Rocha	Amostra	SiO_2	Al_2O_3	Cr_2O_3	MgO	MnO	FeO	NiO	Total	Si	Al	Cr	Mg	Mn	Fe^{2+}	Ni	Total	Fo
		36.23	0.01	0.00	34.42	0.44	27.58	0.14	98.8	0.98	0.00	0.00	1.39	0.01	0.62	0.00	3.00	69.0
		34.06	0.05	0.01	32.05	0.50	27.75	0.09	94.5	0.97	0.00	0.00	1.36	0.01	0.66	0.00	3.00	67.3
		36.69	0.00	0.00	34.50	0.56	27.34	0.14	99.2	0.99	0.00	0.00	1.38	0.01	0.61	0.00	3.00	69.2
		36.93	0.00	0.01	33.71	0.63	28.00	0.22	99.5	0.99	0.00	0.00	1.35	0.01	0.63	0.00	3.00	68.2
		36.86	0.00	0.00	31.07	0.49	28.80	0.09	97.3	1.02	0.00	0.00	1.29	0.01	0.67	0.00	2.99	65.8
		36.57	0.00	0.00	35.04	0.45	27.26	0.11	99.4	0.98	0.00	0.00	1.40	0.01	0.61	0.00	3.00	69.6
		36.58	0.36	0.09	35.38	0.48	26.87	0.12	99.9	0.97	0.01	0.00	1.40	0.01	0.60	0.00	3.00	70.1
		37.16	0.03	0.00	30.79	0.51	29.15	0.08	97.7	1.03	0.00	0.00	1.27	0.01	0.68	0.00	3.00	65.3
		36.89	0.00	0.01	32.01	0.42	28.57	0.17	98.1	1.01	0.00	0.00	1.31	0.01	0.66	0.00	3.00	66.6
		36.23	0.00	0.01	34.35	0.54	27.49	0.06	98.7	0.98	0.00	0.00	1.38	0.01	0.62	0.00	3.00	69.0
Intrusão 2 Wehrlito	A-23B	39.15	0.00	0.00	43.16	0.19	19.33	0.10	101.9	0.98	0.00	0.00	1.61	0.00	0.40	0.00	3.00	79.9
		38.88	0.01	0.07	43.13	0.23	18.47	0.12	100.9	0.98	0.00	0.00	1.62	0.00	0.39	0.00	3.00	80.6
		39.18	0.00	0.00	42.78	0.38	19.24	0.10	101.7	0.98	0.00	0.00	1.60	0.01	0.40	0.00	3.00	79.9
		38.61	0.01	0.00	42.22	0.24	18.92	0.13	100.1	0.98	0.00	0.00	1.60	0.01	0.40	0.00	3.00	79.9
		38.73	0.00	0.05	42.48	0.26	18.83	0.16	100.5	0.98	0.00	0.00	1.61	0.01	0.40	0.00	3.00	80.1
		38.82	0.00	0.03	42.65	0.15	18.95	0.14	100.7	0.98	0.00	0.00	1.61	0.00	0.40	0.00	3.00	80.0
		39.98	0.00	0.01	44.87	0.27	18.85	0.14	104.1	0.97	0.00	0.00	1.63	0.01	0.38	0.00	3.00	80.9
Intrusão 2 Wehrlito	A-24C	36.00	0.01	0.03	39.62	0.27	17.67	0.16	93.7	0.98	0.00	0.00	1.61	0.01	0.40	0.00	3.00	80.0
		35.73	0.00	0.04	39.77	0.15	17.61	0.08	93.4	0.97	0.00	0.00	1.62	0.00	0.40	0.00	3.00	80.1
		34.68	0.26	1.25	32.13	0.24	12.25	0.11	80.9	1.08	0.01	0.03	1.49	0.01	0.32	0.00	2.94	82.4
		34.94	0.00	0.00	38.72	0.15	17.06	0.09	90.9	0.98	0.00	0.00	1.62	0.00	0.40	0.00	3.00	80.2
		35.84	0.02	0.04	39.23	0.19	16.08	0.09	91.5	0.99	0.00	0.00	1.62	0.00	0.37	0.00	3.00	81.3
		26.65	0.14	0.02	29.65	0.12	8.36	0.11	65.0	1.02	0.01	0.00	1.69	0.00	0.27	0.00	2.99	86.3
		37.21	0.02	0.00	36.44	0.07	7.47	0.18	81.4	1.14	0.00	0.00	1.66	0.00	0.19	0.00	3.00	89.7
Intrusão 4 Troctolito	A-38B	37.73	0.01	0.00	33.95	0.22	28.37	0.02	100.3	1.01	0.00	0.00	1.35	0.01	0.63	0.00	3.00	68.1
		36.17	0.01	0.00	34.52	0.25	27.54	0.07	98.6	0.98	0.00	0.00	1.39	0.01	0.62	0.00	2.99	69.1
		36.36	0.00	0.00	34.47	0.36	28.43	0.07	99.7	0.97	0.00	0.00	1.38	0.01	0.64	0.00	3.00	68.4
		36.42	0.00	0.00	33.93	0.31	27.87	0.10	98.6	0.99	0.00	0.00	1.37	0.01	0.63	0.00	3.00	68.5
		36.13	0.00	0.01	34.54	0.29	28.09	0.02	99.1	0.97	0.00	0.00	1.39	0.01	0.63	0.00	3.00	68.7

Rocha	Amostra	SiO_2	Al_2O_3	Cr_2O_3	MgO	MnO	FeO	NiO	Total	Si	Al	Cr	Mg	Mn	Fe^{2+}	Ni	Total	Fo
		36.48	0.02	0.01	34.59	0.35	28.03	0.04	99.5	0.98	0.00	0.00	1.38	0.01	0.63	0.00	3.00	68.7
		37.37	0.00	0.00	33.79	0.14	28.51	0.08	99.9	1.00	0.00	0.00	1.35	0.00	0.64	0.00	3.00	67.9
		36.21	0.00	0.00	34.51	0.31	27.87	0.11	99.0	0.98	0.00	0.00	1.39	0.01	0.63	0.00	3.00	68.8
		37.06	0.01	0.00	33.67	0.30	28.61	0.08	99.7	1.00	0.00	0.00	1.35	0.01	0.64	0.00	3.00	67.7
		36.21	0.00	0.00	34.14	0.28	28.69	0.10	99.4	0.97	0.00	0.00	1.37	0.01	0.65	0.00	3.00	68.0
		37.27	0.00	0.00	33.71	0.24	28.75	0.08	100.0	1.00	0.00	0.00	1.35	0.01	0.64	0.00	3.00	67.6
		36.08	0.00	0.00	34.17	0.25	28.50	0.07	99.1	0.97	0.00	0.00	1.38	0.01	0.64	0.00	3.00	68.1
		37.16	0.02	0.02	33.89	0.33	28.36	0.16	99.9	1.00	0.00	0.00	1.35	0.01	0.64	0.00	3.00	68.1
		36.40	0.02	0.00	34.48	0.25	27.79	0.07	99.0	0.98	0.00	0.00	1.38	0.01	0.63	0.00	3.00	68.9
		36.48	0.01	0.00	34.46	0.32	27.62	0.05	98.9	0.98	0.00	0.00	1.39	0.01	0.62	0.00	3.00	69.0
		36.33	0.03	0.00	34.19	0.33	27.77	0.11	98.8	0.98	0.00	0.00	1.38	0.01	0.63	0.00	3.00	68.7
		36.47	0.02	0.00	34.14	0.34	28.38	0.12	99.5	0.98	0.00	0.00	1.37	0.01	0.64	0.00	3.00	68.2
		36.19	0.03	0.00	33.46	0.37	28.10	0.08	98.2	0.99	0.00	0.00	1.36	0.01	0.64	0.00	3.00	68.0
		36.08	0.00	0.04	34.05	0.23	28.49	0.05	98.9	0.98	0.00	0.00	1.37	0.01	0.64	0.00	3.00	68.1
Intrusão 4 Troctolito	A-38D	36.45	0.02	0.00	35.05	0.11	27.48	0.03	99.1	0.98	0.00	0.00	1.40	0.00	0.62	0.00	3.00	69.5
		36.59	0.00	0.00	35.27	0.34	27.38	0.09	99.7	0.98	0.00	0.00	1.40	0.01	0.61	0.00	3.00	69.7
		36.79	0.04	0.06	35.45	0.28	27.40	0.04	100.1	0.98	0.00	0.00	1.40	0.01	0.61	0.00	2.99	69.8
		36.41	0.02	0.00	35.33	0.32	27.10	0.05	99.2	0.97	0.00	0.00	1.41	0.01	0.61	0.00	3.00	69.9
		36.57	0.00	0.00	35.23	0.18	27.44	0.12	99.5	0.98	0.00	0.00	1.40	0.00	0.61	0.00	3.00	69.6
		36.48	0.00	0.04	34.51	0.24	28.04	0.04	99.3	0.98	0.00	0.00	1.38	0.01	0.63	0.00	3.00	68.7
		36.63	0.02	0.00	34.28	0.26	27.70	0.03	98.9	0.99	0.00	0.00	1.38	0.01	0.62	0.00	3.00	68.8
		36.91	0.00	0.00	34.79	0.24	27.57	0.08	99.6	0.99	0.00	0.00	1.39	0.01	0.62	0.00	3.00	69.2
		36.29	0.01	0.05	34.87	0.27	27.38	0.11	99.0	0.97	0.00	0.00	1.40	0.01	0.62	0.00	3.00	69.4

*Fórmula estrutural calculada na base de 4 oxigênios.

Tabela 10: Química mineral dos clinopiroxênios estudados.

	Amostra	SiO_2	TiO_2	Al_2O_3	Cr_2O_3	MgO	CaO	MnO	FeO	NiO	Na_2O	Total	Si	Ti	Al	Cr	Mg	Ca	Mn	Fe^{2+}	Ni	Na	Total	%En	Mineral
Intrusão 2 - Wehrlito	A-01C	51.02	0.44	4.46	0.36	17.15	21.04	0.13	4.72	0.00	0.16	99.5	1.87	0.01	0.19	0.01	0.93	0.82	0.00	0.09	0.00	0.01	3.9	49.11	Aug
		51.21	0.23	2.91	0.23	16.03	23.75	0.17	3.96	0.00	0.14	98.6	1.90	0.01	0.13	0.01	0.88	0.94	0.01	0.04	0.00	0.01	3.9	45.38	Di
		50.45	0.15	4.48	0.32	15.64	22.96	0.14	4.07	0.00	0.25	98.5	1.87	0.00	0.20	0.01	0.86	0.91	0.00	0.06	0.00	0.02	3.9	45.43	Di
		56.42	0.25	2.03	0.14	23.05	12.94	0.05	3.19	0.04	0.20	98.3	2.04	0.01	0.09	0.00	1.24	0.50	0.00	0.10	0.00	0.01	4.0	67.52	Aug
		51.21	0.10	3.09	0.23	16.28	24.00	0.11	3.29	0.01	0.15	98.5	1.89	0.00	0.13	0.01	0.90	0.95	0.00	0.02	0.00	0.01	3.9	46.02	Di
		50.44	0.05	4.21	0.53	15.87	23.07	0.08	4.28	0.01	0.22	98.8	1.86	0.00	0.18	0.02	0.87	0.91	0.00	0.04	0.00	0.02	3.9	45.54	Di
		51.00	0.25	3.45	0.31	15.46	23.05	0.16	4.70	0.00	0.31	98.7	1.89	0.01	0.15	0.01	0.85	0.92	0.00	0.06	0.00	0.02	3.9	44.59	Di
		50.39	0.46	4.24	0.32	15.51	23.38	0.13	4.23	0.00	0.24	98.9	1.86	0.01	0.18	0.01	0.85	0.93	0.00	0.05	0.00	0.02	3.9	44.72	Di
	A-23B	50.96	0.05	3.55	0.18	18.50	18.24	0.16	7.19	0.03	0.21	99.1	1.87	0.00	0.15	0.01	1.01	0.72	0.00	0.11	0.00	0.02	3.9	51.92	Aug
		50.95	0.39	4.23	0.27	15.61	22.91	0.13	4.11	0.06	0.37	99.0	1.88	0.01	0.18	0.01	0.86	0.90	0.00	0.07	0.00	0.03	3.9	45.40	Di
		51.38	0.29	5.07	0.35	15.08	23.22	0.06	4.48	0.03	0.42	100.4	1.87	0.01	0.22	0.01	0.82	0.91	0.00	0.06	0.00	0.03	3.9	43.99	Di
		51.74	0.22	4.25	0.34	15.44	22.72	0.16	4.71	0.09	0.33	100.0	1.89	0.01	0.18	0.01	0.84	0.89	0.00	0.08	0.00	0.02	3.9	44.87	Di
		51.31	0.16	4.55	0.53	15.84	22.80	0.10	4.62	0.00	0.31	100.2	1.87	0.00	0.20	0.02	0.86	0.89	0.00	0.08	0.00	0.02	3.9	45.50	Di
		50.89	0.18	4.23	0.36	18.76	14.96	0.17	9.40	0.00	0.23	99.2	1.87	0.01	0.18	0.01	1.03	0.59	0.01	0.22	0.00	0.02	3.9	53.94	Aug
		51.76	0.33	4.02	0.41	15.66	23.39	0.17	4.54	0.02	0.30	100.6	1.88	0.01	0.17	0.01	0.85	0.91	0.01	0.06	0.00	0.02	3.9	44.73	Di
		52.19	0.23	3.80	0.24	15.86	22.80	0.15	4.27	0.02	0.23	99.8	1.91	0.01	0.16	0.01	0.87	0.89	0.00	0.08	0.00	0.02	4.0	45.79	Di
		51.27	0.23	4.23	0.31	15.63	23.02	0.09	4.50	0.00	0.44	99.7	1.88	0.01	0.18	0.01	0.85	0.90	0.00	0.06	0.00	0.03	3.9	45.04	Di
		51.48	0.19	4.55	0.57	15.36	22.82	0.12	4.49	0.04	0.28	99.9	1.88	0.01	0.20	0.02	0.84	0.90	0.00	0.08	0.00	0.02	3.9	44.81	Di
		50.99	0.46	4.85	0.49	15.56	22.33	0.11	4.49	0.00	0.37	99.7	1.87	0.01	0.21	0.01	0.85	0.88	0.00	0.09	0.00	0.03	4.0	45.59	Di
		50.87	0.46	4.52	0.46	15.04	22.65	0.16	4.75	0.04	0.38	99.3	1.88	0.01	0.20	0.01	0.83	0.89	0.00	0.07	0.00	0.03	3.9	44.27	Di
		50.47	0.42	4.58	0.18	15.73	22.14	0.15	5.05	0.07	0.39	99.2	1.86	0.01	0.20	0.01	0.86	0.87	0.00	0.07	0.00	0.03	3.9	45.63	Di
		50.67	0.22	4.51	0.39	16.10	21.60	0.09	5.23	0.00	0.32	99.1	1.86	0.01	0.20	0.01	0.88	0.85	0.00	0.09	0.00	0.02	3.9	46.60	Aug
		51.28	0.51	3.77	0.24	15.65	22.75	0.15	5.12	0.00	0.44	99.9	1.88	0.01	0.16	0.01	0.85	0.89	0.00	0.07	0.00	0.03	3.9	44.89	Di
		50.65	0.24	4.73	0.38	15.41	22.14	0.12	5.18	0.05	0.41	99.3	1.86	0.01	0.20	0.01	0.85	0.87	0.00	0.09	0.00	0.03	3.9	45.02	Di
	A-24C	47.56	0.25	3.59	0.23	15.65	20.66	0.06	2.90	0.00	0.17	91.1	1.89	0.01	0.17	0.01	0.93	0.88	0.00	0.06	0.00	0.01	4.0	48.71	Di
		46.97	0.25	7.82	0.13	18.95	11.42	0.02	4.06	0.05	0.97	90.6	1.84	0.01	0.36	0.00	1.10	0.48	0.00	0.11	0.00	0.07	4.0	64.39	Aug
		48.95	0.02	0.74	0.05	16.36	21.44	0.19	2.31	0.07	0.07	90.2	1.97	0.00	0.03	0.00	0.98	0.92	0.01	0.05	0.00	0.01	4.0	49.47	Di

Amostra		SiO_2	TiO_2	Al_2O_3	Cr_2O_3	MgO	CaO	MnO	FeO	NiO	Na_2O	Total	Si	Ti	Al	Cr	Mg	Ca	Mn	Fe^{2+}	Ni	Na	Total	%En	Mineral
Intrusão 4 Troctolito	A-38B	52.78	0.19	2.75	0.12	15.22	23.78	0.13	5.45	0.07	0.29	100.8	1.92	0.01	0.12	0.00	0.83	0.93	0.00	0.05	0.00	0.02	3.9	43.04	Di
		52.48	0.20	2.29	0.09	15.30	23.56	0.05	5.53	0.00	0.21	99.7	1.93	0.01	0.10	0.00	0.84	0.93	0.00	0.05	0.00	0.02	3.9	43.31	Di
		51.52	0.14	2.02	0.01	16.01	23.37	0.20	5.17	0.00	0.23	98.7	1.91	0.00	0.09	0.00	0.89	0.93	0.01	0.05	0.00	0.02	3.9	44.84	Di
		51.43	0.05	2.71	0.13	16.30	22.56	0.15	5.15	0.00	0.21	98.7	1.90	0.00	0.12	0.00	0.90	0.89	0.00	0.08	0.00	0.01	3.9	46.05	Di
		51.66	0.09	2.35	0.03	16.14	22.91	0.01	5.05	0.00	0.20	98.4	1.92	0.00	0.10	0.00	0.89	0.91	0.00	0.07	0.00	0.01	3.9	45.55	Di
Intrusão 3 - Clinopiroxenito	A-44	51.49	0.37	1.71	0.00	12.06	22.80	0.90	9.81	0.00	0.58	99.7	1.94	0.01	0.08	0.00	0.68	0.92	0.03	0.01	0.00	0.04	3.7	35.51	Di
		51.51	0.09	1.47	0.00	12.48	23.57	1.03	9.36	0.00	0.50	100.0	1.93	0.00	0.06	0.00	0.70	0.95	0.02	0.00	0.00	0.04	3.7	36.00	Di
		51.98	0.00	1.80	0.00	11.98	22.92	0.72	9.86	0.06	0.65	100.0	1.95	0.00	0.08	0.00	0.67	0.92	0.02	0.01	0.00	0.05	3.7	35.25	Di
		51.47	0.04	1.46	0.00	12.07	23.41	0.78	9.41	0.00	0.73	99.4	1.94	0.00	0.06	0.00	0.68	0.94	0.00	0.00	0.00	0.05	3.7	35.31	Di
		50.63	0.17	2.50	0.00	12.02	21.25	0.79	10.94	0.00	0.64	98.9	1.92	0.00	0.11	0.00	0.68	0.86	0.03	0.06	0.00	0.05	3.7	35.95	Di
		50.70	0.22	2.33	0.10	12.01	21.69	0.99	10.52	0.04	0.70	99.3	1.92	0.01	0.10	0.00	0.68	0.88	0.03	0.04	0.00	0.05	3.7	35.86	Di
		51.21	0.00	1.72	0.06	11.75	23.39	0.76	9.89	0.00	0.58	99.4	1.93	0.00	0.08	0.00	0.66	0.95	0.01	0.00	0.00	0.04	3.7	34.46	Di
		51.93	0.07	0.86	0.00	12.72	23.73	0.82	9.53	0.00	0.43	100.1	1.94	0.00	0.04	0.00	0.71	0.95	0.02	0.00	0.00	0.03	3.7	36.22	Di
		51.54	0.16	1.49	0.04	11.95	23.61	0.87	9.86	0.04	0.59	100.1	1.93	0.00	0.07	0.00	0.67	0.95	0.01	0.00	0.00	0.04	3.7	34.68	Di
		51.50	0.00	1.17	0.00	12.22	23.37	0.96	9.68	0.00	0.48	99.4	1.94	0.00	0.05	0.00	0.69	0.94	0.02	0.00	0.00	0.03	3.7	35.48	Di

*Fórmula estrutural calculada na base de 6 oxigênios.

Tabela 11. Química mineral dos ortopiroxênios estudados.

Amostra		SiO_2	TiO_2	Al_2O_3	Cr_2O_3	MgO	CaO	MnO	FeO	NiO	Na_2O	Total	Si	Ti	Al	Cr	Mg	Ca	Mn	Fe^{2+}	Ni	Na	Total	%En	Mineral
Intrusão 2 - wehrlito	A-23B	55.04	0.00	0.74	0.08	31.33	0.19	0.22	12.31	0.00	0.00	99.9	1.94	0.00	0.03	0.00	1.65	0.01	0.01	0.28	0.00	0.00	3.9	81.65	En
		55.02	0.00	0.94	0.00	30.47	0.24	0.19	12.52	0.00	0.06	99.4	1.95	0.00	0.04	0.00	1.61	0.01	0.01	0.32	0.00	0.00	3.9	80.91	En
		53.74	0.07	2.93	0.11	30.31	0.23	0.29	12.21	0.01	0.01	99.9	1.90	0.00	0.10	0.00	1.60	0.01	0.01	0.29	0.00	0.00	3.9	81.21	En
		53.07	0.08	3.47	0.08	30.21	0.25	0.20	12.25	0.00	0.03	99.6	1.88	0.00	0.12	0.00	1.59	0.01	0.01	0.27	0.00	0.00	3.9	81.09	En
		53.56	0.00	2.96	0.23	29.92	0.31	0.15	12.34	0.00	0.00	99.5	1.90	0.00	0.10	0.01	1.58	0.01	0.00	0.30	0.00	0.00	3.9	80.72	En
		53.58	0.00	2.77	0.08	29.96	0.38	0.29	12.76	0.02	0.01	99.8	1.90	0.00	0.10	0.00	1.58	0.01	0.01	0.29	0.00	0.00	3.9	80.12	En

Amostra		SiO_2	TiO_2	Al_2O_3	Cr_2O_3	MgO	CaO	MnO	FeO	NiO	Na_2O	Total	Si	Ti	Al	Cr	Mg	Ca	Mn	Fe^{2+}	Ni	Na	Total	%En	Mineral
Intrusão 4 - Troctolito	A-01C	53.84	0.10	2.97	0.09	29.69	0.19	0.18	11.96	0.05	0.02	99.1	1.92	0.00	0.08	0.00	1.58	0.01	0.01	0.33	0.00	0.00	3.9	81.26	En
		53.50	0.17	1.99	0.05	30.26	0.17	0.21	12.21	0.00	0.03	98.6	1.91	0.00	0.08	0.00	1.61	0.01	0.01	0.29	0.00	0.00	3.9	81.27	En
	A-38B	54.53	0.07	1.50	0.06	26.56	0.29	0.19	16.95	0.06	0.01	100.2	1.97	0.00	0.03	0.00	1.43	0.01	0.01	0.51	0.00	0.00	4.0	73.21	En
		54.86	0.13	1.01	0.01	27.39	0.34	0.27	16.95	0.02	0.02	101.0	1.96	0.00	0.04	0.00	1.46	0.01	0.01	0.48	0.00	0.00	4.0	73.75	En
		53.52	0.13	1.35	0.05	26.48	0.31	0.23	16.74	0.00	0.00	98.8	1.96	0.00	0.04	0.00	1.45	0.01	0.01	0.50	0.00	0.00	4.0	73.37	En
		53.49	0.02	0.88	0.00	27.52	0.31	0.33	16.67	0.04	0.00	99.2	1.94	0.00	0.04	0.00	1.49	0.01	0.01	0.43	0.00	0.00	3.9	74.20	En
		53.57	0.00	2.51	0.00	26.13	0.29	0.14	16.82	0.09	0.00	99.6	1.95	0.00	0.05	0.00	1.42	0.01	0.00	0.51	0.00	0.00	3.9	73.04	En
		51.50	0.00	2.23	0.04	26.08	0.21	0.33	16.93	0.00	0.00	97.3	1.91	0.00	0.09	0.00	1.44	0.01	0.01	0.45	0.00	0.00	3.9	73.00	En
		47.70	0.07	1.31	0.03	22.81	0.31	0.23	19.83	0.08	0.00	92.4	1.90	0.00	0.06	0.00	1.35	0.01	0.01	0.52	0.00	0.00	3.9	66.79	En
		53.69	0.00	1.90	0.04	25.91	0.39	0.17	17.15	0.04	0.00	99.3	1.96	0.00	0.04	0.00	1.41	0.02	0.01	0.52	0.00	0.00	4.0	72.35	En
		52.64	0.00	1.84	0.00	26.58	0.29	0.13	16.98	0.00	0.01	98.5	1.93	0.00	0.07	0.00	1.45	0.01	0.00	0.46	0.00	0.00	3.9	73.19	En
		53.13	0.06	1.35	0.04	27.44	0.34	0.21	16.64	0.02	0.00	99.2	1.93	0.00	0.06	0.00	1.49	0.01	0.01	0.42	0.00	0.00	3.9	74.12	En
		52.92	0.15	1.93	0.00	26.27	0.30	0.23	17.32	0.06	0.02	99.2	1.93	0.00	0.07	0.00	1.43	0.01	0.01	0.48	0.00	0.00	3.9	72.56	En
	A-38D	51.51	0.15	2.74	0.02	26.66	0.30	0.28	16.22	0.06	0.04	98.0	1.89	0.00	0.11	0.00	1.46	0.01	0.01	0.41	0.00	0.00	3.9	74.11	En
		52.32	0.08	2.82	0.07	26.37	0.27	0.29	16.65	0.00	0.04	98.9	1.91	0.00	0.09	0.00	1.43	0.01	0.01	0.45	0.00	0.00	3.9	73.45	En
		51.94	0.00	2.61	0.00	26.77	0.32	0.26	16.15	0.02	0.00	98.1	1.91	0.00	0.09	0.00	1.46	0.01	0.01	0.42	0.00	0.00	3.9	74.24	En
		52.52	0.00	2.86	0.00	26.58	0.30	0.34	16.27	0.00	0.00	98.9	1.91	0.00	0.09	0.00	1.44	0.01	0.01	0.45	0.00	0.00	3.9	73.99	En
		53.32	0.06	1.89	0.04	27.37	0.25	0.29	16.30	0.06	0.03	99.6	1.93	0.00	0.07	0.00	1.47	0.01	0.01	0.43	0.00	0.00	3.9	74.58	En
		52.43	0.00	2.34	0.01	27.39	0.30	0.26	16.40	0.03	0.02	99.2	1.90	0.00	0.10	0.00	1.48	0.01	0.01	0.40	0.00	0.00	3.9	74.41	En
		52.47	0.00	1.66	0.00	27.23	0.19	0.27	16.34	0.10	0.00	98.3	1.92	0.00	0.07	0.00	1.49	0.01	0.01	0.42	0.00	0.00	3.9	74.54	En
		53.11	0.13	1.72	0.01	27.02	0.30	0.25	16.25	0.07	0.01	98.9	1.94	0.00	0.06	0.00	1.47	0.01	0.01	0.45	0.00	0.00	3.9	74.32	En
		52.43	0.05	2.20	0.07	27.05	0.19	0.31	16.42	0.04	0.02	98.8	1.91	0.00	0.09	0.00	1.47	0.01	0.01	0.42	0.00	0.00	3.9	74.33	En
		51.86	0.07	2.74	0.04	26.29	1.79	0.22	15.35	0.06	0.01	98.4	1.90	0.00	0.10	0.00	1.43	0.07	0.01	0.38	0.00	0.00	3.9	72.65	En
		52.35	0.14	2.53	0.00	26.93	0.36	0.28	16.52	0.04	0.00	99.1	1.90	0.00	0.10	0.00	1.46	0.01	0.01	0.42	0.00	0.00	3.9	73.88	En
		52.28	0.00	2.68	0.07	26.82	1.42	0.22	15.37	0.00	0.00	98.9	1.90	0.00	0.10	0.00	1.45	0.06	0.01	0.38	0.00	0.00	3.9	73.56	En
		52.21	0.00	2.86	0.00	27.25	0.34	0.35	15.64	0.09	0.01	98.8	1.90	0.00	0.10	0.00	1.48	0.01	0.01	0.39	0.00	0.00	3.9	75.14	En
		52.17	0.00	2.59	0.00	26.65	0.32	0.27	16.71	0.06	0.00	98.8	1.90	0.00	0.10	0.00	1.45	0.01	0.01	0.43	0.00	0.00	3.9	73.51	En

*Fórmula estrutural calculada na base de 6 oxigênios.

Tabela 12: Química mineral dos plagioclásios estudados.

Intrusão 4 - Troctolito	Amostra	Na_2O	K_2O	SiO_2	Al_2O_3	FeO	CaO	Total	Na	K	Si	Al	Fe^{2+}	Ca	Total	% An
	A-38B	2.10	0.02	46.20	33.72	0.08	16.08	98.18	0.19	0.00	2.15	1.85	0.00	0.80	4.99	80.84
		1.71	0.03	45.21	34.18	0.07	16.69	97.87	0.15	0.00	2.11	1.88	0.00	0.84	4.99	84.24
		1.68	0.05	45.38	34.17	0.05	16.64	97.96	0.15	0.00	2.12	1.88	0.00	0.83	5.00	84.31
		1.64	0.01	46.28	33.94	0.03	17.06	98.95	0.15	0.00	2.14	1.85	0.00	0.85	4.99	85.14
		1.85	0.02	45.88	34.40	0.05	16.34	98.54	0.17	0.00	2.13	1.88	0.00	0.81	4.99	82.90
		1.28	0.02	44.44	34.81	0.09	17.23	97.87	0.12	0.00	2.08	1.92	0.00	0.87	4.99	88.08
		0.46	0.02	43.42	35.54	0.06	18.79	98.29	0.04	0.00	2.03	1.96	0.00	0.94	4.97	85.63
	A-38D	1.64	0.03	44.60	33.09	0.10	16.60	96.06	0.15	0.00	2.13	1.86	0.00	0.85	4.99	84.66
		1.91	0.03	45.64	33.43	0.07	16.39	97.46	0.17	0.00	2.14	1.85	0.00	0.82	4.99	82.45
		1.98	0.00	46.31	33.16	0.07	16.31	97.82	0.18	0.00	2.16	1.82	0.00	0.82	4.98	82.01
		1.62	0.03	45.05	33.35	0.08	16.80	96.92	0.15	0.00	2.13	1.86	0.00	0.85	4.99	85.01
		1.91	0.02	46.47	33.29	0.02	16.47	98.18	0.17	0.00	2.17	1.83	0.00	0.82	4.99	82.58
		1.16	0.03	44.23	34.17	0.02	17.26	96.86	0.11	0.00	2.10	1.91	0.00	0.88	4.99	88.99
		2.03	0.00	46.16	33.01	0.08	16.24	97.53	0.18	0.00	2.16	1.82	0.00	0.81	4.98	81.51
		2.21	0.03	46.82	33.03	0.11	16.65	98.85	0.20	0.00	2.17	1.80	0.00	0.83	4.99	80.46
		1.17	0.03	46.71	31.30	0.65	18.52	98.38	0.11	0.00	2.19	1.73	0.03	0.93	4.99	89.57
		2.05	0.06	46.88	33.38	0.07	16.84	99.26	0.18	0.00	2.16	1.81	0.00	0.83	4.99	81.68
		1.62	0.03	45.93	34.02	0.05	17.27	98.93	0.15	0.00	2.13	1.86	0.00	0.86	4.99	85.32
		2.20	0.03	46.78	34.00	0.08	15.98	99.07	0.20	0.00	2.16	1.85	0.00	0.79	4.99	79.90
		2.00	0.04	47.16	34.14	0.13	16.90	100.37	0.18	0.00	2.15	1.83	0.00	0.83	4.99	82.17
		1.49	0.04	45.43	34.59	0.05	18.05	99.65	0.13	0.00	2.09	1.88	0.00	0.89	4.99	86.79
		1.30	0.01	45.93	33.21	0.24	18.30	98.98	0.12	0.00	2.14	1.82	0.00	0.91	4.98	88.57
		1.01	0.01	45.07	33.04	0.35	19.13	98.60	0.09	0.00	2.11	1.82	0.00	0.96	4.98	91.27
		1.19	0.03	45.92	31.50	0.57	18.86	98.06	0.11	0.00	2.16	1.75	0.00	0.95	4.97	89.65
		1.08	0.01	44.51	34.88	0.06	18.27	98.81	0.10	0.00	2.07	1.91	0.00	0.91	4.99	90.31
		1.84	0.07	46.22	33.63	0.04	17.22	99.03	0.16	0.00	2.14	1.83	0.00	0.85	5.00	83.48
		1.11	0.03	44.88	34.42	0.08	18.37	98.90	0.10	0.00	2.09	1.88	0.00	0.91	4.99	89.94
		0.96	0.02	44.20	34.95	0.07	18.62	98.81	0.09	0.00	2.06	1.92	0.00	0.93	4.99	91.38
		1.85	0.02	45.97	33.23	0.12	17.06	98.24	0.17	0.00	2.14	1.83	0.00	0.85	4.99	83.55

Amostra	Na_2O	K_2O	SiO_2	Al_2O_3	FeO	CaO	Total	Na	K	Si	Al	Fe^{2+}	Ca	Total	% An
	1.80	0.04	46.72	33.00	0.10	16.88	98.55	0.16	0.00	2.17	1.81	0.00	0.84	4.99	83.59
	1.83	0.02	45.80	33.60	0.00	16.86	98.11	0.17	0.00	2.14	1.85	0.00	0.84	4.99	83.47
	1.60	0.01	46.01	33.66	0.06	17.40	98.74	0.14	0.00	2.14	1.85	0.00	0.87	5.00	85.67
	1.01	0.04	44.04	34.54	0.06	18.24	97.93	0.09	0.00	2.07	1.91	0.00	0.92	4.99	90.67

*Fórmula estrutural calculada na base de 8 oxigênios.

Tabela 13: Química mineral dos anfibólios estudados.

	Amostra	SiO_2	TiO_2	Al_2O_3	FeO	MnO	MgO	CaO	Na2O	K_2O	Cl	Cr_2O3	V_2O_3	NiO	SrO	Total	Si	Al	Total	Al	Ti	Fe^{3+}	V	Cr	Mg	Ni	Fe^{2+}	Mn	Total	Ca	Na	K	Total	Mineral
Intrusão 3	A-44	41.76	0.45	11.14	17.30	0.56	11.11	12.09	1.52	1.48	0.07	0.00	0.05	0.00	0.02	97.6	6.27	1.73	8.0	0.24	0.05	0.73	0.01	0.00	2.49	0.00	1.44	0.05	5.0	1.94	0.44	0.28	2.7	Mg-Hs
		42.06	0.62	10.88	17.11	0.57	10.91	11.97	1.44	1.44	0.04	0.10	0.05	0.02	0.05	97.3	6.33	1.67	8.0	0.27	0.07	0.62	0.01	0.01	2.45	0.00	1.53	0.04	5.0	1.93	0.42	0.28	2.6	Mg-Hs
		42.63	0.68	11.37	16.92	0.63	11.40	11.95	1.40	1.41	0.04	0.00	0.02	0.00	0.00	98.4	6.31	1.69	8.0	0.29	0.08	0.71	0.00	0.00	2.51	0.00	1.38	0.03	5.0	1.89	0.40	0.27	2.6	Mg-Hs
		42.62	0.49	11.38	17.05	0.70	11.07	11.85	1.44	1.48	0.04	0.03	0.01	0.00	0.00	98.1	6.34	1.66	8.0	0.33	0.05	0.65	0.00	0.00	2.45	0.00	1.47	0.04	5.0	1.89	0.42	0.28	2.6	Mg-Hs
		41.66	0.59	10.51	17.25	0.67	10.87	11.89	1.28	1.41	0.05	0.03	0.02	0.02	0.03	96.3	6.33	1.67	8.0	0.21	0.07	0.74	0.00	0.00	2.46	0.00	1.45	0.06	5.0	1.94	0.38	0.27	2.6	Mg-Hs
		42.21	0.63	10.92	16.81	0.64	10.95	12.17	1.54	1.52	0.05	0.00	0.00	0.00	0.00	97.4	6.35	1.65	8.0	0.29	0.07	0.52	0.00	0.00	2.46	0.00	1.59	0.06	5.0	1.96	0.45	0.29	2.7	Mg-Hs
	A-44C	45.10	0.27	10.18	8.55	0.12	16.31	11.70	1.73	0.28	0.11	0.09	0.00	0.00	0.00	94.4	6.63	1.37	8.0	0.39	0.03	0.56	0.00	0.01	3.57	0.00	0.44	0.00	5.0	1.84	0.49	0.05	2.4	Mg-Hbl
		54.66	0.00	1.87	11.34	0.26	22.08	6.01	0.36	0.04	0.03	0.04	0.00	0.04	0.06	96.8	7.71	0.29	8.0	0.02	0.00	0.24	0.00	0.00	4.65	0.00	0.08	0.00	5.0	0.91	0.10	0.01	1.0	Mg-Hbl
		51.27	0.01	5.85	7.13	0.10	19.02	12.07	0.83	0.16	0.07	0.00	0.00	0.00	0.05	96.5	7.24	0.76	8.0	0.22	0.00	0.47	0.00	0.00	4.01	0.00	0.30	0.00	5.0	1.83	0.23	0.03	2.1	Act
		46.64	0.18	10.17	9.07	0.20	16.68	12.04	1.48	0.26	0.04	0.00	0.00	0.00	0.01	96.8	6.67	1.33	8.0	0.39	0.02	0.62	0.00	0.00	3.56	0.00	0.42	0.00	5.0	1.85	0.41	0.05	2.3	Mg-Hbl
		46.88	0.00	9.73	8.73	0.17	16.70	11.95	1.48	0.37	0.08	0.08	0.02	0.06	0.06	96.3	6.75	1.25	8.0	0.40	0.00	0.54	0.00	0.01	3.58	0.01	0.46	0.00	5.0	1.84	0.41	0.07	2.3	Mg-Hbl
		45.79	0.00	10.59	9.07	0.08	16.58	11.70	1.61	0.33	0.08	0.03	0.01	0.05	0.00	95.9	6.61	1.39	8.0	0.41	0.00	0.69	0.00	0.00	3.57	0.01	0.32	0.00	5.0	1.81	0.45	0.06	2.3	Mg-Hbl
		44.14	0.00	9.97	8.70	0.04	15.42	11.76	1.31	0.37	0.10	0.01	0.02	0.01	0.00	91.8	6.68	1.32	8.0	0.46	0.00	0.53	0.00	0.00	3.48	0.00	0.53	0.00	5.0	1.91	0.38	0.07	2.4	Mg-Hbl
		46.15	0.31	10.27	8.97	0.13	16.49	11.87	1.54	0.33	0.05	0.04	0.00	0.04	0.00	96.2	6.65	1.35	8.0	0.40	0.03	0.58	0.00	0.00	3.54	0.00	0.44	0.00	5.0	1.83	0.43	0.06	2.3	Mg-Hbl
		47.88	0.05	6.32	7.81	0.08	17.92	11.83	0.97	0.22	0.08	0.01	0.03	0.03	0.00	93.2	7.05	0.95	8.0	0.14	0.01	0.63	0.00	0.00	3.93	0.00	0.27	0.00	5.0	1.87	0.28	0.04	2.2	Mg-Hbl
		54.94	0.00	0.86	14.97	0.48	23.09	1.31	0.14	0.03	0.02	0.00	0.02	0.02	0.00	95.9	7.86	0.14	8.0	0.01	0.00	0.11	0.00	0.00	4.88	0.00	0.00	0.00	5.0	0.20	0.04	0.01	0.2	Act
		51.62	0.10	4.55	7.17	0.11	19.41	12.04	0.70	0.08	0.02	0.05	0.00	0.00	0.00	95.8	7.33	0.67	8.0	0.09	0.01	0.53	0.00	0.01	4.11	0.00	0.25	0.00	5.0	1.83	0.19	0.01	2.0	Mg-Hbl
		29.09	0.07	6.45	9.20	0.19	11.26	9.41	0.90	0.41	0.22	0.00	0.00	0.00	0.06	67.2	6.22	1.63	7.9	0.00	0.00	0.90	0.00	0.00	3.59	0.00	0.51	0.00	5.0	1.73	0.37	0.11	2.2	Ts
		50.92	0.03	6.22	7.82	0.18	18.69	11.98	0.85	0.15	0.02	0.05	0.02	0.02	0.04	97.0	7.18	0.82	8.0	0.21	0.00	0.55	0.00	0.01	3.93	0.00	0.31	0.00	5.0	1.81	0.23	0.03	2.1	Mg-Hbl
		44.63	0.29	11.63	9.56	0.12	16.23	11.40	1.60	0.42	0.03	0.05	0.00	0.00	0.12	96.1	6.44	1.56	8.0	0.42	0.03	0.78	0.00	0.01	3.49	0.00	0.28	0.00	5.0	1.76	0.45	0.08	2.3	Ts
		44.79	0.29	11.24	9.45	0.15	15.85	11.82	1.73	0.43	0.06	0.00	0.00	0.04	0.00	95.8	6.51	1.49	8.0	0.44	0.03	0.61	0.00	0.00	3.43	0.00	0.48	0.00	5.0	1.84	0.49	0.08	2.4	Ts
	A-44D	48.62	0.31	5.83	14.28	0.44	13.75	12.35	0.79	0.60	0.00	0.00	0.03	0.00	0.00	97.0	7.15	0.85	8.0	0.16	0.03	0.34	0.00	0.00	3.01	0.00	1.42	0.03	5.0	1.95	0.23	0.11	2.3	Mg-Hbl
		46.42	0.10	7.21	15.60	0.53	12.77	11.78	1.11	0.85	0.03	0.00	0.03	0.01	0.04	96.5	6.92	1.08	8.0	0.19	0.01	0.51	0.00	0.00	2.84	0.00	1.44	0.01	5.0	1.88	0.32	0.16	2.4	Mg-Hbl
		46.22	0.25	7.20	15.36	0.62	12.83	11.99	1.08	0.92	0.04	0.00	0.00	0.00	0.00	96.5	6.90	1.10	8.0	0.16	0.03	0.50	0.00	0.00	2.85	0.00	1.42	0.04	5.0	1.92	0.31	0.17	2.4	Mg-Hbl
		46.36	0.38	7.09	15.59	0.56	12.62	11.86	1.12	0.90	0.02	0.04	0.01	0.05	0.09	96.7	6.92	1.08	8.0	0.17	0.04	0.42	0.00	0.00	2.81	0.01	1.52	0.02	5.0	1.90	0.32	0.17	2.4	Mg-Hbl
		45.94	0.21	7.06	15.32	0.46	12.14	11.96	0.92	0.83	0.03	0.05	0.01	0.00	0.00	94.9	6.98	1.02	8.0	0.24	0.02	0.36	0.00	0.01	2.75	0.00	1.59	0.03	5.0	1.95	0.27	0.16	2.4	Mg-Hbl

Amostra		SiO_2	TiO_2	Al_2O_3	FeO	MnO	MgO	CaO	Na2O	K_2O	Cl	Cr_2O3	V_2O_3	NiO	SrO	Total	Si	Al	Total	Al	Ti	Fe^{3+}	V	Cr	Mg	Ni	Fe^{2+}	Mn	Total	Ca	Na	K	Total	Mineral
Intrusão 4	A-38B	40.99	0.57	15.53	8.85	0.12	15.20	11.53	2.74	0.45	0.02	0.02	0.09	0.00	0.14	96.2	5.97	2.03	8.0	0.63	0.06	0.61	0.01	0.00	3.30	0.00	0.39	0.00	5.0	1.80	0.77	0.08	2.7	Mg-Hs
		41.65	0.63	15.51	8.40	0.04	15.58	11.78	2.60	0.33	0.03	0.05	0.05	0.00	0.00	96.7	6.00	2.00	8.0	0.64	0.07	0.62	0.01	0.01	3.35	0.00	0.31	0.00	5.0	1.82	0.73	0.06	2.6	Mg-Hs
		41.32	0.24	16.15	8.67	0.07	15.34	11.60	2.72	0.31	0.05	0.08	0.00	0.00	0.08	96.6	5.96	2.04	8.0	0.71	0.03	0.67	0.00	0.01	3.30	0.00	0.29	0.00	5.0	1.79	0.76	0.06	2.6	Mg-Hs
		41.19	1.26	14.96	8.90	0.01	14.84	12.05	2.12	1.05	0.02	0.06	0.10	0.06	0.00	96.6	6.01	1.99	8.0	0.58	0.14	0.46	0.01	0.01	3.23	0.01	0.58	0.00	5.0	1.88	0.60	0.20	2.7	Mg-Hs
		41.09	1.15	15.56	9.10	0.00	14.61	11.79	2.15	1.03	0.03	0.00	0.04	0.00	0.06	96.6	5.99	2.01	8.0	0.66	0.13	0.46	0.00	0.00	3.17	0.00	0.57	0.00	5.0	1.84	0.61	0.19	2.6	Mg-Hs
		42.38	0.09	14.89	8.55	0.15	15.54	12.02	2.48	0.17	0.05	0.00	0.02	0.00	0.12	96.5	6.12	1.88	8.0	0.66	0.01	0.62	0.00	0.00	3.35	0.00	0.37	0.00	5.0	1.86	0.70	0.03	2.6	Mg-Hs
		43.01	0.07	14.40	9.13	0.04	15.60	11.64	2.43	0.09	0.03	0.00	0.00	0.00	0.00	96.4	6.19	1.81	8.0	0.64	0.01	0.69	0.00	0.00	3.35	0.00	0.32	0.00	5.0	1.80	0.68	0.02	2.5	Mg-Hs
		42.27	0.12	14.82	9.01	0.12	15.18	11.84	2.26	0.38	0.04	0.00	0.04	0.00	0.07	96.1	6.13	1.87	8.0	0.67	0.01	0.63	0.01	0.00	3.28	0.00	0.40	0.00	5.0	1.84	0.64	0.07	2.5	Mg-Hs
	A-38E	43.37	0.38	13.81	9.44	0.15	15.19	12.01	1.81	0.20	0.14	0.10	0.03	0.00	0.00	96.6	6.25	1.75	8.0	0.59	0.04	0.71	0.00	0.01	3.26	0.00	0.38	0.00	5.0	1.85	0.51	0.04	2.4	Ts
		45.66	0.33	11.29	9.01	0.07	16.33	12.03	1.51	0.14	0.05	0.00	0.01	0.01	0.06	96.5	6.55	1.45	8.0	0.46	0.04	0.64	0.00	0.00	3.49	0.00	0.37	0.00	5.0	1.85	0.42	0.03	2.3	Mg-Hbl
		43.69	0.24	12.45	9.70	0.09	15.59	12.11	1.63	0.20	0.09	0.00	0.03	0.05	0.03	95.9	6.34	1.66	8.0	0.46	0.03	0.80	0.00	0.00	3.37	0.01	0.34	0.00	5.0	1.88	0.46	0.04	2.4	Ts
		42.42	0.74	13.72	9.96	0.11	14.99	11.94	1.54	0.68	0.12	0.06	0.00	0.00	0.15	96.4	6.16	1.84	8.0	0.51	0.08	0.76	0.00	0.01	3.25	0.00	0.40	0.00	5.0	1.86	0.43	0.13	2.4	Ts
		42.48	0.80	14.16	10.05	0.20	14.79	12.08	1.69	0.71	0.08	0.00	0.06	0.00	0.00	97.1	6.14	1.86	8.0	0.55	0.09	0.69	0.01	0.00	3.18	0.00	0.48	0.00	5.0	1.87	0.47	0.13	2.5	Ts
		42.64	0.16	14.29	9.21	0.16	15.31	12.11	1.74	0.12	0.06	0.00	0.06	0.00	0.14	96.0	6.17	1.83	8.0	0.60	0.02	0.80	0.01	0.00	3.30	0.00	0.27	0.00	5.0	1.88	0.49	0.02	2.4	Ts
		43.52	0.14	13.28	9.72	0.13	15.54	11.85	1.72	0.17	0.09	0.00	0.03	0.00	0.17	96.4	6.28	1.72	8.0	0.53	0.01	0.82	0.00	0.00	3.34	0.00	0.29	0.00	5.0	1.83	0.48	0.03	2.3	Ts
		41.23	0.88	14.41	9.91	0.09	14.97	12.02	1.61	0.39	0.11	0.01	0.06	0.06	0.11	95.9	6.00	2.00	8.0	0.48	0.10	0.93	0.01	0.00	3.25	0.01	0.23	0.00	5.0	1.87	0.45	0.07	2.4	Ts
		42.23	0.52	14.67	9.26	0.11	14.65	12.36	1.65	0.37	0.08	0.09	0.00	0.05	0.10	96.1	6.14	1.86	8.0	0.65	0.06	0.64	0.00	0.01	3.17	0.01	0.46	0.00	5.0	1.92	0.47	0.07	2.5	Ts
		42.83	0.00	13.92	9.66	0.06	14.76	11.79	1.97	0.08	0.08	0.01	0.00	0.00	0.22	95.4	6.26	1.74	8.0	0.66	0.00	0.64	0.00	0.00	3.22	0.00	0.48	0.00	5.0	1.85	0.56	0.02	2.4	Ts
Intrusão 2		53.70	0.00	4.14	4.88	0.07	20.93	12.74	0.86	0.10	0.03	0.34	0.05	0.03	0.11	98.0	7.44	0.56	8.0	0.11	0.00	0.27	0.00	0.04	4.32	0.00	0.25	0.00	5.0	1.89	0.23	0.02	2.1	Mg-Hbl
		53.54	0.06	4.54	5.10	0.06	20.53	12.81	0.78	0.13	0.02	0.43	0.02	0.09	0.25	98.3	7.41	0.59	8.0	0.15	0.01	0.22	0.00	0.05	4.23	0.01	0.33	0.00	5.0	1.90	0.21	0.02	2.1	Mg-Hbl
	A-23A	43.53	0.80	15.75	7.03	0.15	16.12	12.36	2.26	0.69	0.01	0.08	0.05	0.04	0.02	98.9	6.12	1.88	8.0	0.74	0.08	0.36	0.01	0.01	3.38	0.00	0.42	0.00	5.0	1.86	0.61	0.12	2.6	Mg-Hbl
		43.20	0.29	14.98	6.93	0.10	16.26	12.25	2.15	0.77	0.00	0.20	0.10	0.00	0.00	97.2	6.17	1.83	8.0	0.69	0.03	0.44	0.01	0.02	3.46	0.00	0.34	0.00	5.0	1.87	0.60	0.14	2.6	Mg-Hbl
		49.48	0.44	6.67	9.74	0.15	16.67	12.63	0.60	0.36	0.04	0.33	0.07	0.10	0.04	97.3	7.07	0.93	8.0	0.19	0.05	0.44	0.01	0.04	3.55	0.01	0.71	0.00	5.0	1.93	0.16	0.07	2.2	Mg-Hbl
		51.37	0.19	4.41	8.92	0.21	17.99	12.68	0.54	0.26	0.02	0.20	0.03	0.09	0.05	97.0	7.32	0.68	8.0	0.06	0.02	0.42	0.00	0.02	3.82	0.01	0.64	0.00	5.0	1.94	0.15	0.05	2.1	Mg-Hbl
		49.90	0.20	6.08	9.70	0.16	17.09	12.74	0.59	0.34	0.01	0.13	0.02	0.04	0.04	97.0	7.13	0.87	8.0	0.16	0.02	0.47	0.00	0.01	3.64	0.01	0.69	0.00	5.0	1.95	0.16	0.06	2.2	Mg-Hbl
	A-25	52.17	0.30	5.53	6.29	0.07	20.34	12.26	0.86	0.17	0.04	0.00	0.01	0.05	0.00	98.1	7.23	0.77	8.0	0.13	0.03	0.49	0.00	0.00	4.20	0.01	0.15	0.00	5.0	1.82	0.23	0.03	2.1	Mg-Hbl
		50.25	0.14	6.94	6.88	0.21	18.57	12.79	0.79	0.13	0.03	0.13	0.06	0.00	0.00	96.9	7.09	0.91	8.0	0.25	0.01	0.44	0.01	0.01	3.91	0.00	0.37	0.00	5.0	1.94	0.22	0.02	2.2	Mg-Hbl
		51.83	0.16	5.77	6.76	0.12	19.25	12.78	0.74	0.12	0.03	0.11	0.00	0.05	0.04	97.8	7.24	0.76	8.0	0.19	0.02	0.40	0.00	0.01	4.01	0.01	0.37	0.00	5.0	1.91	0.20	0.02	2.1	Mg-Hbl
		52.56	0.08	4.15	6.54	0.08	19.49	12.22	0.61	0.19	0.01	0.15	0.04	0.10	0.00	96.2	7.44	0.56	8.0	0.13	0.01	0.35	0.00	0.02	4.11	0.01	0.37	0.00	5.0	1.85	0.17	0.03	2.1	Mg-Hbl

Amostra		SiO_2	TiO_2	Al_2O_3	FeO	MnO	MgO	CaO	Na2O	K_2O	Cl	Cr_2O3	V_2O_3	NiO	SrO	Total	Si	Al	Total	Al	Ti	Fe^{3+}	V	Cr	Mg	Ni	Fe^{2+}	Mn	Total	Ca	Na	K	Total	Mineral
		52.00	0.18	5.71	6.60	0.08	19.78	12.31	0.78	0.17	0.02	0.11	0.00	0.04	0.00	97.8	7.23	0.77	8.0	0.17	0.02	0.49	0.00	0.01	4.10	0.00	0.21	0.00	5.0	1.83	0.21	0.03	2.1	Mg-Hbl
		52.77	0.19	4.57	6.23	0.11	19.74	12.70	0.61	0.15	0.00	0.06	0.01	0.06	0.00	97.2	7.39	0.61	8.0	0.15	0.02	0.32	0.00	0.01	4.12	0.01	0.37	0.00	5.0	1.91	0.17	0.03	2.1	Mg-Hbl
		52.15	0.12	5.48	6.61	0.15	19.61	12.22	0.83	0.13	0.04	0.24	0.02	0.04	0.00	97.6	7.27	0.73	8.0	0.17	0.01	0.45	0.00	0.03	4.08	0.00	0.26	0.00	5.0	1.82	0.22	0.02	2.1	Mg-Hbl
		52.37	0.28	5.04	6.35	0.11	19.98	12.61	0.63	0.12	0.02	0.21	0.00	0.08	0.00	97.8	7.28	0.72	8.0	0.10	0.03	0.48	0.00	0.02	4.14	0.01	0.21	0.00	5.0	1.88	0.17	0.02	2.1	Mg-Hbl
	A-01A	46.77	0.00	9.48	8.07	0.04	17.63	12.38	1.33	0.21	0.12	0.03	0.04	0.01	0.00	96.1	6.70	1.30	8.0	0.30	0.00	0.72	0.00	0.00	3.77	0.00	0.20	0.00	5.0	1.90	0.37	0.04	2.3	Mg-Hbl
	A-01A	46.95	0.21	9.76	7.72	0.15	17.73	12.24	1.18	0.28	0.09	0.00	0.08	0.05	0.13	96.6	6.69	1.31	8.0	0.32	0.02	0.70	0.01	0.00	3.76	0.01	0.17	0.00	5.0	1.87	0.32	0.05	2.2	Mg-Hbl
	A-01A	44.22	0.13	12.48	8.73	0.00	16.06	12.30	1.59	0.47	0.22	0.00	0.01	0.01	0.15	96.4	6.39	1.61	8.0	0.51	0.01	0.67	0.00	0.00	3.46	0.00	0.34	0.00	5.0	1.90	0.44	0.09	2.4	Ts
	A-01A	44.24	0.12	12.57	8.93	0.05	15.83	12.31	1.77	0.46	0.20	0.00	0.00	0.04	0.07	96.6	6.39	1.61	8.0	0.53	0.01	0.61	0.00	0.00	3.41	0.00	0.43	0.00	5.0	1.90	0.49	0.09	2.5	Ts
	A-01B	50.33	0.50	7.23	8.46	0.13	18.25	11.64	0.82	0.12	0.06	0.10	0.00	0.04	0.00	97.7	7.06	0.94	8.0	0.25	0.05	0.57	0.00	0.01	3.81	0.00	0.30	0.00	5.0	1.75	0.22	0.02	2.0	Mg-Hbl
	A-01B	46.64	0.47	10.70	8.81	0.14	16.48	11.52	1.15	0.18	0.08	0.06	0.03	0.06	0.06	96.4	6.66	1.34	8.0	0.47	0.05	0.67	0.00	0.01	3.51	0.01	0.29	0.00	5.0	1.76	0.32	0.03	2.1	Mg-Hbl
	A-01C	47.15	0.17	8.73	7.00	0.26	22.20	9.34	0.20	0.03	0.04	0.00	0.04	0.00	0.11	95.3	6.65	1.35	8.0	0.10	0.02	1.01	0.00	0.00	3.86	0.00	0.00	0.00	5.0	1.16	0.05	0.01	1.2	Mg-Hbl
	A-01C	45.58	0.00	12.61	5.47	0.19	18.11	12.36	1.41	0.16	0.15	0.04	0.02	0.07	0.22	96.4	6.47	1.53	8.0	0.58	0.00	0.58	0.00	0.00	3.83	0.01	0.00	0.00	5.0	1.88	0.39	0.03	2.3	Ts
	A-22	45.98	0.60	9.09	9.88	0.07	16.09	12.81	0.93	0.71	0.01	0.05	0.04	0.07	0.07	96.4	6.68	1.32	8.0	0.23	0.06	0.56	0.00	0.01	3.48	0.01	0.64	0.01	5.0	1.99	0.26	0.13	2.4	Mg-Hbl
	A-22	47.52	0.31	7.99	8.80	0.15	16.83	13.11	0.81	0.56	0.02	0.00	0.02	0.06	0.04	96.2	6.87	1.13	8.0	0.23	0.03	0.46	0.00	0.00	3.63	0.01	0.60	0.02	5.0	2.00	0.23	0.10	2.3	Mg-Hbl
	A-22	51.40	0.36	4.81	7.74	0.15	18.91	12.85	0.55	0.25	0.03	0.00	0.09	0.04	0.04	97.2	7.26	0.74	8.0	0.06	0.04	0.46	0.01	0.00	3.98	0.00	0.45	0.00	5.0	1.94	0.15	0.04	2.1	Mg-Hbl
	A-22	47.05	0.66	8.28	9.33	0.07	16.61	12.75	0.97	0.60	0.03	0.10	0.06	0.02	0.09	96.6	6.80	1.20	8.0	0.21	0.07	0.47	0.01	0.01	3.58	0.00	0.65	0.00	5.0	1.97	0.27	0.11	2.4	Mg-Hbl
	A-22	46.00	0.49	6.78	9.79	0.32	15.48	12.37	0.81	0.46	0.19	0.09	0.04	0.01	0.00	92.8	6.95	1.05	8.0	0.16	0.06	0.48	0.01	0.01	3.49	0.00	0.76	0.04	5.0	2.00	0.24	0.09	2.3	Mg-Hbl
	A-22	46.97	0.14	7.92	8.89	0.19	16.91	12.84	0.82	0.55	0.03	0.00	0.02	0.04	0.00	95.3	6.84	1.16	8.0	0.20	0.02	0.60	0.00	0.00	3.67	0.00	0.49	0.02	5.0	2.00	0.23	0.10	2.3	Mg-Hbl
Intrusão 1	A-19	58.02	0.00	0.98	2.50	0.14	23.99	12.43	0.33	0.04	0.00	0.01	0.00	0.05	0.01	98.5	7.86	0.14	8.0	0.02	0.00	0.09	0.00	0.00	4.84	0.01	0.04	0.00	5.0	1.80	0.09	0.01	1.9	Tr
Intrusão 1	A-19	58.52	0.00	0.75	2.27	0.00	24.18	12.78	0.22	0.02	0.00	0.00	0.00	0.00	0.00	98.7	7.89	0.11	8.0	0.01	0.00	0.08	0.00	0.00	4.86	0.00	0.05	0.00	5.0	1.85	0.06	0.00	1.9	Tr
Intrusão 1	A-19	57.30	0.19	1.54	2.90	0.30	23.81	12.47	0.37	0.05	0.02	0.03	0.00	0.06	0.01	99.0	7.75	0.25	8.0	0.00	0.02	0.10	0.00	0.00	4.80	0.01	0.07	0.00	5.0	1.81	0.10	0.01	1.9	Tr
Intrusão 1	A-19	57.94	0.05	0.46	2.13	0.13	23.97	12.54	0.14	0.01	0.00	0.06	0.00	0.01	0.06	97.5	7.93	0.07	8.0	0.00	0.00	0.01	0.00	0.01	4.89	0.00	0.09	0.00	5.0	1.84	0.04	0.00	1.9	Tr
Intrusão 1	A-19	55.02	0.29	2.15	2.72	0.09	23.08	11.61	0.26	0.06	0.06	0.01	0.00	0.03	0.07	95.4	7.69	0.31	8.0	0.05	0.03	0.19	0.00	0.00	4.73	0.00	0.00	0.00	5.0	1.74	0.07	0.01	1.8	Tr

*Fórmula estrutural calculada na base de 23 oxigênios.